Reliable emergency service for 5G networks

Vishaka Basnayake Mudiyanselage

THÈSE DE DOCTORAT EN CO-TUTELLE

DE L'ÉTABLISSEMENT UNIVERSITÉ BOURGOGNE FRANCHE-COMTÉ

PRÉPARÉE À L'UNIVERSITÉ DE FRANCHE COMTÉ, FRANCE

ET DE L'ÉTABLISSEMENT ÉCOLE DES ÉTUDES SUPÉRIEURES ET DE LA RECHERCHE, SRI LANKA TECHNOLOGICAL CAMPUS, SRI LANKA

École doctorale n°37

Sciences Pour l'Ingénieur et Microtechniques

Doctorat d'Informatique

par

VISHAKA BASNAYAKE

Reliable Emergency Service for 5G Networks

Service de communication sans fil d'urgence 5G fiable

Thèse présentée et soutenue à Montbéliard, le 2 Juin 2023

Composition du Jury :

NATHALIE MITTON MME	Directeur de recherche, INRIA Lille	Président
GENTIAN JAKLLARI M	Professeur des universités, Toulouse INP–ENSEEIHT	Rapporteur
G. LAKSHMI SUTHA MME	Professeur associé, Institut national de technologie de Puducherry, Inde	Examinateur
HAKIM MABED M	Professeur associé à l'Université de Bourgogne Franche-Comté, France	Directeur de thèse
PHILIPPE CANALDA M	Professeur associé à l'Université de Bourgogne Franche-Comté, France	Co-Directeur de thèse
DUSHANTHA JAYAKODY M	Professeur à l'Lusófona University et Sri Lanka Technological Campus, Sri Lanka	Co-Directeur de thèse

N° | X | X | X |

école doctorale **sciences pour l'ingénieur et microtechniques**

Title: Service de communication sans fil d'urgence 5G fiable

Keywords: Asynchronous Non-Orthogonal Multiple Access, Device-to-Device, Emergency Communication Systems, Localization, Multi-Hop Emergency Call Protocol, Out-of-Coverage

Abstract:
During large-scale disasters, emergency communication systems that are reliable, responsive, and energy-efficient are crucial. This thesis focuses on designing reliable emergency communication systems for disaster scenarios in out-of-coverage areas. The proposed systems are designed to work seamlessly across the data link, network, and application layers. At the data link layer, a new decoding scheme named Cyclic Triangular Successive Interference Cancellation (Cyclic T-SIC) is proposed to enhance the reliability in Asynchronous NOMA-assisted D2D communications. Moreover, at the network layer, new multi-hop protocols namely Multi-Hop Emergency caLl Protocol (M-HELP) and 5G Standalone Service (5G-SOS) that comply with 3GPP standards are introduced to reduce control traffic and improve emergency information transfer reliability. Moreover, a new Multi Victim Localization Algorithm *(MVLA)* is proposed at the application layer to locate victim devices during emergencies. This scheme uses radio data from outband D2D-assisted multi-hop emergency calls and applies constraint satisfaction methods to locate victims in a progressive propagation manner. Additionally, an emergency service architecture is also proposed comprising an optimized machine learning model to locate population-congested areas during pandemics. By comparing and evaluating the proposed methods and schemes with conventional state-of-the-art approaches, valuable insights are obtained into the design of efficient and optimal emergency communication systems for areas with limited network coverage.

Titre : Service de communication sans fil d'urgence 5G fiable

Mots-clés : Accès Multiple Asynchrone Non-Orthogonal, Périphérique à Périphérique, Systèmes de Communication d'Urgence, Localisation, Protocole d'Appel d'Urgence Multi-Sauts, Hors de la Couverture

Résumé :
Pendant les catastrophes à grande échelle, les systèmes de communication d'urgence fiables, réactifs et économes en énergie sont cruciaux. Cette thèse se concentre sur la conception de systèmes de communication d'urgence fiables pour les scénarios de catastrophe dans les zones sans couverture réseau. Les systèmes proposés sont conçus pour fonctionner de manière transparente à travers les couches de liaison de données, de réseau et d'application. Au niveau de la liaison de données, un nouveau schéma de décodage nommé Cyclic Triangular Successive Interference Cancellation (Cyclic T-SIC) est proposé pour améliorer la fiabilité dans les communications D2D assistées par Asynchronous NOMA. De plus, au niveau du réseau, de nouveaux protocoles multi-sauts, à savoir Multi-Hop Emergency caLl Protocol (M-HELP) et 5G Standalone Service (5G-SOS), conformes aux normes 3GPP, sont introduits pour réduire le trafic de contrôle et améliorer la fiabilité de transfert d'informations d'urgence. De plus, un nouvel algorithme de localisation multi-victimes *(MVLA)* est proposé au niveau de l'application pour localiser les dispositifs des victimes pendant les situations d'urgence. Ce schéma utilise les données radio des appels d'urgence multi-sauts assistés par D2D hors bande et applique des méthodes de satisfaction de contraintes pour localiser les victimes de manière progressive. De plus, une architecture de service d'urgence est également proposée comprenant un modèle d'apprentissage automatique optimisé pour localiser les zones de forte densité de population pendant les pandémies. En comparant et en évaluant les méthodes et schémas proposés avec les approches conventionnelles de pointe, des informations précieuses sont obtenues sur la conception de systèmes de communication d'urgence efficaces et optimaux pour les zones avec une couverture réseau limitée.

UBFC UNIVERSITÉ BOURGOGNE FRANCHE-COMTÉ
Université Bourgogne Franche-Comté
32, avenue de l'Observatoire
25000 Besançon, France

ACKNOWLEDGEMENTS

I would like to express my sincere gratitude to several individuals without whom this Ph.D. thesis would not have been possible. First and foremost, I would like to express my sincere appreciation to my supervisors, Prof. Hakim Mabed, Prof. Dushantha Nalin K. Jayakody, and Prof. Philippe Canalda for their guidance, patience, and encouragement throughout my Ph.D. program. Their expertise, knowledge, and support have been instrumental in shaping my research and developing my academic abilities. I am grateful for their mentorship, and I have learned invaluable lessons from their dedication and commitment to research.

Moreover, I would like to thank my parents and siblings for their constant love, support, and encouragement throughout my academic journey. Their unwavering belief in me has been a driving force behind my success, and I am grateful for their sacrifices and unconditional love.

I would also like to extend my heartfelt thanks to my colleagues and friends who have supported me throughout my Ph.D. journey. Their support, encouragement, and camaraderie have been invaluable, and I am grateful for the friendships and memories made.

Finally, I would like to acknowledge the assistance given by two research institutions, Université de Bourgogne Franche-Comté (UBFC) and Sri Lanka Technological Campus (SLTC), for providing financial and technical support towards my research. Their assistance has been critical in enabling me to conduct research and achieve my academic goals.

"Tu n’échoues qu’au moment ou tu arrêtes d’essayer."

-Albert Einstein

CONTENTS

I

Problem and State Of The Art

1

INTRODUCTION

1.1/ MOTIVATION

Recent catastrophes such as the Tsunami of the Indian Ocean in 2004, Hurricane Katrina in 2005, Fukushima disaster in 2011, and Haiti Earthquake in 2010 have demonstrated that a robust networking system is indispensable to protect human lives. In such situations, mobile networks present a more resilient way to transfer urgent information and coordinate the work of rescue teams compared to landline connections [1]. Although it is difficult to prevent natural disasters and pandemics, a proper disaster management scheme allows us to mitigate their effects and improve the impact assessment and response phases [2–4] as depicted in Figure. 1.1.

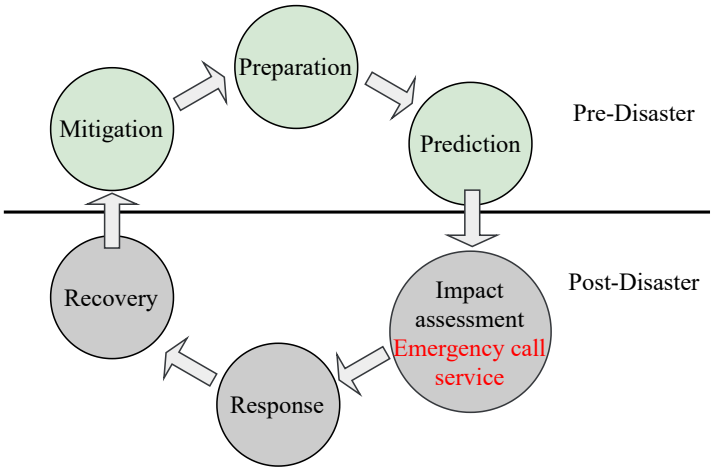

Figure 1.1: The phases of disaster management cycle during pre-disaster and post-disaster stages.

In such situations, the ubiquity of mobile phone devices and wireless emergency communication networks assist in establishing stability before, during, and after crises and managing their impact on the community. However, the user equipment is not owned by the network system itself making the protocol implementation more strict than in private/community networks such as Mobile Ad hoc Network (MANET), and Vehicular Ad hoc network (VANET) systems [5, 6]. In this context, researchers worldwide are taking large strides in developing optimal systems to deal with emergency situations. Moreover,

it is noted that the underpinning concept behind every emergency application includes wireless communication systems.

An appropriate wireless emergency communication system can help individuals with critical information and instant notifications, irrespective of their positions. It helps to respond, recover, and mitigate potential damages. However, achieving such objectives is highly complicated, as the wireless communications systems may lack interoperability with the other communication systems, or fails to support crucial data transfer in a huge emergency situation. Despite the extensive use of modern devices such as smartphones and computers, there is no guarantee that emergency notifications reach the end-users or that emergency calls reach the appropriate services.

Cellular network-assisted emergency services still remain less efficient, even though multiple research works have been done on disaster-resilient Ad Hoc networks [7–9]. The efficiency of a wireless emergency communication network is measured according to its reliability, latency, adaptability to the emergency situation, and its compatibility with the technical standards set by the 3rd Generation Partnership Project (3GPP). The key issues in emergency call services in out-of-coverage can be summarized as follows:

- Lack of reliable links with the network infrastructure
- Limited cellular resources for communication
- Lack of reliable multiple access decoding schemes
- Energy limitations at the device level
- Delays in emergency device call dissemination
- Lack of intelligent adaptive emergency services
- Uncertainty in emergency device localization

Reliable transfer of emergency calls to emergency services can be challenging during disasters especially when the damages impact the cellular network infrastructure. In such cases, the network may entail larger out-of-coverage areas. Moreover, it is important to maintain connectivity among user devices, i.e., potential victims, in such a manner that all the emergency messages get collected reliably as the emergency data is crucial for rescue actions. In this context, Device-to-Device (D2D) technology represents an excellent way to extend cellular network coverage. The scarcity of resources allocated for D2D communication in out of coverage leads to collision among transmissions and hence reliable communication mechanisms are required.

Furthermore, massive D2D networks are in demand due to their key merits namely i) infrastructure-free network, ii) ability to operate with limited resources and iii) ubiquitous connectivity to the end-users. Moreover, the consideration of D2D mechanisms for out-of-coverage communications requires the optimization of two networking layers: the data link layer and the network layer. Concerning the data link layer, Non-Orthogonal Multiple Access (NOMA) schemes are a possible solution to address resource limitation issues.

However, complex decoding procedures can be observed in NOMA-based networks. This complexity is increased under a massive NOMA-assisted D2D network [10,11]. Moreover, it has been shown, [12], that decoding complexity increases in NOMA scheme when the number of interfering users increases. The computational and energy limitation of mobile devices necessitates optimizing the energy efficiency of D2D communications. In this context, it is noted that a reliable and efficient Asynchronous NOMA scheme (A-NOMA) for massive D2D networks is understudied. In addition, the management of the trade-off between the energy consumption of mobile devices and communication reliability in out-of-coverage areas is under-explored [13, 14].

Furthermore, it is important to define the network layer protocols which govern the routing of an emergency call received from another device. Therefore an extended multi-hop routing protocol using a 4/5G enabled D2D is required. The objective of such a protocol is to guarantee that each emergency call reaches the core network without overloading the system with highly redundant messages, which reduces the devices' lifetime and increases interference. The emergency calls routing protocol should be self-adaptive regarding the density of the mobile devices and the number of emergency calls.

In disaster scenarios, accurately locating victims, especially in out-of-coverage areas, is a major challenge. Current localization methods struggle to process data received through multi-hop protocols and with minimal delay. To tackle this problem, efficient, and accurate localization schemes are needed. Hence, developing reliable localization schemes based on data received through multi-hop protocols with minimal delay in the application layer is crucial for effective rescue efforts in out-of-coverage areas.

1.2/ Objectives of the Thesis

This thesis aims to address the challenge of designing optimal emergency communication systems for disaster situations in areas with limited network coverage. The new schemes proposed for improvements in three critical layers of the Open Systems Interconnection (OSI) model: the data link, network, and application layers can be further articulated as follows:

1. A communication scheme is proposed for emergency call forwarding at the data link layer that utilizes A-NOMA, specifically in areas with limited network coverage. The proposed method involves implementing an A-NOMA decoding scheme to improve the reception of reliable information in D2D asynchronous communications. New algorithms are developed to enhance decoding reliability and efficiency, including the use of Triangular Successive Interference Cancellation (T-SIC) techniques. The goal is to optimize network performance for increased energy efficiency and reduced bit error rate. This proposed scheme also seeks to enhance the communication system's secrecy capacity in the presence of jamming users using optimization techniques and its performance is compared to conventional approaches.
2. Network protocols are proposed that comply with 3GPP standards, 5G New Radio (5G-NR), and with a focus on minimizing control traffic at the network layer. The

aim is to investigate emergency services that can be deployed during catastrophic events by proposing a self-adaptive, distributed mechanism that ensures connectivity and enhances the reliability of emergency information transfer. This includes proposing an optimized Multi-Hop Emergency call Protocol (M-HELP) service in 5G mobile networks. Additionally, an adaptive emergency call protocol named 5G Standalone Service (5G-SOS) is presented. The parameters of the 5G-SOS protocol are designed to be adaptable, taking into account observed neighborhood emergency call congestion data and prior knowledge of local network congestion limits.

3. Schemes for determining the location of victim devices during emergency situations are proposed at the application layer. First, a new localization procedure that utilizes the radio measurements received from outband D2D-assisted multi-hop emergency calls and applies constraint satisfaction methods is proposed. This proposed approach is compared against a conventional localization method to evaluate its performance.

4. An optimized service architecture is presented to enhance the detection of population clusters during a pandemic like Covid-19 and reduce the computational costs involved in local D2D networks.

1.3/ Structure of the Thesis

This dissertation is divided into two main sections and is organized as follows:

- **Section 1: Problem and State of the Art**: This section provides an in-depth overview of the previous research and existing work related to out-of-coverage D2D networks, multi-hop protocols, multiple access schemes, asynchronous non-orthogonal multiple access, localization, and optimization techniques.
- **Section 2: Contributions** This section presents the research contributions of the thesis in each chapter:
  - Chapter 3: This chapter presents several new developments in the field of signal decoding for communication systems that experience co-channel interference and data rate constraints. The first contribution is the creation of a new algorithm that can quickly and effectively identify the optimal combination of data symbols from a superimposed signal. The second contribution is the introduction of a new Cyclic T-SIC scheme, which improves the efficiency and accuracy of signal decoding when compared to existing methods. The third contribution is research on how to balance the trade-off between data accuracy and energy efficiency when using the proposed Cyclic T-SIC scheme. The fourth contribution is the demonstration that the new method is less computationally complex and faster than previous techniques. Additionally, it presents a binary optimization problem that is proposed to enhance the secrecy capacity of a specific type of communication system while facing jamming users

and compare the proposed optimized scheme with the conventional secrecy capacity values.

– Chapter 4: The goal of this chapter is to explore the emergency services that can be deployed during catastrophic and unpredictable events. The proposed solution is a self-adapting, distributed mechanism that maintains connectivity for users who are out of coverage and potential victims when part of the network infrastructure is damaged. To improve the reliability of emergency information transfer, an optimized multi-hop emergency call service in 5G mobile networks is suggested, which enables the autonomous transfer of emergency calls to the core network after a call has been made. Moreover, this chapter presents an adaptive emergency call protocol named 5G-SOS that is compatible with 3GPP and 5G New Radio (5G-NR). The protocol is designed to forward emergency calls autonomously and reliably to the network infrastructure during massive network failures using multi-hop D2D relaying across the sidelink channel, with zero additional control traffic, fully distributed, and adaptive to local emergency call congestion. It utilizes distributed learning and adapts its parameters according to observed neighborhood emergency call congestion data and prior knowledge of local network congestion limits. Algorithms are proposed for user devices to follow the 5G-SOS protocol, and it is shown to have significant performance improvements compared to existing protocols such as M-HELP and FINDER in terms of transmission success rate, network traffic control, and energy management during emergency scenarios.

– Chapter 5: The main contributions of this chapter are proposing a service architecture that allows users to access the localization of population clusters, providing a new method to improve population cluster detection and decrease computational cost in a local D2D network by adopting the Maximum Volume Inscribed Ellipse (MVIE) in a convex hull principle in unsupervised learning, and comparing the proposed method with two baseline clustering methods, K-means and Gaussian Mixture Model (GMM), in network regions with different population sizes such as remote, rural, suburban, and urban.

– Chapter 6: This chapter presents a new localization procedure designed for emergency situations, where the focus is on obtaining data for localization using only emergency calls received and without generating additional control traffic. The proposed scheme utilizes outband D2D-assisted multi-hop protocols and relies on radio measurement data from emergency calls sent by victims or relayed by other phones. The scheme assigns a priority value to each device that participated in disseminating emergency calls to the core network, which is used to organize received emergency data and localize source/relay devices in order of priority. The proposed localization solution uses a dynamic constraint satisfaction method to estimate the localization of target victim devices against the progression in time, and a constraint satisfaction-based algorithm for multiple victims' localization using cumulative path information where the absolute positions of the relay devices are unknown is proposed. The proposed algorithm extracts a combination of localization data such as GPS, AoA,

RSSI, and ToA from the received emergency call, and a hybrid localization technique consisting of all such measurements is utilized for localizing each device. The performance of the proposed algorithm is shown to be significant when compared with a competitive existing algorithm named RSSI-Montecarlo boxed localization in terms of localization error, and end-to-end delay under extreme emergency scenarios.

– Chapter 7: This chapter presents the conclusion and future Works of the thesis.

1.4/ Publications Arising from the Thesis

The list of publications arising from the thesis is summarized as follows.

1.4.1/ International Peer Reviewed Journal Articles

1. V. Basnayake, D. N. K. Jayakody, V. Sharma, N. Sharma, P. Muthuchidambaranathan, and H. Mabed, “A New Green Prospective of Non-orthogonal Multiple Access (NOMA) for 5G,” *Information*, vol. 11, no. 2, p. 89, Feb. 2020, doi: 10.3390/info11020089 (Q2).

2. V. Basnayake, H. Mabed, D. N. K. Jayakody, P. Canalda, and M. Beko, “Adaptive Emergency Call Service for Disaster Management,” *Journal of Sensor and Actuator Networks*, vol. 11, no. 4, p. 83, Nov. 2022, doi: 10.3390/jsan11040083 (Q1).

3. V. Basnayake, D. N. K. Jayakody, H. Mabed, A. Kumar and T. D. Ponnimbaduge Perera, "M-Ary QAM Asynchronous-NOMA D2D Network With Cyclic Triangular-SIC Decoding Scheme," *IEEE Access*, vol. 11, pp. 6045-6059, 2023, doi: 10.1109/ACCESS.2023.3236966 (Q1).

4. V. Basnayake, H. Mabed, P. Canalda, and D. N. K. Jayakody, ’D2D Communications for Victims Localization in Post-Disaster Situation’, *IEEE Transactions in Mobile Computing*, (Minor Revision).

1.4.2/ International Peer Reviewed Conference Papers

1. V. Basnayake, H. Mabed, P. Canalda, and D. N. K. Jayakody, "M-HELP - Multi-Hop Emergency Call Protocol in 5G," *2020 IEEE 19th International Symposium on Network Computing and Applications (NCA)*, 2020, pp. 1-8, doi: 10.1109/NCA51143.2020.9306713.

2. V. Basnayake, H. Mabed, P. Canalda and D. N. K. Jayakody, "Enhanced Convex Hull based Clustering for High Population Density Avoidance under D2D Enabled Network," *2021 IEEE 94th Vehicular Technology Conference (VTC2021-Fall)*, 2021, pp. 1-7, doi: 10.1109/VTC2021-Fall52928.2021.9625054.

3. V. Basnayake, Ambrish Kumar, D. N. K. Jayakody, "Optimization of Secure Emergency Call Services in Asynchronous-NOMA D2D Network", *International Research Conference 2022 (IRC 2022)*, Sri Lanka Technological Campus, Sri Lanka, September 2022. The paper was awarded First Runner-Up in the Best Paper category.

4. V. Basnayake, H. Mabed, P. Canalda, and D. N. K. Jayakody, "Post-Disaster Victim Localization via D2D Communications," *Track 4: Applications, Platforms, and Business, IEEE International Symposium on Personal, Indoor and Mobile Radio Communications*, Toronto, Canada, September 2023.

2

BACKGROUND

This Chapter provides information about the technological context of the thesis and fundamental techniques and protocols proposed in the field of D2D communication. It will cover the fundamental protocols and methods used in D2D communication, as well as multi-hop D2D protocols and techniques for determining the location of mobile devices.

2.1/ MOBILE CELLULAR NETWORKS

Mobile cellular networks play a vital role in modern communications and are used by billions of people around the world to access the Internet and communicate with each other. The demand for mobile communication has risen exponentially due to the availability of affordable mobile devices, the popularity of internet-based services, and the development of new technologies. Moreover, mobile devices use a variety of technologies, such as cellular radio, satellite, and Wi-Fi, to provide coverage over a wide area and enable mobile devices to connect to the Internet from anywhere.

2.1.1/ HISTORY

Mobile cellular networks have evolved over several different generations including 1G, 2G, 3G, 4G, and 5G. Each generation represents a significant advance in the capabilities and performance of the network, with increasing data rates, better latency, and capacity. The history of mobile cellular networks dates back to the 1950s when the first analog cellular networks were developed. These early networks used a system called frequency division multiple access (FDMA), in which each cell used a different frequency band to transmit and receive signals. In the 1980s, the second generation (2G) of mobile cellular networks introduced digital signaling and the use of time division multiple access (TDMA) to allow multiple users to share the same frequency band. In the 1990s, the third generation (3G) of mobile cellular networks was developed. 3G introduced high-speed data services and the use of code division multiple access (CDMA) to allow multiple users to share the same frequency band. 3G networks also introduced the concept of multimedia services, such as video calls and Internet access.

The fourth generation (4G) of mobile cellular networks was developed in the early 2000s,

introducing even higher data rates and using multiple-input multiple-output (MIMO) technology to improve the capacity and performance of the network. 4G networks also introduced the concept of all-IP networks, which allowed all types of communication to be transmitted over the same network. The fifth generation (5G) of mobile cellular networks is currently being developed, with the goal of providing even higher data rates, lower latency, and improved capacity and coverage. 5G networks are expected to enable a wide range of new applications and services, such as virtual reality [15], the Internet of Things [16], and software-defined networking [17].

2.1.2/ ARCHITECTURE

The architecture of mobile cellular networks is designed to allow mobile devices, such as wireless phones, smartphones, and tablets, to connect to the radio network in order to communicate with each other or access other devices or services over the Internet. A mobile cellular network consists of a set of hierarchical cells (macro-cell, micro-cell, pico-cell, femtocell), where each cell represents a base station that covers a specific geographic area. The basic network architecture is shown in Figure. 2.1.

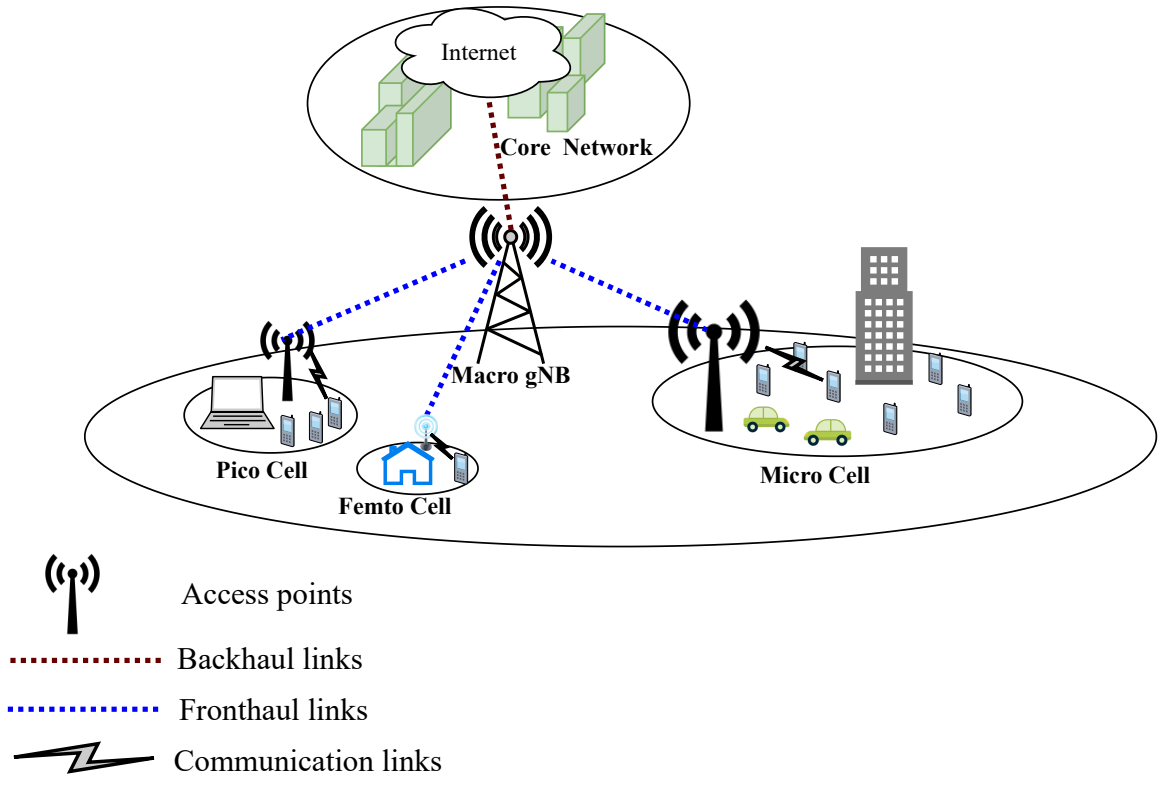

Figure 2.1: Hierarchy of cells and the connection link between devices and e-UTRAN that is connected to core network

The base station in 5G is referred to as gNodeB (gNB) and is responsible for connecting mobile devices to the core network in both the downlink and uplink directions. The core network, also called the backbone network, is connected to the public internet through

high-capacity links such as fiber optic cables or satellite connections that connect major Internet Service Providers (ISPs). These ISPs communicate with each other using the Border Gateway Protocol (BGP), which routes data packets and finds the most efficient path for the data to travel from source to destination. The core network, consisting of high-capacity links and routers, serves as the backbone of the internet and enables efficient communication between different parts of the internet. Traditionally, communication between mobile devices was done through the core network infrastructure. However, the idea of directly linking mobile devices using sidelink channels was introduced in the 4G standardization process.

2.1.3/ Cellular network for Public Safety Communications

Wireless communication-assisted public safety services are more robust during catastrophes since the wired connections may get damaged when the scale of the disaster is large. In these circumstances, the ubiquity of mobile phone devices and radio access infrastructure make mobile communication the default method of communication and can make positive contributions before, during, and after the disaster. Besides, the familiarity of people with mobile applications (SMS, voice call, chat) increases the frequency and the efficiency of their usage [1, 18]. On top of that, one of the main goals of the beyond 5G (B5G) and 6G networks is to facilitate reliable communications during emergencies and natural disasters [19]. Many applications and protocols [20, 21] are proposed for public safety services based on cellular network technologies [22]. To that end, the architecture of mobile cellular networks can assist emergency response in several ways:

- Wide coverage: Mobile cellular networks are designed to provide coverage over a wide area, which allows emergency devices to communicate with each other and with other devices from any location. This is particularly important in rural or remote areas, where traditional communication infrastructure may not be available. Furthermore, public safety communications are applied mainly to extend existing network coverage to high-cost and unreachable locations.
- High-speed and low latency communications: The improvement of communications data-rate and latency is one of the main objectives of mobile network evolution. These two characteristics allow emergency responders to access important, various, and voluminous information
- Reliable connectivity: Mobile cellular networks are designed to be reliable, with multiple levels of redundancy ensured by both the cells' hierarchy (macro/micro/pico/femto) and cells' overlapping. This allows emergency responders to rely on the network when localized troubles occur.
- Advanced services: Unlike the previous cellular network generations (1G/2G), new mobile communication protocols are not only dedicated to voice communications. Since the 3rd generation of mobile networks, a wide range of advanced telecommunication services are supported, such as video calls, multimedia data transfer,

location tracking, gaming, and data sharing. These new communication modes are very useful for emergency management process. For example, video calls can be used for remote consultation with medical experts, while location tracking can be used to track the movement of emergency responders and other assets.

Thus, the cellular network is the optimal tool for supporting emergency call services. The challenge lies in maintaining the cellular network as a reliable medium for emergency calls even in the event of a disaster that affects the network. Moreover, the third-generation partnership project (3GPP) is an organization that proposes standards and protocols for cellular network technologies. Thereby, is it useful to propose schemes that are 3GPP compatible such that those schemes can be implemented easily in industry and academic domains.

2.2/ Overview of 3GPP D2D Communications

Two main approaches were proposed by the 3GPP standard concerning proximity services: extending the base stations coverage by using the D2D protocols [23,24], and supporting the group calling communication, also called, Push To Talk service (PTT) [25,26].

- *PTT communication* is described in TS 22.179 of 3GPP standard [27] and [28]. In push-to-talk protocol, the user requests permission to transmit at the touch of a button, then all subscribers of the PTT service receive a call. The user with the higher priority overrides the current talker to transfer its emergency message and speaking time is limited to prevent resource starvation.

- *Device to Device (D2D) communication* is a technology that enables direct communication between mobile devices, without passing through the network infrastructure. D2D enhances service quality in densely populated networks by reducing the radio link distances. It was first introduced in the 3GPP release 12 [29, 30], and allows the use of short-range radio technologies such as WiFi, Bluetooth, Zigbee, LoRa, Thread, EnOcean, and SigFox to communicate [31–34].

Moreover, the use of D2D mode in Proximity Services (ProSe) [35, 36] is proposed as one of the key components in providing mission-critical services. The evolution of such specifications with their respective 3GPP release is illustrated in Figure 2.2. Examples of mission-critical services that can benefit from D2D communication in LTE 3GPP include public safety, industrial automation, and healthcare. Moreover, under public safety, D2D communication can be used for secure, real-time communication between devices in emergency situations. In LTE 3GPP, D2D communication is supported through various features and technologies, including ProSe, Multi-point Relay (MPR), and direct mode. These features provide a robust and flexible infrastructure for supporting D2D communication and enabling mission-critical services. Consequently, many applications were proposed [25,37,38] to use proximity services protocols for public safety services [39].

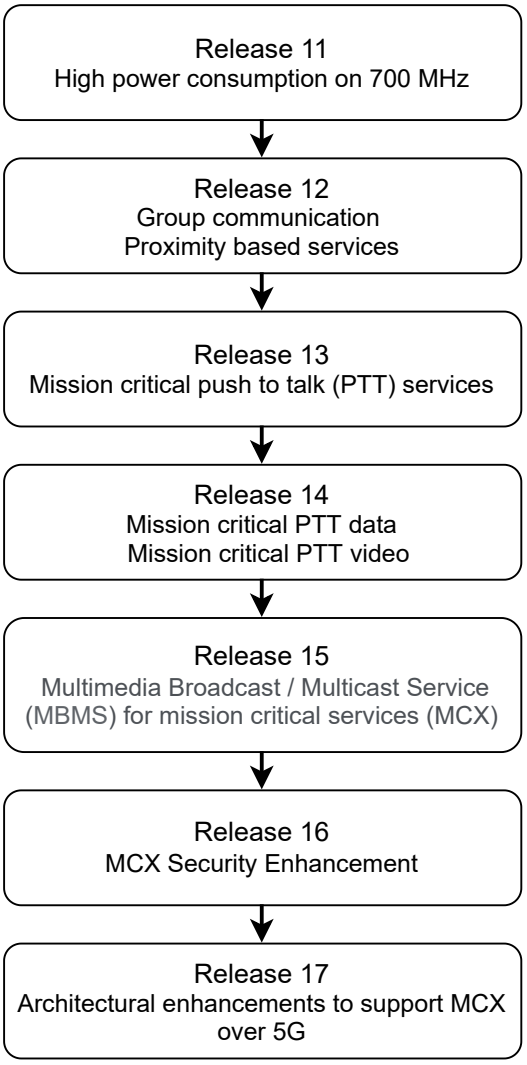

Figure 2.2: Evolution of the 3GPP specifications for missions critical/emergency scenarios using proximity-based services under each release from 11–17.

2.2.1/ 3GPP D2D FUNCTIONALITIES

In order to support LTE D2D ProSe, 3GPP defined a new direct link mode between UEs named Sidelink [40] at the access stratum layers. ProSe-enabled UEs can use Sidelink channels to exchange information when they are in close proximity. Three LTE D2D functionalities are defined under ProSe: direct communication, direct discovery, and synchronization [41]. The direct communication functionality allows the UEs to establish a communication link between them without the need of routing the data via the gNBs. The direct discovery functionality allows to announce and detect useful information provided by the UEs in proximity without the need of establishing a communication link. Finally, the synchronization functionality provides the mechanisms needed by the UEs in proximity to follow the same synchronization reference and suitably align in time and frequency.

2.2.2/ D2D Operating Scenarios

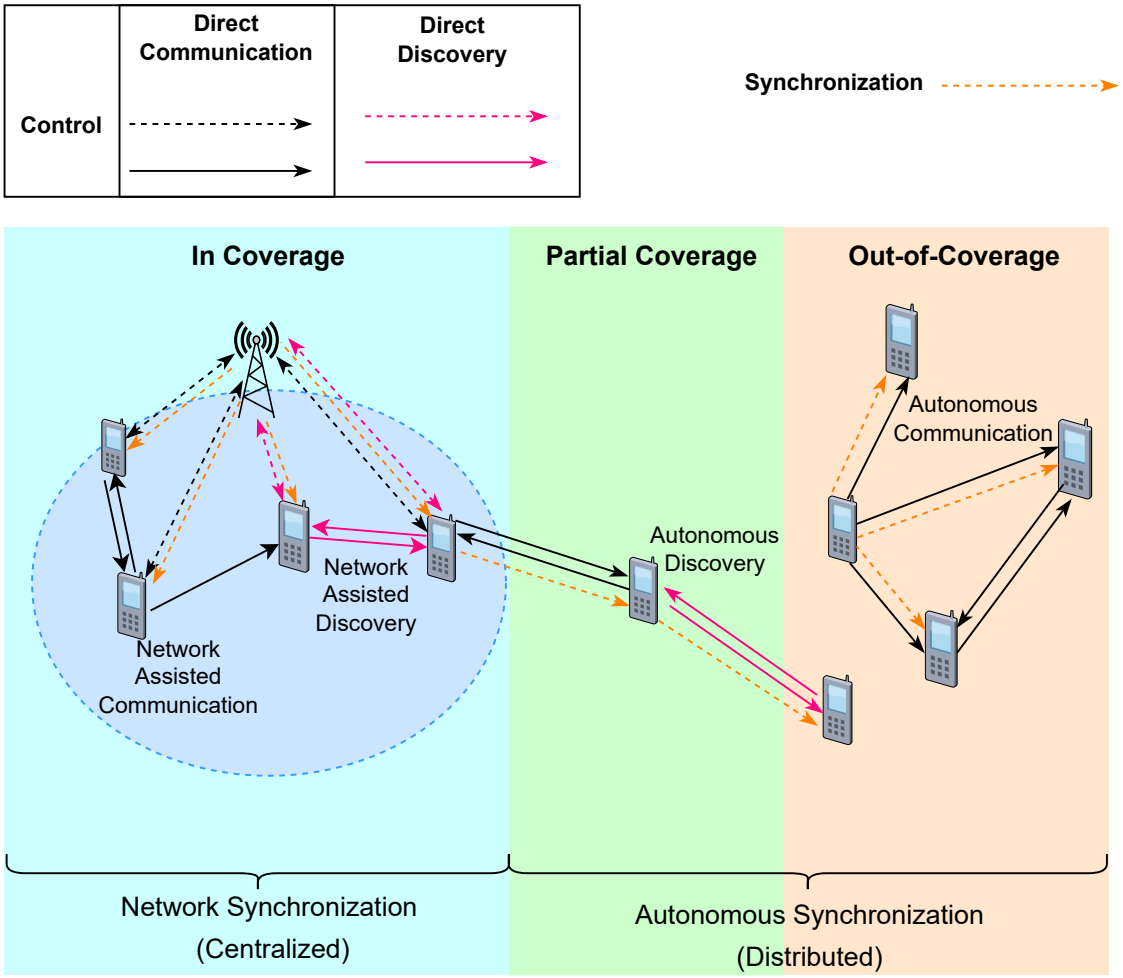

Figure 2.3: Overview of D2D Operating Scenarios and Functionalities

The LTE D2D functionalities can operate regardless of the network status of the UEs. Thus, three scenarios were identified by 3GPP: in-coverage, partial coverage, and out-of-coverage, as illustrated in Figure 2.5. When the UEs are in-coverage, the functionalities are network assisted, i.e., the UEs use the configuration and control information provided dynamically by the network, as well as preconfigured parameters. When the UEs are out-of-coverage, they rely on preconfigured parameters, enabling autonomous operations. Partial coverage is a hybrid between the other two scenarios, in which UEs within network coverage can provide system information to out-of-coverage UEs.

D2D communication over Sidelink is performed over periodically repeating periods in the time domain [42]. Each Sidelink period is composed of two channels spaced out in time, the Physical Sidelink Control Channel (PSCCH) and the Physical Sidelink Shared Channel (PSSCH), as depicted in Figure 2.4. Each channel is defined by a resource pool, i.e., a combination of certain Resource Blocks (RBs) in the frequency domain, and certain subframes in the time domain [42]. A detailed resource pool analysis for the PSCCH and its resource scheduling procedures can be found in [43]. The PSCCH is used by ProSe-

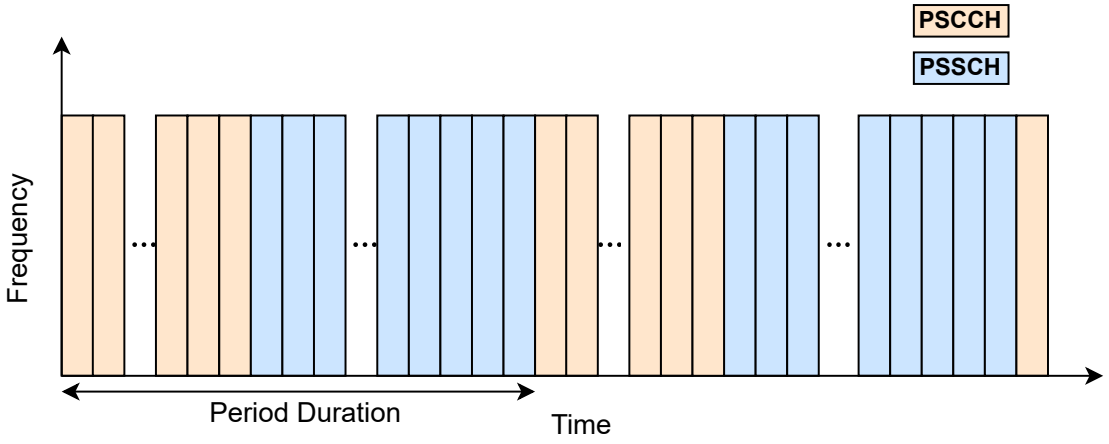

Figure 2.4: Sidelink Communication Period

enabled UEs to send a Sidelink Control Information (SCI) message, to indicate to who this message is addressed, how and where the data will be transmitted, i.e., the group destination ID, the Modulation and Coding Scheme (MCS), and the PSSCH resource assignment in time and frequency, among other parameters. Each UE can be associated with one or more group IDs, and must scan through the control channel time duration to detect if another UE is going to transmit something addressed to their group. Upon successful reception of an SCI message, pertaining UEs can then proceed to tune to the corresponding resources in the PSSCH.

LTE Release 12 introduced two resource allocation modes for D2D communication: Mode 1 and Mode 2, The base station, eNodeB (eNB) or gNodeB (gNB), configures in-coverage UEs to operate on either mode. However, out-of-coverage UEs can operate only in Mode 2. In Mode 1, D2D communications are assisted by the base station, i.e., resource scheduling is performed dynamically by the eNB/gNB. In Mode 2, UEs manage resource scheduling autonomously relying on preconfigured settings, and both, PSCCH and PSSCH, resources are selected at random from their respective resource pools.

2.3/ MULTI-HOP D2D PROTOCOLS

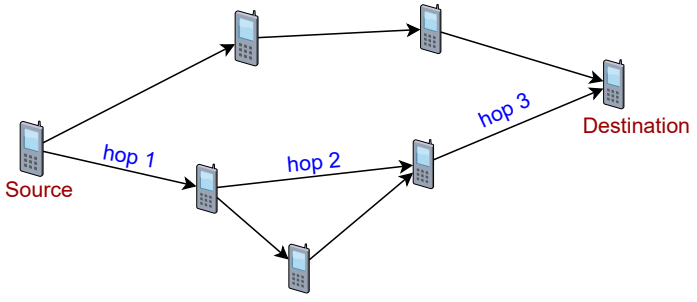

Figure 2.5: Multi-Hop Communications

It is noted that 3GPP standards do not specify how a UE with out-coverage can transmit data to remote devices or services. However, multi-hop D2D communication consists of linking the out-coverage UEs to the core networks using a set of other UEs that relay the received packets to the destination (a base station). Therefore, multi-hop D2D communications can extend the coverage of the cellular network and improve the UEs' connectivity. Typically, D2D-assisted multi-hop communications have been proposed in research works to enhance the reliability, security, and latency of the communication [44–46]. Indeed, transmission over multiple short links might require less transmission power and energy than over long links. Multi-hop D2D communication is also studied for improving cellular network resilience against failure situations [47, 48]. Also, they enable higher data rates resulting in higher throughput and more efficient use of the wireless medium. Multi-hop wireless networks avoid the wide deployment of cables and can be deployed in a cost-efficient way. In the case of dense multi-hop networks, multiple communication paths to the end destination become available which increases the robustness of the network.

2.4/ Localization in Wireless Networks

Smartphones have greatly improved communication, navigation, and positioning due to the variety of technologies such as Global Navigation Satellite Systems (GNSS) [49–52], Multi-Input and Multiple-Output (MIMO) antennas [53,54], and D2D communications [55]. These technologies are particularly useful for localization tasks, especially during disaster scenarios where it is important to locate victim devices with high accuracy and minimal delay in order to rescue them promptly [56].

2.4.1/ Homogeneous and Hybrid Localization

There are two main categories of localization measurement based on the number of measurement used: homogeneous and hybrid [57]. The homogeneous localization approach refers to positioning using one type of measurement such as Global Positioning System (GPS), Received Signal Strength Indicator (RSSI) [58], Time of Arrival (ToA) [59], or Angle of Arrival (AoA) [60]. On the other hand, in hybrid localization, a combination of different types of measurements is used to support a localization algorithm. Such hybrid localization approaches are used to improve the overall performance or to support an algorithm that cannot be applied standalone given the lack of signal measurements [61,62]. With the increasing demand for high-accuracy positioning, hybrid signal-based localization is gaining more attention [63]. Experimental analysis in [55, 64] shows that hybrid localization produces a better localization accuracy compared to homogeneous localization. Table. 2.1 presents the accuracy obtained from using homogeneous localization approaches.

Moreover, in classical localization, homogeneous or hybrid localization measurement are used under a fully operational radio network infrastructure, where devices' signals received by the base station are combined to extract the positions of the devices. However,

Table 2.1: Confidence intervals of different localization methods

Measurement type	**Environment**	**Measurement error (min, max)**	**Citation**
GPS	Outdoor (NLOS)	(5 - 99.7) m	[65]
GPS	Indoor Building (1-2 floors) (NLOS)	(1 - 2) m	[66]
GPS	Indoor Building (> 2 floors) (NLOS)	(2 - 21.7) m	[66]
RSSI	NLOS	(1.5 - 5) m	[67, 68]
ToA	NLOS	(1 - 5.23) m	[69]
AoA	NLOS	$(\pi/18 - \pi/3)$ rad	[69, 70]

under a large disaster situation impacting the network infrastructure, the device position is extracted using the ad-hoc D2D signals received by neighbor devices. Furthermore, Figure 5.1 shows the difference between these classical and ad-hoc localization approaches.

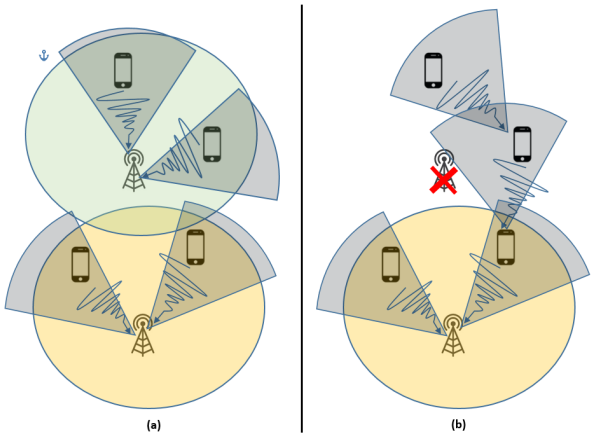

Figure 2.6: Comparison between (a) classical localization approach under operational network and (b) our localization approach under dysfunctional network. In the classical approach, the localization system uses the signals received by the base stations from the devices. In our case, the localization system uses mainly signals received by the devices from other devices. The sectors in the figure refer to the signal AoA estimation and the wavy arrows to the signal quality measured by the RSSI.

2.4.2/ GPS ASSISTED LOCALIZATION

GPS-assisted localization is a method of determining the location of a device using satellite signals received from a network of satellites orbiting the earth. By measuring the time delay between the transmission and reception of the satellite signals, a device can estimate the distance from each satellite and determine its location using trilateration [71]. The accuracy of the GPS location estimate can vary on several factors such as the number of satellites in view, the strength of the satellite signals, and the presence of interference or obstructions. Nevertheless, GPS offers a high localization accuracy [72] and due to its simplicity, and availability in most phones, i.e., smart and feature phones [73].

However, a minimum of four satellites in view of the user device is required to obtain a high level of accuracy. Further, GPS has several disadvantages such as consuming too much power and requiring the line of sight to satellites [55].

2.4.3/ AoA assisted Localization

Table 2.2: Specifications of commercially available smartphones with MIMO

Smartphone	**MIMO Model**	**Capacity**	**Price (eur)**	**Network**
iPhone SE	2×2	64 - 256GB	399 - 600	LTE
iPhone XR	2×2	64 - 512GB	499 - 878	LTE
iPhone XS and XS max	4×4	64 - 512 GB	199 - 400	LTE
iPhone 12	4×4	64 - 256 GB	678 - 799	LTE/5G
Samsung's Galaxy S9 and S9+	4×4	64 - 256 GB	350 - 575	LTE
Samsung's Galaxy 21	4×4	64 - 256 GB	859 - 1149	LTE/5G
Google's Pixel 3 and Pixel 3 XL	4×4	64 - 128 GB	489 - 815	LTE
Google's Pixel 5	4×4	128 GB	629 - 700	LTE/5G

AoA-assisted localization is a method of determining the location of a device using the angles at which signals from multiple transmitters or reference points arrive at the device. Furthermore, AoA localization is possible even if the device is not in the direct line of sight of the transmitters. Furthermore, in order to implement AoA-assisted localization, the device must be equipped with suitable sensors or antenna arrays, i.e., MIMO antennas, that are capable of measuring the AoA. As of now MIMO antennas are also present on modern smartphones and Table. 2.2 gives some examples of MIMO enabled smartphones and their characteristics [74]. For instance, Martin Schüssel [70] shows that the AoA technique estimates the transmitter direction with an error of about 60^0 using a Nexus 5X smartphone equipped with a 2×2 MIMO antennas. The accuracy of AoA-assisted localization can be affected by various factors such as the accuracy of the AoA measurement, the presence of obstacles or interference, and the number of transmitters used.

2.4.4/ RSSI assisted Localization

RSSI-assisted localization is a method that determines the position of a device using the strength of wireless signals received from multiple reference points or transmitters [75]. The technique involves measuring the RSSI of the signals and then triangulating the position of the device using techniques such as trilateration or multilateration [76]. RSSI-assisted localization is less complex and cost-effective compared to other techniques because it does not require synchronization between the transmitter and receiver [59, 77]. It is also useful because it can provide quality indicators, such as signal-to-interference-noise ratio (SINR) [78] and channel quality indicator (CQI), up to a distance of 75 km from the reference point [79, 80]. The RSSI value is determined based on an empirical propagation model and is used to estimate the distance from the device to the transmitter [59, 81]. If the location of the transmitters is known, the location of the receiver can

be determined using the RSSI value and other factors such as the nominal transmission signal power of a cellular device, the reference distance, and the path loss exponent. RSSI-assisted distance estimation between the transmitter and the receiver, d, is mathematically defined as:

$$d = d_0 10^{\frac{\mathcal{P}_0 - \text{RSSI}}{10 n_p}}, \tag{2.1}$$

where $RSSI$ and P_0, n_p are respectively, the measured RSSI power, the nominal transmission signal power of a cellular device received at a reference distance d_0, and the path loss exponent. The d_0 is usually taken as 1 km for a macro cell and 1 m to 10 m for a micro cell. and n_p is determined based on the environment [82].

2.4.5/ ToA assisted Localization

ToA-assisted localization is a technique used in wireless communication systems to estimate the location of a device based on the time it takes for a signal to travel from the transmitter to the receiver. The ToA-assisted distance estimation can be defined as:

$$d = \frac{ToA \times v}{2}, \tag{2.2}$$

where ToA and v are respectively the time of arrival of the signal at the receiver, measured in seconds, and the speed of light in the medium through which the signal is transmitted, typically measured in meters per second. The distance between the transmitter and receiver, d, is determined by the ToA and v. In practice, the accuracy of ToA-assisted localization may be affected by various factors, such as the clock's synchronization between the transmitter and the receiver, the presence of obstacles or reflections in the environment, and the presence of multipath fading. As a result, ToA-assisted localization may not be as accurate as other techniques, such as AoA or received signal strength (RSS) in out-of-coverage scenarios. The need for synchronization between the transmitter and the receiver makes that ToA-assisted localization is mostly used when the device is under gNB coverage because the gNB is able to maintain precise synchronization with the in-coverage devices.

2.5/ Non-Orthogonal Multiple Access Schemes for Massive networks

Providing reliable connectivity for massive networks is required during network connection failures which can occur during large-scale catastrophes. The forthcoming beyond-5G/6G network is expected to provide reliable, error-free, and energy-efficient services with ubiquitous connectivity [13,83,84]. In this context, widely used 5G Orthogonal Multiple Access (OMA) schemes such as Orthogonal Frequency Division Multiple Access (OFDMA) [85] and CDMA [86] can support a large number of devices by utilizing the existing network resources effectively. Nevertheless, in such OMA schemes, the number of sub-carriers within the bandwidth is limited, and hence, supporting a large number of devices is a

major challenge. As a solution, NOMA schemes are proposed in the literature.

2.5.1/ An Overview of NOMA

NOMA schemes are shown to improve spectral efficiency by allowing users to access the same resource blocks (RBs) simultaneously [83, 87]. In the NOMA scheme, multiple users share the same time-frequency resources and transmit their data simultaneously. In a NOMA system, the transmitter uses superposition coding to combine the data streams of multiple users into a single signal, which is then transmitted over the same frequency band. The receiver uses successive interference cancellation (SIC) to separate the data streams and decode the individual messages. There are several different types of NOMA schemes, including power-domain NOMA, code-domain NOMA, and hybrid NOMA. Each of these schemes uses different techniques to combine and separate the data streams of multiple users, and they may be suitable for different types of communication systems.

Overall, NOMA is a promising technology for improving the spectral efficiency of wireless communication systems and enabling more users to connect to the network at the same time. It is being actively researched and developed for use in a variety of applications, including 5G and beyond. Also, NOMA scheme is included in 3GPP as a promising multiple access scheme for B5G/6G [88].

In power-domain NOMA, the superposition coding of multiple users' signals is done over the same subcarrier with different power levels that enables the receiver to decode the signal by using the SIC technique [89, 90]. At the receiver, the SIC treatment is applied to decode the data of the user having the strongest channel conditions up to the last user in descending order of Signal to Noise Ratios (SNRs). Once the strongest signal is directly decoded, the detected data is passed through to an iterative SIC algorithm. Next, the strongest signal is reconstructed based on the prior knowledge of Channel State Information (CSI) and the modulation scheme used for transmission. Finally, the reconstructed signal is subtracted from the received superimposed symbol to reduce its interference and increase accuracy in decoding the rest of the user signals.

2.5.2/ Interference Mitigation and Cancellation Techniques

Mitigating interference is one of the major challenges in NOMA and specifically in massive networks. In [91] a method of minimizing interference between individual cells using a coordinated approach between the cells and improving user throughput is explained. In addition, interference cancellation using practical SIC techniques are addressed in [92]. In general, both conventional SIC and asynchronous SIC can be used in NOMA systems to improve the performance of the receiver by reducing the effect of interference from multiple transmitters. However, asynchronous SIC may be more flexible and adaptable, as it can adjust to the changing interference environment in real-time, whereas conventional SIC relies on a predetermined order of processing the received signals. Hence, conventional SIC decoding is shown to be less reliable in decoding NOMA signals when there is an asynchrony between received user signals [87–90, 93–96]. [87–90, 93–96].

2.5.3/ ASYNCHRONOUS-NOMA

Under realistic channel conditions, a synchronous NOMA scheme is impractical in the uplink and D2D communications. As a consequence, NOMA signals arrive at the receiving terminal with varying time offsets [97]. Thereby, in [98], an A-NOMA scheme has been proposed taking into account the interference induced by co-channel users' overlapping symbols to the desired user's data symbols at the receiver terminal. Recently, in [98], an iterative signal processing based T-SIC technique has been proposed to decode A-NOMA signals received at a user terminal. Under the reception of A-NOMA signals T-SIC decoding technique has provided significant Bit Error Rate (BER) performance improvement compared to conventional SIC [98].

2.5.3.1/ CONVENTIONAL SIC DECODING

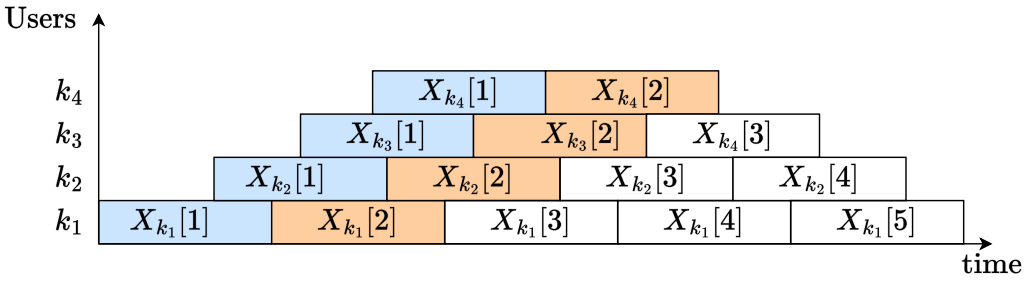

Figure 2.7: Conventional SIC decoding process

When the conventional SIC scheme is used to decode an A-NOMA signal, the receiver processes the received signals in a predetermined order, based on the strength of the signals. To decode the asynchronous NOMA signal, the receiver first processes the received signal symbol-by-symbol, starting with the strongest signal. The receiver then moves on to the next strongest signal and uses the predetermined order of symbols to decode each of its data. The conventional SIC decoding scheme does not take into account the interference from misaligned symbols, instead it only considers the data symbols which are in alignment with the desired symbol for SIC procedure. In this case, interference from all the overlapping symbols is not considered and hence the existing interference is neglected. Moreover, the decoding process of conventional SIC is depicted in Figure 2.7. In contrast, the decoding procedure in an A-NOMA system using an asynchronous SIC scheme involves processing the received signal symbol-by-symbol in and cancelling out the interference caused by the stronger signals at each symbol, in order to improve the performance of the receiver and accurately decode the data of all of the users.

2.5.3.2/ CONVENTIONAL TRIANGULAR-SIC (CONV T-SIC) DECODING

The added interference due to asynchrony need to be addressed and hence the T-SIC procedure proposed in [98] is detailed as follows. The T-SIC decoding scheme [98] is applicable at the receiver terminal for a communication system containing $k \in K$ transmitters

as shown in Figure 2.8. The T-SIC decoding procedure is followed once an asynchronous superimposed signal with misaligned data symbols is received at R_X. First, an Interference Cancellation (IC) triangle is constructed by exploiting the triangular pattern of data symbols detected as illustrated in Figure 2.8. The weakest symbol received out of such data symbols is added to the IC triangle as the last symbol to be detected. Next, the symbols that overlap with the weakest user's symbol are added to the IC triangle. Then, all the symbols that overlaps the second weakest users' symbols are included to the IC triangle. This procedure is repeated until the strongest users' symbols are entered to the IC triangle.

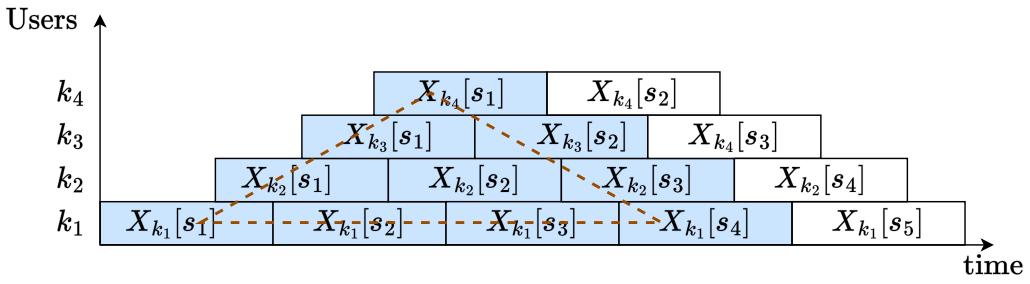

Figure 2.8: Asynchronous T-SIC decoding process

Once such an IC triangle is constructed for n number of transmissions received from k_1 to k_n users, the first symbol of the strongest user, k_1, is decoded. Next the consecutive symbols of k_1 are decoded. Afterwards, the first symbol of the second strongest user, k_2 is decoded by subtraction of prior estimated symbols of k_1. Then, the second symbol of the k_2 user is decoded by subtracting the prior estimated symbols belonging to k_1 and k_2. Next, the first symbol of k_3 user is decoded by subtracting all the prior estimated symbols that belong to both k_1, k_2 from the received signal Y. Similarly, the rest of the symbols of k_3, up to k_n users are decoded by subtracting the prior symbols estimated.

Moreover, the conventional T-SIC [98] is repeated iteratively between users for a fixed number of times, $N_{\text{T-SIC}}$. Specifically, the conventional T-SIC not only utilizes strong user signals to decode weak user signals but also uses weak user signals to decode strong user signals iteratively. In the Conv T-SIC scheme [98], the $N_{T_{SIC}}$ is within the range $1 \leq N_{T_{SIC}} \leq N_{T_{SIC\text{max}}}$, where it is used primarily to improve the T-SIC accuracy in terms of BER. The basis of the T-SIC decoding technique lies in constructing an IC triangle to decode each user symbol while considering the interference from all neighboring users to the desired users' symbol. Due to the triangular pattern used for decoding symbols in T-SIC, the interference caused by multiple asynchronous data symbols on each desired user's symbols is considered to enhance the symbol detection and residual interference cancellation. Further, the proposed scheme uses the latest prior estimates of decoded symbols to define the SINR and thereby the BER of each user.

BER Analysis of T-SIC decoding:

The average theoretical BER of k^*th user data, P_{bit,k^*}, in asynchronous transmissions can be formulated in [98] as follows. First, by considering the latest detected

symbols, the SINR of the sth symbol of the k^*th user is expressed with respect to $\tilde{\eta}_{k^*}[s]$ as [98],

$$(\gamma_{k^*}[s]|\mathbf{z}, h_{k^*}, \Delta_{k^*}) = \frac{P_{k^*} g_{k^*}}{\mathsf{Var}(\tilde{\eta}_{k^*}[s]|\mathbf{z}, h_{k^*}, \Delta_{k^*}) + \sigma^2}, \tag{2.3}$$

$$\gamma_{k^*}[s] = \frac{P_{k^*} g_{k^*}}{\mathsf{Var}(\tilde{\eta}_{k^*}[s]|\mathbf{z}, h_{k^*}, \Delta_{k^*}) + \sigma^2}, \tag{2.4}$$

where $\mathbf{z}$ represents the latest detection status of the interfering symbols, i.e. correct or erroneous. Further, the error probability of sth symbol detection can be presented with respect to the $(\tilde{\gamma}_k[s]|\mathbf{z}, h_{k^*}, \Delta_{k^*}[s])$ as [98],

$$P(e_{k^*}[s]|\mathbf{z}, h_{k^*}, \Delta_{k^*}[s]) = 1 - \left(1 - Q\left(\sqrt{\frac{3.(\tilde{\gamma}_k[s]|\mathbf{z}, h_{k^*}, \Delta_{k^*}[s])}{2.(M-1)}}\right)\right)^2, \tag{2.5}$$

where, Q(·) represent the Q function and M denotes the order in M-QAM [99].

$$(\tilde{\gamma}_k[s]|\mathbf{z}, h_{k^*}, \Delta_{k^*}[s]) = \mathsf{Var}(\tilde{\eta}_k[s]|\mathbf{z}, \Delta_{k^*}[s]) + \sigma^2 > d_{e_k^*} \tag{2.6}$$

where $d_{e_k^*}$ is half the distance between two nearest constellation points given by $\sqrt{\frac{3.P_{k^*}h_{k^*}}{2.(M-1)}}$ [100]. Further, the conditional error probability of the sth symbol detection can be obtained as [98],

$$P(e_{k^*}[s]|h_{k^*}, \Delta_{k^*}[s]) = \sum_{i=1}^{2^{2(K-1)}} P(e_{k^*}[s]|iP_{z(\mathcal{L})}, h_{k^*}, \Delta_{k^*}[s]). \prod_{k\in K, \zeta\in(s-1,s+1), k\neq k^*} Pr_{i,k}^{(\mathcal{L})}[\zeta], \tag{2.7}$$

where,

$$P(e_{k^*}[s]) = \frac{1}{\tau_{max} - \tau_{min}}. \int_{\tau_{min}}^{\tau_{max}} \int_0^{\infty} P(e_{k^*}[s]|h_{k^*}, \Delta_{k^*}[s]).e^{-h_{k^*}}.dh_{k^*}.d\Delta_{k^*}[s], \tag{2.8}$$

$$P_{bit,k^*} = \frac{P(e_{k^*}[s])}{\log_2(M)}, \tag{2.9}$$

where $P(e_{k^*}[s])$, $P(e_{k^*}[s]|\alpha_{k^*}, \Delta_{k^*}[s])$ denote respectively, the probability of error and conditional probability of error on the sth symbol of the k^*th user. Also, sth symbol of the k^* user is the desired symbol to be detected and M is the modulation order. Further, h_{k^*} denotes the magnitude of fading for the sth symbol of the k^*th user. The $\Delta_{k^*}[s]$ denotes the percentage of symbol time that the overlapping symbols of the ith user has on the sth symbol of the k^*th user. Moreover, iP_z, denotes probability of the ith permutation of $\mathbf{z}$, $1 \leq i \leq 2^{2(K-1)}$ and $Pr_{i,k}[\zeta]$ denotes the probability of detection being correct or in error.

Furthermore, Conv T-SIC may not be optimal for decoders, particularly in massive D2D communication networks with energy-limited nodes. Thereby, energy efficient decoding schemes are required for A-NOMA assisted D2D communications

2.5.4/ ENERGY-EFFICIENT NOMA

Mathematically, energy efficiency (EE) in a communication system is defined as the amount of information that can be reliably transmitted per Joule of consumed energy; which is denoted using units of bits-per-Joule [101]. In other words, EE is defined as the ratio between the total achievable rates and total power consumption of the communication system [84] as follows:

$$\text{EE} = \frac{\text{Throughput (bits/s)}}{\text{Power Consumption (W)}} = \frac{R}{P_c} \text{ bits/J.} \tag{2.10}$$

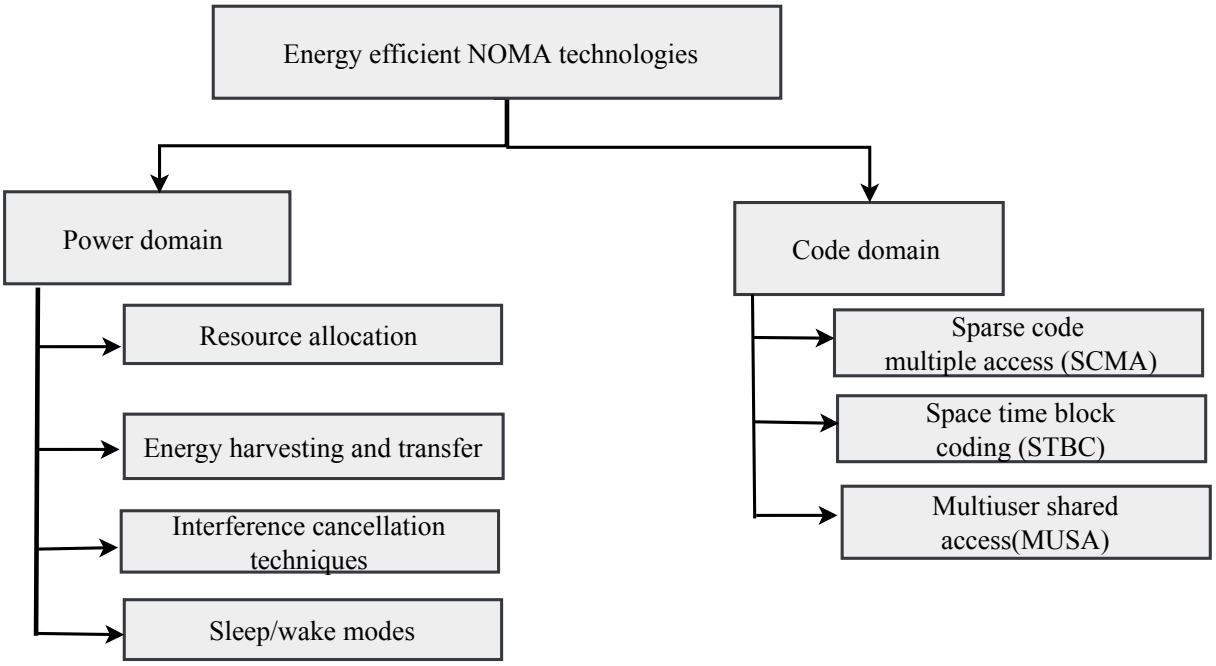

Figure 2.9: Classification of green technologies used in NOMA

Facing massive connections and unavoidable interference, the ways of providing green communications for emerging mobile networks are important. Thus, it is our goal to review and investigate available strategies for maintaining and increasing the energy efficiency of all users in a NOMA scheme-assisted network. In most of the existing literature, [102–113], proposed algorithms are derived using probability, optimization, and signal processing principles and are used to derive optimal or sub-optimal energy-efficient algorithms. The approaches for green NOMA of wireless networks can be classified under two major categories namely power domain and code domain NOMA as illustrated in Figure 2.9. Besides, the trending and extended schemes of enhancing energy efficiency of NOMA-based wireless networks are illustrated in Figure. 2.10.

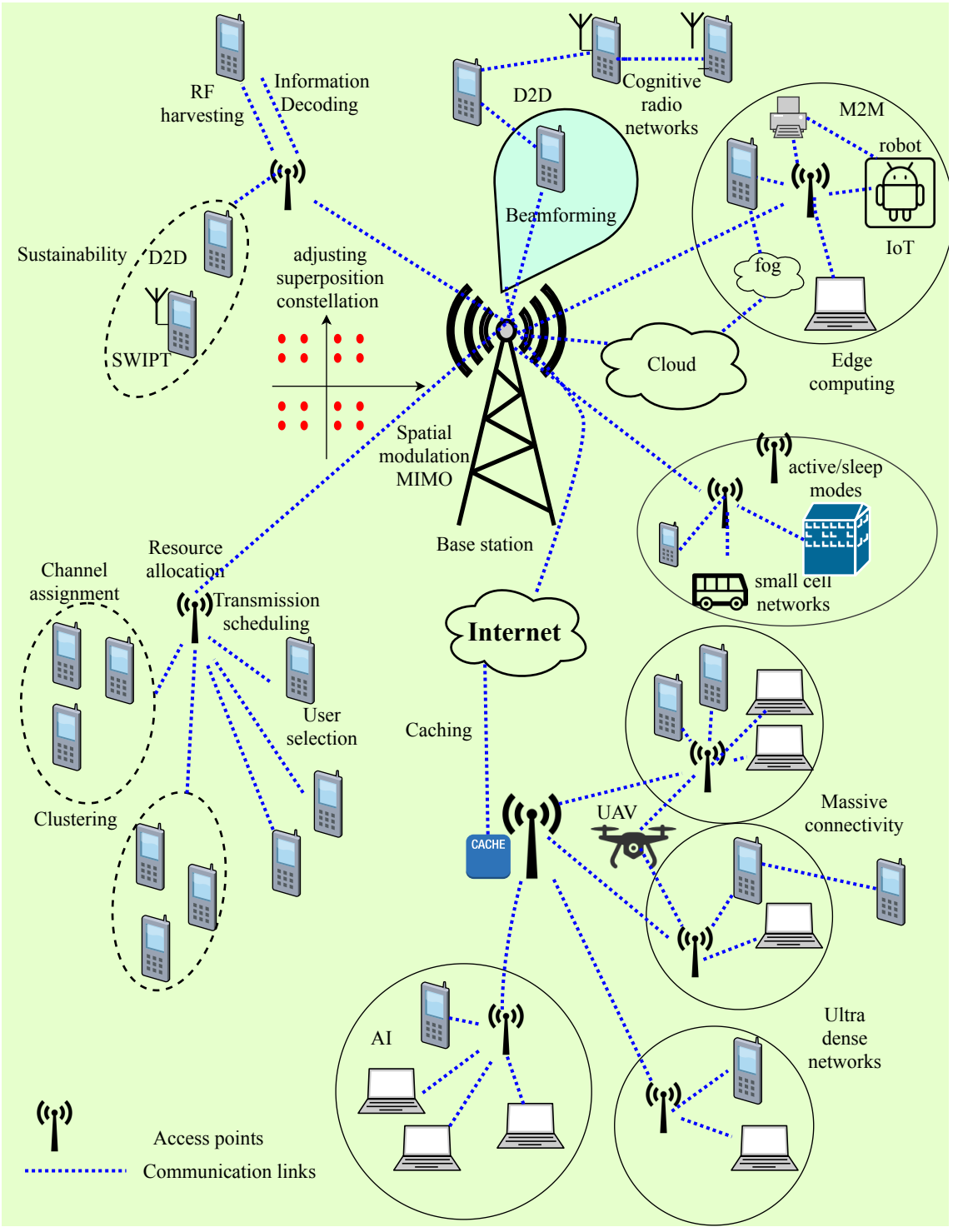

Figure 2.10: Schemes for enhancing energy efficiency of NOMA-based wireless networks such as optimal resource allocation, sleeping modes, RF energy harvesting, cooperative communications (D2D, M2M), cloud computing, caching, beamforming, AI, UAV, modulation optimization

2.5.5/ Secrecy Capacity

The secrecy capacity of wireless networks refers to the maximum amount of secure information that can be transmitted by a legitimate user over a wireless channel. It is limited by the strength of the eavesdropper's signal and noise level on the channel. The secrecy capacity of a wireless network is defined mathematically as:

$$C_s = \frac{\log(1+\gamma_l)}{\log(1+\gamma_e)} \tag{2.11}$$

where γ_l and γ_e denote respectively, the SINR of the legitimate user and SINR of the eavesdropper. Furthermore, secrecy capacity is an important metric in the field of information theory. It can be applied in a wide range of fields such as military communications, financial transactions, secure messaging, etc.

2.6/ Optimization Techniques

The typical procedure to design an optimal wireless communication system is to find the optimal design parameters with respect to a set of prioritized criteria or constraints. Furthermore, research works in wireless optimization involve the analysis and mathematical modelling of problems in wireless networks and the design of efficient algorithms for solving them. Moreover, in this section, optimization procedures using Lagrangian approximation, stochastic gradient descent algorithm, successive linear programming, and constraint satisfaction-assisted techniques are discussed.

2.6.1/ Lagrangian Approximation

The optimal solution of a convex optimization problem can be derived by applying Lagrangian multipliers/KKT conditions. A convex optimization problem of the form given in (2.12a) can be transformed to its Lagrangian dual form as in (2.13).

$$\begin{aligned} \underset{d_u}{\text{minimize}} \quad & f(x) && \text{(2.12a)} \\ \text{subject to} \quad & h(x) = b,, && \text{(2.12b)} \\ & g(x) \leq c, && \text{(2.12c)} \end{aligned}$$

$$L(x,\lambda) = f(x) + \lambda(b - h(x)) + \mu(c - g(x)) \tag{2.13}$$

2.6.2/ Gradient Descent Algorithm

Gradient descent (GD) is an iterative method for optimizing an objective function with suitable smoothness properties. A general Stochastic Gradient Descent (SGD) algorithm is presented in Algorithm (1). Gradient descent is an iterative algorithm, that starts from a random point on a function, f, and travels down its slope in steps until it reaches the lowest point of f. The descending is started with a random point in f and updated in each iteration by sending with a step size t. This process is repeated until the gradient between the current point and the previous point is almost 0.

Algorithm 1 Gradient Descent

Set error tolerances for algorithm termination, ϵ, step size, t
Initialize $i = 1$
repeat
  Update d_u as in $d_u(i+1) = d_u(i) - t\nabla^i_{d_u} f$
  $i = i + 1$
until d_u converged;
Return d_u

2.6.3/ Successive Linear Programming (SLP)

A SLP algorithm [114] converts the nonlinear inequalities system into the approximated linear system (polyhedral areas). The linear approximation is possible using the Taylor series expansion of such nonlinear inequalities. Consider the nonlinear function related to such inequality, $g(x)$, which can be expanded as follows,

$$\tilde{g}(x, x^{(n)}) = g(x^{(n)}) + \Delta g(x^{(n)})(x - x^{(n)}). \tag{2.14}$$

Next, the batch of linear inequalities related to an unknown parameter is solved for n number of iterations until the solution is converged to a fixed point. The use of SLP algorithm guarantees better time resolution when the linear approximation is adopted. An SLP algorithm presents a relevant choice particularly when the amount of data is high. The use of the SLP algorithm guarantees better time resolution when the linear approximation is adopted. SLP algorithm presents a relevant choice particularly when the amount of data and the number of cellular phones is high.

Algorithm 2 Successive Linear Programming

Input data: step size, ϵ
Set a random value to $\boldsymbol{d_u}$
repeat
  Substitute $\boldsymbol{d_u(i)}$ in the Taylor expansion of the non linear inequality g(x)
  Solve the optimization problem with g(x) and find the updated solution of $\boldsymbol{d_u}$
  $d_u(i+1) = d_u(i)$
until $\boldsymbol{d_u}$ converged, i.e. $\boldsymbol{d_u(i+1) - d_u(i) \leq \epsilon}$;
Return $\boldsymbol{d_u(i+1)}$

2.6.4/ Constraint Satisfaction Programming

Constraint Satisfaction Programming (CSP) based optimization can be used for tasks such as localization, scheduling, route planning. First a Constraint Satisfaction Problem (CSP) is defined. This CSP consists of, given a finite collection of variables and a set of constraints. The goal is to find a solution that satisfies all constraints and possibly optimizes an objective function. Thereby, once a CSP is defined as a triple $< V, D, C >$ that consists of a set of variables $(V_1, V_2, V_3, ..., V_n)$, a discrete domain $(D_1, D_2, D_3, ..., D_n)$ for each variable, and a set of constraints (C = $\{C_1, C_2, C_3, ..., C_n\}$), the optimal values that fulfill all the constraints, i.e., $V_1^o, V_2^o, V_3^o, ..., V_n^o$, are determined as the solution of the CSP.

$$[V_1^o, V_2^o, V_3^o, ..., V_n^o] = \begin{cases} \text{Variables:} V_1, V_2, V_3, ..., V_n \\ C_1 \leq 0 \\ C_2 \leq 0 \\ C_3 \leq 0 \\ \vdots \\ C_n \leq 0 \end{cases} \tag{2.15}$$

Moreover, CSP based algorithms have been used in many combinatorial problems such as scheduling, packing, and routing. Furthermore, CSP has been used in wireless ad hoc network localization applications [115–121]. Such CSPs are usually solved via search, in a form of backtracking or local search. It is noted that methods such as priority ordering, filtering, and iterative min-conflict have been used to enhance the performance of CSP algorithms [122–124].

2.7/ Cross layer Integration of A-NOMA Scheme with Outband D2D Multi-hop Protocols

Cross-layer integration refers to the desigining of different layers of communication such as phyiscal layer and network layer to work together seamlessly. In the domain of D2D communications in wireless network, cross layer integration of multiple acess schemes with network protocols optimize the performance and efficiency of the D2D communication. Different multiple access schemes can be integrated with network layer protocols to optimize the utilization of the wireless spectrum and improve the D2D communication efficiency. Additionally, cross-layer integration of A-NOMA with outband D2D multi-hop communications is a challenging task due to variations in the radio channel and network congestion conditions.

The network layer performance of A-NOMA assisted D2D communications can be evaluated under metrics such as network congestion, stability, compatibility, complexity, and deployability. Moreover, the design of such communications must take into account the strict and closed 3GPP standards for D2D communications. In addition, the proposed network layer protocols have to be as light as possible with less control and redundancy traffic. Also, one of the main challenges under both physical and network layers of future

B5G/6G D2D networks is to optimize such metrics under massive connection [83,84,125].

Moreover, the physical layer performance of multiple access schemes can be evaluated under metrics such as reliability, end-to-end latency, energy efficiency, complexity, and security [83, 84, 125]. Other than spectral efficiency and reliability metrics, one of the main targets of future 6G D2D networks is to optimize its EE [83,84,125]. Furthermore, a massive NOMA-assisted D2D network conventionally suffers from high complexity during the decoding phase [10–14]. Also, less complex systems with algorithms are required for outband D2D assisted multi-hop communication networks [126]. Hence, it is noted that, a reliable and energy efficient A-NOMA for massive D2D networks is understudied. Hence, schemes required to achieve the optimal performance for an A-NOMA-assisted out-of-coverage D2D emergency call service are discussed in this thesis.

II

CONTRIBUTIONS

3

ASYNCHRONOUS-NOMA D2D NETWORK WITH CYCLIC TRIANGULAR-SIC SCHEME

In the context of conventional wireless networks that use NOMA to support multiple users, one challenge is the high computational complexity and energy consumption at the receiver side for decoding the received signals using SIC. The complexity of decoding NOMA signals increases as the number of users increases, as discussed in Section 2.7 [127]. Additionally, under realistic channel conditions, it is impractical to use the synchronous NOMA scheme in uplink D2D transmission. To address these issues, the first section of this chapter proposes an A-NOMA-based cyclic T-SIC scheme for a massive D2D network. The second section of this chapter investigates the issue of improving the secrecy capacity of D2D communications in disaster scenarios in the presence of jammers in close proximity. In the next chapter, we present a multi-hop protocol that enables the network layer functioning of the Cyclic T-SIC based NOMA assisted D2D emergency call transmissions, with a focus on disaster situations where robust networking systems are crucial for protecting human lives.

The proposed Cyclic T-SIC assisted A-NOMA scheme aims to reduce the decoding complexity, energy consumption, and BER of a superimposed signal received in an outband D2D network. This scheme consists of three stages: optimization, decoding, and retransmission. In the optimization stage, a dual Lagrangian objective function is employed to maximize the number of data symbols that can be decoded at the receiver by determining an optimal interference cancellation triangle, subject to co-channel interference and data rate constraints. In the decoding stage, the data in the optimal interference cancellation triangle is decoded using a conventional T-SIC technique. Then the remaining users' data are decoded in sequential iterations of the proposed scheme using the retransmissions from such users. The proposed scheme is evaluated in terms of energy efficiency, BER, computational complexity, and decoding delay metrics. The proposed scheme is shown to outperform the conventional T-SIC decoding scheme under massive D2D networks. An A-NOMA-assisted transmission scheme is considered due to the resource limitations and the asynchrony in signal receptions in out-of-coverage D2D scenarios. A binary optimization problem is proposed to select the optimal data to enhance the sum

secrecy capacity of the transmissions. The results show that the proposed optimized scheme outperforms the conventional secrecy capacity.

3.1/ M-ary QAM Asynchronous-NOMA assisted D2D Network with Cyclic Triangular-SIC Scheme

3.1.1/ Introduction

A synchronous NOMA scheme is impractical in the uplink and D2D communications. In D2D networks, the users are geographically distributed and their respective signals propagate over different paths that encounter distinct channel effects [128]. As a consequence, transmitted NOMA signals arrive at the receiving terminal with varying time offsets. Hence, time-synchronous data reception is not possible at the receiver terminal of a D2D network [97]. In [98], an A-NOMA scheme has been proposed under the consideration that the interference is induced by co-channel during the decoding process of the desired user's data symbols at the receiver terminal. Therefore, the studies in [93, 98, 129–131] have illustrated that the use of the A-NOMA scheme can improve the decoding ability of the receiver terminal as well as enhance the D2D network performance. Such studies claim that the asynchrony between user signals can in fact enhance spectral efficiency. In [132], it has been proven that the asynchrony in the transmission can enhance the signal detection at the receiver terminal in an uplink A-NOMA scheme even under equal-power asynchronous transmissions. Moreover, in [133], it has been defined that the optimal mismatch between user signals in an uplink A-NOMA can enhance the throughput and energy efficiency. Authors in [129] have proposed and experimentally implemented an A-NOMA scheme for an uplink optical access scenario, which has a higher BER reduction of one order magnitude than the synchronous NOMA schemes. Moreover, in [130], an uplink A-NOMA with a sufficiently large data frame length has been shown to outperform synchronous NOMA in sum throughput.

Other than spectral efficiency and reliability metrics, one of the main targets of future 6G D2D networks is to optimize its' EE [83, 84, 125, 134, 135]. Nowadays, massive D2D networks are in demand due to their key merits namely i) infrastructure-free network, ii) ability to operate with limited resources, and iii) ubiquitous connectivity to the end-users. Indeed, a massive NOMA-assisted D2D network conventionally suffers from high complexity during the decoding phase [10, 11]. Moreover, the authors in [12] have shown that there is an increase in decoding complexity in the NOMA scheme when the number of users increases for more than three. Thus, an increment incurs high complexity that reduces the energy efficiency of the D2D networks. The energy consumption of mobile devices can be higher, particularly in energy-limited D2D communication scenarios such as emergency disaster scenarios, since such devices cannot cope flexibly with energy-consuming computations [13, 14]. Additionally, with limited resources for allocation, complex SIC decoding procedures can be observed in NOMA-based massive D2D networks. Hence, it was noted that a reliable and efficient A-NOMA for massive D2D networks is understudied.

Recently, in [98], an iterative signal processing based T-SIC technique has been proposed to enhance the spectral efficiency of A-NOMA uplink transmissions. Due to the triangular pattern used for decoding symbols in T-SIC, the interference caused by multiple asynchronous data symbols on each desired user's symbols is considered to enhance the symbol detection and residual interference cancellation in the D2D network. Therefore, the T-SIC technique can also be exploited to optimize the decoding ability and spectrum efficiency of the A-NOMA D2D network. To the best of the authors' knowledge, it is yet not been used in D2D networks to date. The overall objective of this chapter is to investigate and optimize the performance of massive A-NOMA D2D transmissions under a modulation such as M-ary QAM. The fourfold contributions of this chapter are summarized as follows:

- A new binary optimization algorithm is proposed to decide the optimal combination of data symbols in the received superimposed signal to be decoded under maximum co-channel interference and minimum data rate constraints. The corresponding optimization problem is a hard constraint problem due to its binary optimization variables and non-linear constraints. Hence, such binary variables and non-linear constraints are reformulated to form continuous and linear constraints, and a Lagrangian dual objective function is formed. Then, this can be solved efficiently by applying the Lagrangian dual algorithm.

- A new Cyclic T-SIC scheme is proposed to ensure the decoding of each user's data in consecutive iterations, considering also the retransmissions by the users whose data were not yet decoded in a prior iteration of optimization. Moreover, the EE and BER performance of the Cyclic T-SIC is shown to be significant in comparison to Conv T-SIC.

- The optimal trade-off between the BER and EE of the proposed Cyclic T-SIC is studied, and compared with conventional Conv T-SIC. The Cyclic T-SIC achieves a higher EE and reduced BER with a lower transmit SNR, lower received power ratio, and higher asynchrony among user signals as compared to a competitive scheme, Conv T-SIC.

- The computational complexity of the proposed Cyclic T-SIC is evaluated and It is seen that the complexity of the proposed Cyclic T-SIC scheme is less than that of the Conv T-SIC scheme when the error tolerance for algorithm termination, ϵ, is in the order of 10^{-1} magnitude. Further, the total simulation delay is shown to be lesser in Cyclic T-SIC than in Conv T-SIC due to its reduced computational complexity.

The remaining of this chapter is organized as follows. In Section II, the existing A-NOMA T-SIC scheme is introduced, and in the Section III the received signal structure and the iterative signal processing at the receiver are presented. Section IV presents the problem formulation and the proposed Cyclic T-SIC scheme is presented in Section V. Next, the performance analysis is given in Section VI. Furthermore, a numerical result analysis is presented in Section VII. Finally, conclusions are drawn with remarks in Section VIII.

3.1.2/ System Model

In this section, a D2D A-NOMA signal model and its preliminaries are presented. Hence, an A-NOMA assisted D2D network with $k \in K$ geographically distributed transmitting users, where K is the maximum number of transmitters, and one receiving terminal, R_X, within a small neighborhood is considered as shown in Figure 3.1. It is assumed that there are K NOMA users sharing each subcarrier with N subcarriers, and $K \geq 1$. It is assumed that the transmitted signals are not aligned at the receiver, and hence the channel is symbol asynchronous. Therefore, a power domain A-NOMA scheme-assisted decoding method is applied in our proposed work where the waveform technique used is based on Orthogonal Frequency Division Multiplexing (OFDM) [98, 136–140].

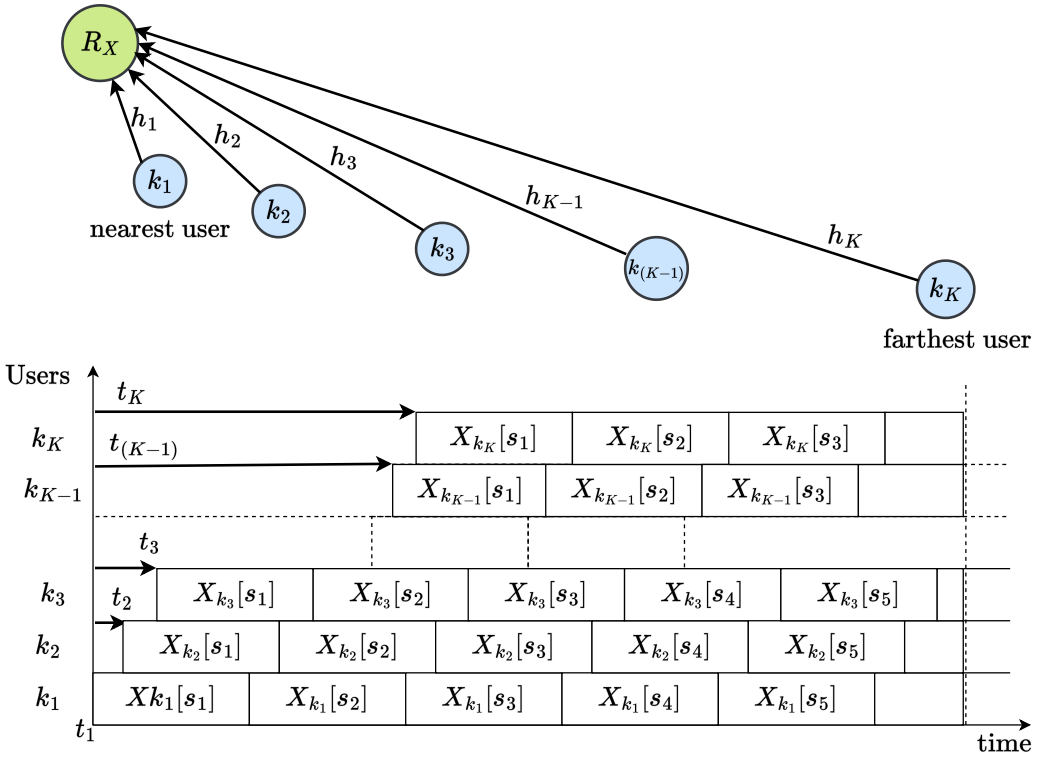

Figure 3.1: A-NOMA assisted D2D communication with a K number of transmitters and one receiving UE.

Moreover, due to the timing offset between users in A-NOMA, Inter-Carrier Interference (ICI) can occur and the resultant OFDM frequency components can get distorted. Such ICI at a subcarrier is formulated as follows. Consider an OFDM signal at time t modeled as:

$$x(t) = \sum_{n=1}^{N} X[n] e^{j2\pi f_n t}, \tag{3.1}$$

where f_n is the frequency of the n^{th} subcarrier, and j denotes the complex number. Moreover, $X[n]$ is the signal transmitted over the nth subcarrier. Furthermore, the frequency offset due to asynchrony in the A-NOMA signal will introduce a multiplicative time-varying distortion, represented as $\beta(t) = e^{j2\pi\rho\Delta f t}$, where $\rho = \frac{\delta f}{\Delta f}$. As a result, the ICI on the m^{th}

subcarrier is modeled as [98]:

$$ICI_m = \sum_{n=1,n\neq m}^{N} \int_0^{T_N} X[n] e^{j2\pi\rho\Delta f t} e^{-j2\pi\Lambda\Delta f t}.dt, \tag{3.2}$$

where the Λ, gives the distance of the interfering subcarrier to the desired subcarrier, and $0 \leq t \leq T_N$, where T_N is the symbol time. Meanwhile, in NOMA systems Multi-Access Interference (MAI) given in (3.4) is another interference that can distort the OFDM symbol of the desired user. Also, it is noted that in A-NOMA, the ICI is comparatively lesser than Multi-Access Interference [98]. Hence, for this analysis, the MAI is considered the dominant source of interference, and one subcarrier is focused on for the analysis. The received signal at R_X for the k^*th[1] user at the sth symbol is given by [98],

$$Y_{k^*}[s] = h_{k^*}.\sqrt{P_{k^*}}.X_{k^*}[s] + \eta_{k^*}[s] + n_0, \tag{3.3}$$

where $X_{k^*}[s]$ denotes the k^*th user's sth data symbol which is complex and output from a M-ary-QAM symbol mapper, and P_{k^*} is the transmit power of $X_{k^*}[s]$, which is same for all symbols of k^*th user for transmission time duration. Hence, the signal transmitted from the k^*th user at the sth symbol can be denoted by $\sqrt{P_{k^*}}X_{k^*}[s]$. The frequency response on one subcarrier for one symbol time period is considered flat and assumed to follow a Rayleigh distribution independently and identically (i.i.d) [141–143]. The symbol time is assumed to be considerably lesser than the channel coherence time. Hence, $h_{k^*}[s]$ is constant for a block of symbols during a transmission period. Further, n_0 is the Additive White Gaussian Noise (AWGN) at the receiver side with variance σ^2 and $\eta_{k^*}[s]$ is the total interference to the k^*th user's sth symbol [98].

$$\eta_{k^*}[s] = \sum_{i\neq k^*}^{K} \sum_{\varsigma=s-1}^{s+1} \Delta_{k^*,i}[s,\varsigma].X_i[\varsigma].h_i.\sqrt{P_i}.e^{j\theta_{k^*,i}}, \tag{3.4}$$

where $e^{j\theta_{k^*,i}}$ depicts the i^{th} user's phase mismatch of the signal to the k^*th and $\Delta_{k^*,i}$ denotes the symbol duration that the i^{th} user's ς symbol overlap with the desired symbol, as a percentage out of the total symbol period, T_{sym}. Moreover, research works such as [144–146] have addressed the problem of estimating the time offset, and carrier offset which leads to estimating $\Delta_{k^*,i}$ and $\theta_{k^*,i}$ with high reliability in D2D communications using time of arrival measurements.

Following the standard SIC procedure, after subtracting the reconstructed interference, $\hat{\eta}_{k^*,i}[s,\varsigma]$, of all overlapping interferes' symbols, the remaining interference cancelled signal for desired symbol is formulated in terms of desired signal, residual interference plus noise as [98],

$$\begin{aligned} \tilde{Y}_{k^*}[s] &= Y_{k^*}[s] - \sum_{i\neq k^*}^{K} \sum_{\varsigma=s-1}^{s+1} \hat{\eta}_{k^*,i}[s,\varsigma], \\ &= X_{k^*}[s].h_{k^*}\sqrt{P_{k^*}} + \tilde{\eta}_{k^*}[s] + n_0, \end{aligned} \tag{3.5}$$

[1] k^* indicates the desired user within a cohort of K users

where the latest residual interference to the desired symbol, $k^*[s]$, is modelled as [98],

$$\tilde{\eta}_{k^*}[s] = \sum_{i \neq k^*}^{K} \sum_{\varsigma=s-1}^{s+1} \Delta_{k^*,i}[s,\varsigma].(X_i[\varsigma] - \hat{X}_i[\varsigma]).h_i \sqrt{P_i}.e^{j\theta_{k^*,i}}. \tag{3.6}$$

Moreover, such residual interference is utilized in the A-NOMA T-SIC scheme to improve the decoding reliability.

3.1.3/ Problem Formulation

The Conv T-SIC decoding scheme [98] detailed in Section 2.5.3.2 is shown to enhance the reliability of decoding in A-NOMA uplink transmissions. Nevertheless, Conv T-SIC may not be optimal for decoders, particularly in massive D2D communication networks with energy-limited nodes. In the forthcoming section, a Cyclic T-SIC decoding scheme is proposed for A-NOMA to improve its decoding efficiency in terms of factors such as energy consumption, reliability, complexity, and delay.

3.1.4/ Cyclic T-SIC Decoding Scheme

A Cyclic T-SIC scheme is proposed for A-NOMA D2D decoders comprising of three stages as, i) Optimization, ii) Decoding, and iii) Re-transmission.

3.1.4.1/ Optimization Stage

Let a superimposed signal is received at the receiver terminal R_X. Furthermore, to conserve the decoder energy consumption and reliability parameters, a binary optimization method is used by R_X as follows,

$$\underset{D_{u_k}}{\text{maximize}} \quad \sum_{k=1}^{K} D_{u_k}(K-k+1) \tag{3.7a}$$

subject to

$$D_{u_k} \in \{0,1\}, \forall k \in K, \tag{3.7b}$$

$$D_{u_{(k+1)}} - D_{u_k} \leq 0, \tag{3.7c}$$

$$D_{u_k}(B\log_2(1 + \sum_{s=1}^{K-k+1} \gamma_k[s]) - R_{\min}) \geq 0, \tag{3.7d}$$

$$0 \leq \sum_{k^*=1}^{K} D_{u_k} \sum_{i \neq k^*}^{K} \sum_{\varsigma=s-1}^{s+1} P_i g_i \Delta_{k^*,i}[s,\varsigma] \leq I_{th}, \tag{3.7e}$$

where a decision vector of the data symbols to be decoded is introduced as $\boldsymbol{D}_u = [D_{u_k}]_{k \in \mathcal{K}}$, and $D_{u_k} = 1$ if the data symbols of the kth user are selected to be decoded. Further, the

duration of symbol time that ith user overlap with the desired k^*th user symbol, co-channel interference threshold, and channel bandwidth are given by $\Delta_{k*,i}, I_{th}$, B respectively. The transmission power of kth user, channel gain of kth user, thermal noise variance, transmission power of ith user, channel gain of ith user are given by $P_k, g_k, \sigma^2, P_i, g_i$, respectively. Also, R_{min} is the minimum rate threshold defined for the communication system.

Moreover, the main aim of the optimization is to maximize the number of decoded data symbols while minimizing the energy consumption over computing, and hence an objective function is formulated using **Lemma 1**.

Proposition 1. *D_{u_k} is approximated to a binary, $D_{u_k} \in \{0, 1\}$, by using a difference of two convex functions/sets constraint (D_b) as follows [147]:*

$$D_b = \left\{(D_{u_k} - D_{u_k}^2) \leq 0, \quad \text{if } 0 \leq D_{u_k} \leq 1\right\},$$

Proof. It is observed that,

$$(D_{u_k} - D_{u_k}^2) \in \{0, 1\}, \tag{3.8}$$

for any D_{u_k} satisfying $0 \leq D_{u_k} \leq 1$. It is noted that, $(D_{u_k} - D_{u_k}^2) > 0$ when $D_{u_k} \in (0, 1)$. Thus satisfies $(D_{u_k} - D_{u_k}^2) <= 0$, which is a convex inequality, only when $D_{u_k} = 0$ or $D_{u_k} = 1$. □

Lemma 1. *The number of symbols selected from an IC triangle per each kth user, N_{sym_k}, is given as,*

$$N_{sym_k} = D_{u_k}(K - k + 1). \tag{3.9}$$

Proof. It is observed that the total number of symbols that is included in an IC triangle is $K!$. Further, the maximum number of symbols that overlap a symbol is two, since each data symbol is received over an equal T_{sym}. Hence, the total number of symbols starting from the weakest symbol increments from 1 to K for each kth user. Thus, for each kth user the number of symbols is $(K - k + 1)$, where $k = 1$ denotes the strongest user. Moreover, the total number of users' data decoded, $k_{\text{opt}} = \sum_{k=1}^{K} D_{u_k}$. □

Moreover, the constraint in (3.7d) corresponds to the minimum rate, and (3.11f) corresponds to the maximum allowable co-channel interference constraint. Note that the optimization algorithm in (3.7a) involves non-linear constraints, such that the optimization is a hard-constrained problem. Hence, it is reformulated by relaxing its binary variables and non-convex constraints. Additionally, the binary constraint in (3.7b) is transformed to linear constraints as given in (3.11b) and (3.11c). Such constraint re-formulation assure that D_{u_k} is approximated to a binary [148] using **Proposition1**. Further, the non-linear constraint with regard to minimum rate constraint in (3.7d) is converted into a linear constraint as in (3.10), where $\tilde{\gamma} = 2^{\frac{R_{min}}{B}} - 1$ [149].

$$D_{u_k}(\sigma^2 + \sum_{i=1}^{K} \sum_{\varsigma=s-1}^{s+1} P_i g_i \Delta_{k,i}[s, \varsigma] - P_k g_k (1 + \frac{1}{\tilde{\gamma}})) \leq 0. \tag{3.10}$$

The relaxed binary optimization with reformulated convex constraints is given as,

$$\underset{D_{u_k}}{\text{maximize}} \quad \sum_{k=1}^{K} D_{u_k}(K-k+1) \tag{3.11a}$$

subject to

$$0 \leq D_{u_k} \leq 1, \forall k \in K, \tag{3.11b}$$

$$\sum_{k=1}^{K}(D_{u_k} - D_{u_k}^2) \leq 0, \tag{3.11c}$$

$$D_{u_{(k+1)}} - D_{u_k} \leq 0, \tag{3.11d}$$

$$D_{u_k}(\sigma^2 + \sum_{i=1}^{K}\sum_{\varsigma=s-1}^{s+1} P_i g_i \Delta_{k,i}[s,\varsigma] - P_k g_k(1+\frac{1}{\tilde{\gamma}})) \leq 0, \tag{3.11e}$$

$$0 \leq \sum_{k^*=1}^{K} D_{u_k} \sum_{i\neq k^*}^{K}\sum_{\varsigma=s-1}^{s+1} P_i g_i \Delta_{k^*,i}[s,\varsigma] \leq I_{th}, \tag{3.11f}$$

Moreover, the reformulated convex optimization problem in (3.11a) is solved efficiently by applying the Lagrangian dual algorithm using **Proposition 2**.

Proposition 2. *The Lagrangian optimization problem is formed as,*

$$\underset{\boldsymbol{\lambda},\boldsymbol{\delta},\boldsymbol{\phi},\boldsymbol{\mu}}{\text{minimize}} \quad \max_{D_u} \mathcal{L}(\boldsymbol{D_u},\boldsymbol{\lambda},\boldsymbol{\delta},\boldsymbol{\phi},\boldsymbol{\mu}) \tag{3.12a}$$

$$\text{subject to} \quad \boldsymbol{\lambda},\boldsymbol{\delta},\boldsymbol{\phi},\boldsymbol{\mu} \succcurlyeq 0. \tag{3.12b}$$

where $\lambda, \delta, \phi, \mu$ are the Lagrangian multipliers corresponding respectively to constraints in the optimization problem in (3.11a).

Proof. The Lagrangian objective function of problem in (3.11a) is formed as,

$$\begin{aligned}\mathcal{L}(\boldsymbol{D_u},\boldsymbol{\lambda},\boldsymbol{\delta},\boldsymbol{\phi},\boldsymbol{\mu}) = &\sum_{k=1}^{K} D_{u_k}(K-k+1) - \sum_{k=1}^{K}\lambda_k D_{u_k} + \sum_{k=1}^{K}\lambda_k D_{u_k}^2 - \sum_{k=1}^{K}\delta_k(D_{u_{(k+1)}} - D_{u_k}) \\ &- \sum_{k=1}^{K}\phi_k\Big(D_{u_k}(\sigma^2 + \sum_{i=1}^{K}\sum_{\varsigma=s-1}^{s+1} P_i g_i \Delta_{k,i}[s,\varsigma] - P_k g_k(1+\frac{1}{\tilde{\gamma}}))\Big) \\ &- \Big(\sum_{k^*=1}^{K}\mu_k D_{u_k}\sum_{i\neq k^*}^{K}\sum_{\varsigma=s-1}^{s+1} P_i g_i \Delta_{k^*,i}[s,\varsigma] - I_{th}\Big),\end{aligned} \tag{3.13}$$

□

Note that the objective function as well as all the constraints of the dual problem are linear with respect to the Lagrangian multipliers. Thus, the dual problem is convex over the dual variables μ, ς which can be optimized through one dimensional searching algorithm. Thus, the optimal $\boldsymbol{D_u}$ can be achieved by running a gradient descent algorithm [150]. First the gradient of the Lagrangian function with respect to D_{u_k} which is formulated as follows.

$$\nabla_{D_{u_k}} \mathcal{L} = -(K-k+1) - \lambda_k + 2\lambda_k D_{u_k}. \tag{3.14}$$

Further, D_{u_k} can be updated as follows,

$$D_{u_k}{}^{(n)} = D_{u_k}{}^{(n-1)} + \beta_u . \nabla_{D_{u_k}{}^{n-1}} \mathcal{L}, \tag{3.15}$$

where β_u denotes the iteration step size of $\boldsymbol{D_u}$. After finding the optimal $\boldsymbol{D_u}$ using the gradient descent algorithm, the optimal λ can be achieved.

Moreover, the dual function in (3.12a) is not guaranteed to be differentiable. Hence, an iterative scheme based on the gradient descent algorithm is used to obtain the optimal $\boldsymbol{\lambda, \delta, \phi, \delta}$ [84] using **Proposition**[3].

Proposition 3. *The sub-gradient of the dual function, $g(\boldsymbol{\lambda, \delta, \phi, \mu}) = \max_{\boldsymbol{D_u}} \mathcal{L}(\boldsymbol{D_u, \lambda, \delta, \phi, \mu})$, with respect to $\boldsymbol{\lambda, \delta, \phi, \mu}$ can be derived as,*

$$\nabla_{\lambda}\, g(\boldsymbol{\lambda, \delta, \phi, \mu}) = \sum_{k=1}^{K} D_{u_k} + \sum_{k=1}^{K} D_{u_k}^2, \tag{3.16}$$

$$\nabla_{\delta}\, g(\boldsymbol{\lambda, \delta, \phi, \mu}) = D_{u_{(k+1)}} - D_{u_k}, \tag{3.17}$$

$$\nabla_{\phi}\, g(\boldsymbol{\lambda, \delta, \phi, \mu}) = \sum_{k=1}^{K} \Big(D_{u_k} (\sigma^2 + \sum_{i=1}^{K} \sum_{\varsigma=s-1}^{s+1} P_i g_i \Delta_{k,i}[s, \varsigma] - P_k g_k (1 + \frac{1}{\tilde{\gamma}})) \Big), \tag{3.18}$$

$$\nabla_{\mu}\, g(\boldsymbol{\lambda, \delta, \phi, \mu}) = \sum_{k^*=1}^{K} D_{u_k} \sum_{i \neq k^*}^{K} \sum_{\varsigma=s-1}^{s+1} P_i g_i \Delta_{k^*,i}[s, \varsigma] - I_{th}. \tag{3.19}$$

Further, the dual variable $\boldsymbol{\lambda, \delta, \phi, \mu}$ can be updated according to the following expression.

$$\lambda_k{}^{(m)} = \lambda_k{}^{(m-1)} + \alpha_u^{(m-1)} \nabla_{\lambda_k^{m-1}} \mathcal{L},\ \forall k \in K, \tag{3.20}$$

$$\delta_k{}^{(m)} = \delta_k{}^{(m-1)} + \alpha_u^{(m-1)} \nabla_{\delta_k^{m-1}} \mathcal{L},\ \forall k \in K, \tag{3.21}$$

$$\phi_k{}^{(m)} = \phi_k{}^{(m-1)} + \alpha_u^{(m-1)} \nabla_{\phi_k^{m-1}} \mathcal{L},\ \forall k \in K, \tag{3.22}$$

$$\mu_k{}^{(m)} = \mu_k{}^{(m-1)} + \alpha_u^{(m-1)} \nabla_{\mu_k^{m-1}} \mathcal{L},\ \forall k \in K, \tag{3.23}$$

where α_u denotes the iteration step size of $\boldsymbol{\lambda, \delta, \phi, \mu}$. The approach to solve the optimization problem in (3.7a) is summarized in Algorithm 3.

Algorithm 3 Optimization of T-SIC triangle

Data: γ_k, Δ_i of each kth user
Result: Optimal $\boldsymbol{D_u}$
Initialize $m = 0$, $\boldsymbol{\lambda^{(0)}, \delta^{(0)}, \phi^{(0)}, \mu^{(0)}} \succcurlyeq 0$
Set error tolerances for algorithm termination, ϵ_1, ϵ_2
repeat
  Let $p = 1$; Initialize $D_{u_1}^{(0)}, D_{u_2}^{(0)}, D_{u_3}^{(0)}, ..., D_{u_K}^{(0)}$
  repeat
    Run optimization problem in (3.11a)
  until D_{u_k} converged, i.e $\|\nabla_{D_u{}^{p-1}} \mathcal{L}\|^2 \leq \epsilon_1$;
  for k = 1:K
  Update $D_{u_k}^{(p)}$ as in (3.15)
  end
  $p = p + 1$
  Update $\lambda^{(m)}, \delta^{(m)}, \phi^{(m)}, \delta^{(m)}$ as in (3.16), (3.17), (3.18), (3.23)
  $m = m + 1$
until $\boldsymbol{\lambda, \delta, \phi, \delta}$ converged,i.e., $\|\lambda^{m-1} - \lambda^m\|^2 \leq \epsilon_2$, $\|\delta^{m-1} - \delta^m\|^2 \leq \epsilon_2$, $\|\phi^{m-1} - \phi^m\|^2 \leq \epsilon_2$, $\|\mu^{m-1} - \mu^m\|^2 \leq \epsilon_2$;
Return $\boldsymbol{D_u}$

3.1.4.2/ Decoding and Re-transmission Stages

Once the optimal set of data symbols is derived using the proposed optimization in (3.11a), they are decoded using the Conv T-SIC scheme. Next, the R_X terminal repeats the process of listening to the same subcarrier and receiving retransmissions from the remaining users. Note that for outband D2D emergency scenarios, user signal retransmissions are necessary in order not to lose any critical data [151]. In addition, it is assumed that the network users follow a D2D protocol such as M-HELP [152], which is used for D2D emergency call transmissions. A M-HELP enabled UE re-transmits their own data after a fixed time interval, when their data have not been forwarded up-to a pre-defined limit, n_{RS}, by neighbor devices. Here, the n_{RS} is calculated by transmitting users, which correspond to the number of relaying of its own data by the neighborhood. The re-transmitted data signals by transmitters share the same subcarrier and are superimposed such that it can be decoded using the optimization problem in (3.11a) at the R_X terminal. Correspondingly, this method is repeated until all K user data are decoded using the proposed optimization-assisted T-SIC.

To sum up, the procedure followed at the transmitting UEs is given in Algorithm 4, where n_{Rt} gives the data signal re-transmissions count. . Further, the Cyclic T-SIC scheme performed at the R_X terminal is summarized in Algorithm 5. Moreover, the method of decoding each user data using the proposed Cyclic T-SIC scheme is presented in Figure 3.2. First, a superimposed signal comprising K user data is received over a T_0 duration. Optimization problem in (3.11a) is utilized to derive the optimal data symbol combination which comprises an IC triangle. Such data symbols are decoded using the T-SIC decoding scheme. In this case, received data symbols of some users can be left undecoded. Hence, after a T_0 duration, retransmissions from such users occur after a t_r time interval and received as superimposed signals. The decoding procedure in Cyclic T-SIC is re-

peated for such a signal received. This procedure is repeated for an arbitrary r number of iterations until the successful decoding of each user data. Note that retransmissions from users are not mandatory in scenarios where all the user data are decoded in one Cyclic T-SIC iteration. Furthermore, the performance analysis of such a D2D A-NOMA decoding scheme in terms of energy efficiency, reliability, computational complexity, and delay aspects has been understudied.

Algorithm 4 At the transmitter

Data: Relaying threshold ($RS_{\text{threshold}}$), Retransmissions threshold, (n_{rth})
Initialize $n_{RS} = 0$, $n_{RT} = 0$
repeat
  Listen to dedicated D2D emergency call channel
    Re-transmitting in the same resource in next period
until $n_{RS} \geq RS_{\text{threshold}}$ or $n_{RT} \geq n_{rth}$;

Algorithm 5 At the receiver: Cyclic T-SIC Decoding

Data: Total number of users, K, sharing same resource
Initialize k_{opt} = 0
repeat
  Receive $n(\leq K)$ user data superimposed signal
    Derive the optimal $\boldsymbol{D_u}$ using (3.11a)
    Decoding the $k_{opt}(\leq n)$ user data
until All K user data decoded;

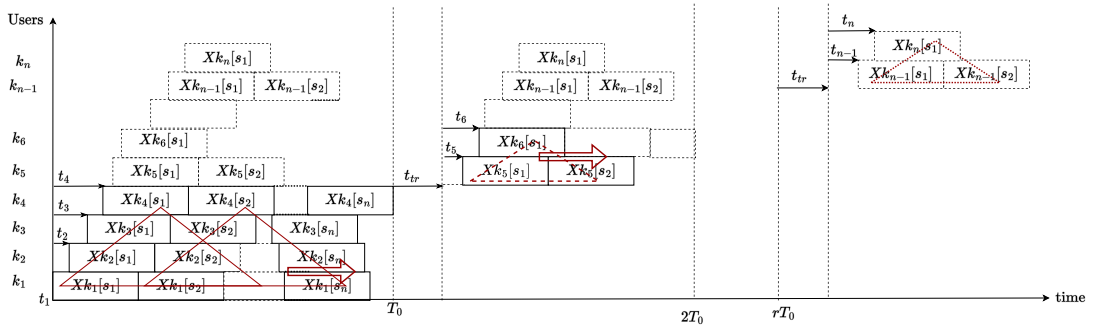

Figure 3.2: Proposed Cyclic T-SIC Decoding Scheme.

3.1.5/ Performance Analysis

In this section the EE, average BER, computational complexity, and simulation delay of the proposed Cyclic T-SIC method are investigated.

3.1.5.1/ EE Analysis

The EE of the A-NOMA D2D scheme can be defined as the ratio between the total achievable rates and total power consumption of the communication system [84]:

$$EE = \frac{\sum_{k=1}^{K} B.\log_2(1+\gamma_k)}{\frac{1}{n_{sym}*T_{sym}}E_c + P_{\text{circuit}} + \varepsilon \sum_{k=1}^{K} P_k}. \tag{3.24}$$

where E_c is the total energy consumption per SIC decoding cycle as defined in **Lemma 2**, P_{circuit} presents the power dissipated by user device hardware circuits [84, 149], and ε denotes the reciprocal of the transmitter power amplifier drain efficiency.

Lemma [2]. *The total energy consumption per decoding instance is denoted by,*

$$\begin{aligned} E_c &= E_{t-1} - E_t \\ &= E_{t-1} - E_{max} e^{-\frac{\log_e \frac{E_{initial}}{E_{final}}}{n_{sym_2} N_{T\text{-}SIC_1} - n_{sym_1} N_{T\text{-}SIC_2}} N_{T\text{-}SIC} \sum_{k=1}^{K} N_{sym_k(t)}}, \end{aligned} \tag{3.25}$$

where E_{max} is the initial maximum energy in a user device, $N_{T\text{-}SIC}$ is the number of repetitive times the same data symbols are decoded, n_{sym_1} is the number of symbols decoded at the initial decoding and $E_{initial}$ is the remaining energy after such decoding instance. Moreover, the total number of symbols decoded at t is $n_{sym}(t) = \sum_{k=1}^{K} N_{sym_k(t)}$. Also, E_{t-1}, E_t are the residual energy levels in the $(t-1)$th and tth instances. Further, n_{sym_2} is the maximum number of symbols possible to decode with E_{max}, and E_{final} is the remaining energy at the end of decoding such n_{sym_2}. Further, the behavior of such energy dissipation is illustrated in Figure 3.3.

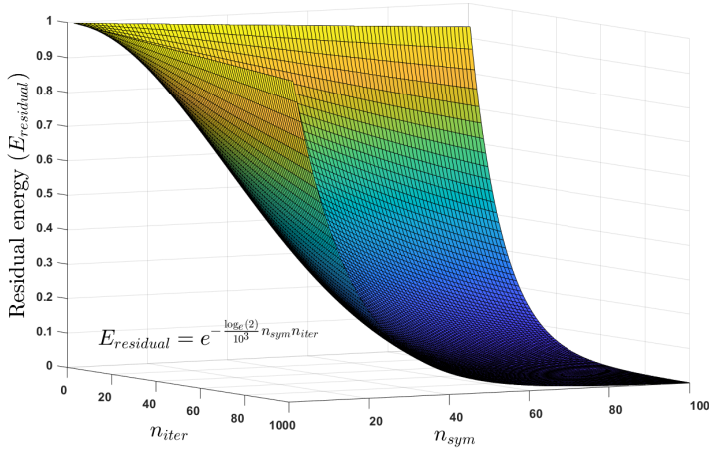

Figure 3.3: Residual energy of a user device in decoding n_{sym} number of symbols under $N_{\text{T-SIC}}$.

Proof. The energy consumption for decoding has an exponential deterioration depending on the n_{sym} [153]. The remaining energy after the initial decoding instance is given as,

$$E_{\text{initial}} = E_{\text{max}} e^{-\alpha_e N_{\text{T-SIC}_1} n_{sym_1}}, \tag{3.26}$$

where α denote the attenuation of energy depending on the receiver physical properties and processing efficiency. Moreover, the final remaining energy at the end of decoding n_{sym_2} is,

$$E_{\text{final}} = E_{\max} e^{-\alpha N_{\text{T-SIC}_2} n_{sym_2}}. \tag{3.27}$$

From (3.26) and (3.27),

$$\alpha_e = \frac{\log_e \frac{E_{\text{initial}}}{E_{\text{final}}}}{n_{sym_2} N_{\text{T-SIC}_1} - n_{sym_1} N_{\text{T-SIC}_2}}. \tag{3.28}$$

□

Hence, the energy consumption per T-SIC decoding cycle for a specific $\sum_{k=1}^{K} N_{\text{sym}_k}$ and n_{iter} is formulated as,

$$\begin{aligned} E_c &= E_{t-1} - E_t, \\ &= E_{t-1} - E_{\max} e^{-\frac{\log_e \frac{E_{\text{initial}}}{E_{\text{final}}}}{n_{sym_2} N_{\text{T-SIC}_1} - n_{sym_1} N_{\text{T-SIC}_2}} N_{\text{T-SIC}} \sum_{k=1}^{K} N_{\text{sym}_{k(t)}}}. \end{aligned} \tag{3.29}$$

3.1.5.2/ BER Analysis

The average theoretical BER of k^*th user data, P_{bit,k^*}, in asynchronous transmissions is formulated in [98] and is updated as follows. First, by considering the latest detected symbols, the SINR of the sth symbol of the k^*th user is expressed with respect to $\tilde{\eta}_{k^*}[s]$ as [98],

$$(\gamma_{k^*}[s]|\mathbf{z}, h_{k^*}, \Delta_{k^*}) = \frac{P_{k^*} g_{k^*}}{\text{Var}(\tilde{\eta}_{k^*}[s]|\mathbf{z}, h_{k^*}, \Delta_{k^*}) + \sigma^2}, \tag{3.30}$$

$$\gamma_{k^*}[s] = \frac{P_{k^*} g_{k^*}}{\text{Var}(\tilde{\eta}_{k^*}[s]|\mathbf{z}, h_{k^*}, \Delta_{k^*}) + \sigma^2}, \tag{3.31}$$

where $\mathbf{z}$ represents the latest detection status of the interfering symbols, i.e. correct or erroneous. Further, the error probability of sth symbol detection can be presented with respect to the $(\tilde{\gamma}_k[s]|\mathbf{z}, h_{k^*}, \Delta_{k^*}[s])$ as [98],

$$P(e_{k^*}[s]|\mathbf{z}, h_{k^*}, \Delta_{k^*}[s]) = 1 - \left(1 - Q\left(\sqrt{\frac{3.(\tilde{\gamma}_k[s]|\mathbf{z}, h_{k^*}, \Delta_{k^*}[s])}{2.(M-1)}}\right)\right)^2, \tag{3.32}$$

where, Q(·) represent the Q function and M denotes the order in M-QAM [99].

$$(\tilde{\gamma}_k[s]|\mathbf{z}, h_{k^*}, \Delta_{k^*}[s]) = \text{Var}(\tilde{\eta}_k[s]|\mathbf{z}, \Delta_{k^*}[s]) + \sigma^2 > d_{e_k^*} \tag{3.33}$$

where $d_{e_k^*}$ is half the distance between two nearest constellation points given by $\sqrt{\frac{3.P_{k^*} h_{k^*}}{2.(M-1)}}$ [100]. Further, the conditional error probability of the sth symbol detection can be obtained as [98],

$$P(e_{k^*}[s]|h_{k^*},\Delta_{k^*}[s]) = \sum_{i=1}^{2^{2(k_{opt}-1)}} P(e_{k^*}[s]|iP_{z(\mathcal{L})},h_{k^*},\Delta_{k^*}[s]).\prod_{k\in k_{opt},\zeta\in(s-1,s+1),k\neq k^*} Pr_{i,k}^{(\mathcal{L})}[\zeta], \quad (3.34)$$

where,

$$P(e_{k^*}[s]) = \frac{1}{\tau_{max}-\tau_{min}}.\int_{\tau_{min}}^{\tau_{max}}\int_{0}^{\infty} P(e_{k^*}[s]|h_{k^*},\Delta_{k^*}[s]).e^{-h_{k^*}}.dh_{k^*}.d\Delta_{k^*}[s], \quad (3.35)$$

$$P_{bit,k^*} = \frac{P(e_{k^*}[s])}{\log_2(M)}, \quad (3.36)$$

where $P(e_{k^*}[s])$, $P(e_{k^*}[s]|\alpha_{k^*},\Delta_{k^*}[s])$ denote respectively, the probability of error and conditional probability of error on the sth symbol of the k^*th user. Also, sth symbol of the k^* user is the desired symbol to be detected and M is the modulation order. Further, h_{k^*} denotes the magnitude of fading for the sth symbol of the k^*th user. The $\Delta_{k^*}[s]$ denotes the percentage of symbol time that the overlapping symbols of the ith user has on the sth symbol of the k^*th user. Moreover, iP_z, denotes probability of the ith permutation of $\mathbf{z}$, $1 \leq i \leq 2^{2(k_{opt}-1)}$ and $Pr_{i,k}[\zeta]$ denotes the probability of detection being correct or in error.

3.1.5.3/ Computational Complexity Analysis

The computational complexity of decoding K user data under Conv T-SIC and Cyclic T-SIC are presented as follows.

1. Conv T-SIC: The total interference to the desired symbol sth symbol of k^*th user, $\eta_{k^*}[s]$, is successively cancelled in Conv T-SIC process and hence the maximum computational complexity depends on the number of user devices, K, which is approximately of order $O(K^2)$ [84].
2. Cyclic T-SIC: The decoding process of the proposed method has a complexity of $O(k_{opt}^2)$, where $k_{opt} \leq K$. On top of that, the computational complexity for the stochastic gradient descent method based optimization in the Cyclic T-SIC scheme is in the order of $O(log(\frac{1}{\epsilon}))$ [84]. To sum up, the proposed Cyclic T-SIC method has a computational complexity of $O(log(\frac{1}{\epsilon})k_{opt}^2)$ per single decoding iteration. Further, it is proven from **Lemma 3** that the computational complexity in Cyclic T-SIC scheme is lower than the Conv T-SIC scheme.

Lemma 3. *The computational complexity of Cyclic T-SIC decoding of k_i users' data over n iterations is less than that of Conventional SIC decoding of K users' data in one iteration [84]. Note that k_i corresponds to k_{opt} in the i^{th} iteration and the sum of k_i equals K.*

$$\log\left(\frac{1}{\epsilon}\right)\sum_{i=1}^{n} k_i^2 \leq K^2, \quad (3.37)$$

where, $0.1 < \epsilon < 1$, $k_i \leq K$ and $\sum_{i=1}^{n} k_i = K$.

Proof. Consider

$$K = k_1 + k_2 + k_3 + ... + k_i + ... + k_{n-1} + k_n, \tag{3.38}$$

where $k_i \leq K$. Hence,

$$k_i^2 \leq K^2. \tag{3.39}$$

Further, it can be seen that,

$$\sum_{i=1}^{n} k_i^2 \leq \Big(\sum_{i=1}^{n} k_i \Big)^2, \tag{38a}$$

$$\sum_{i=1}^{n} k_i^2 \leq K^2. \tag{38b}$$

Moreover,

$$\log\Big(\frac{1}{\epsilon}\Big) \sum_{i=1}^{n} k_i^2 < K^2, \tag{39}$$

where $0.1 \leq \epsilon < 1$. □

3.1.5.4/ Analysis of the Numerical Simulation Results

In this Section, the numerical simulation results are presented to demonstrate the performance of the proposed system model and the algorithm. User terminals are considered to be randomly located within a radius of 100m to the corresponding receiving UE. Also, for a Monte-Carlo simulation analysis, 10^3 random A-NOMA D2D setups are considered. Different parameters used for simulation analysis are summarized in Table 6.1[2]. Furthermore, the performance of both the Conv T-SIC and Cyclic T-SIC are considered under the condition that each IC triangle formed across the received asynchronous NOMA signal is decoded for one iteration, i.e., $N_{\text{T-SIC}} = 1$.

Figure 3.4a depicts that the EE obtained via the proposed optimization algorithm converges to a stable value within a fixed number of iterations. However, the converging EE value decreases as the K increases. With the increment in the K, the total n_{sym} to be decoded increases, which considerably elevates E_c and reduces the EE. Furthermore, the number of iterations required to converge EE increases with the increment in K. This is mainly due to the fact that the vector size of $\boldsymbol{D_u}$ increments with K.

Figure 3.4b depicts the EE performance versus K with Cyclic and Conv T-SIC under different I_{th} values. It can be seen from the plot that EE decreases when the value K increases. The total n_{sym} symbols increment with K and hence result in a higher E_c. Moreover, when the I_{th} increases, n_{sym} increases and reduces the EE. It is also noteworthy that since Conv T-SIC is not optimizing the K, it is not impacted by I_{th}. Furthermore, in Conv T-SIC, the total K data are decoded during one decoding iteration which leads to a higher number of computations and thereby a higher E_c compared to Cyclic T-SIC. It is noteworthy that in Figure. 3.4a and Figure. 3.4b, Cyclic T-SIC, EE

[2]It is noteworthy that these given values can be modified to any other values depending on the specific scenario under consideration.

Table 3.1: Simulation parameters

Parameter	**Value**
Modulation order, M	16 QAM
Minimum relative symbol time offset, τ_{min}	0.01 sec
Maximum relative symbol time offset , τ_{max}	0.5 sec
Maximum initial energy of user device, E_{max}	1.08 kJ
Power dissipated by user device, P_{circuit}	0.01 W
Maximum transmit power, P_{max} [154]	0.2 W (23 dBm)
Path-loss exponent, η_p	1.5
Minimum throughput threshold, R_{min}	2 Mbits/sec
Interference threshold, (I_{th})	1.2W
Number of repeated times of T-SIC decoding, $N_{\text{T-SIC}}$	1
AWGN power, σ^2	0.01 W
Bandwidth, B	1 MHz
Symbol time duration, T_{sym}	1 sec
Error tolerance for optimal D_u, ϵ_1	0.1
Error tolerance for optimal λ, ϵ_2	0.5
Learning rates, α and β	0.4
Transmission power of an UE	[0,...,P_{max}]
Total number of UEs, K	[2,...25]
Relative symbol time offset, ϕ	[1 - 50]%.T_{sym}
Received power ratio, ν	[1,...,10]
Transmit SNR	[10,...,35] dBm

converges respectively under $K = 5, K = 10$ and $K = 15$, to 1.3×10^5, 8.3×10^4 and 6.4×10^4 bits per Joule at $I_{th} = 1.2W$. Similarly, under Conv T-SIC, EE converges respectively under $K = 5, K = 10$ and $K = 15$, to $7\times10^4, 3.6\times10^4$ and 2×10^4 bits per Joule at $I_{th} = 1.2W$.

Figure 3.4c depicts the variation of EE against the received power ratio, ν. It is seen from the plot that the EE increases as ν increments in both Cyclic and Conv T-SIC schemes. P_k increases with the elevation of ν, which leads to the increment in γ_k and the average sum throughput, which improves the EE. Moreover, Cyclic T-SIC has a significant improvement in comparison to Conv T-SIC, because the increment in ν enables the optimization algorithm to derive $\boldsymbol{D_u}$ easily due to the distinct P_k levels of each user. Hence, the $\boldsymbol{D_u}$ derivation enables the optimal data symbols to be decoded. Also, a convergence in EE in the Cyclic T-SIC is observed when $\nu \geq 5.0$. This is due to the thresholds in the optimization algorithm which limits the k_{opt} decoded per iteration.

Furthermore, it can be seen from the Figure. 3.4b and Figure. 3.4c that Cyclic T-SIC, EE converges respectively under $K = 5, K = 10$ and $K = 15$, to 1.3×10^5, 8.3×10^4 and 6.4×10^4 bits per Joule at $\nu = 5$. Similarly, under Conv T-SIC, EE converges respectively under $K = 5, K = 10$ and $K = 15$, to $7\times10^4, 3.6\times10^4$ and 2×10^4 bits per Joule at $\nu = 5$. In this scenario, the Cyclic T-SIC has relative EE gains by 52.5%, 32.8%, and 38.1% compared to Conv T-SIC under $K = 5, K = 10$, and $K = 15$.

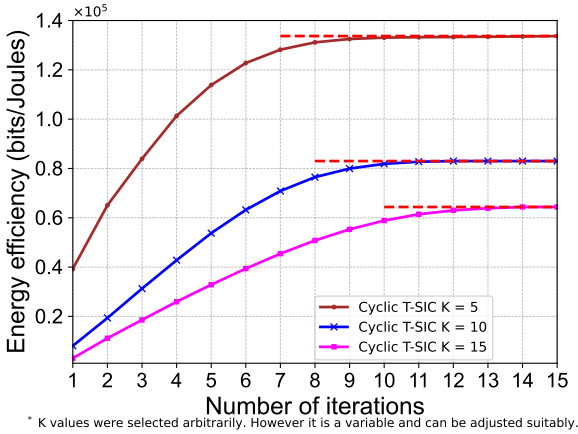

(a) Convergence of EE against the number of iterations. Parameters: ν = 5, I_{th} = 1.2 W, ϕ = 50%.

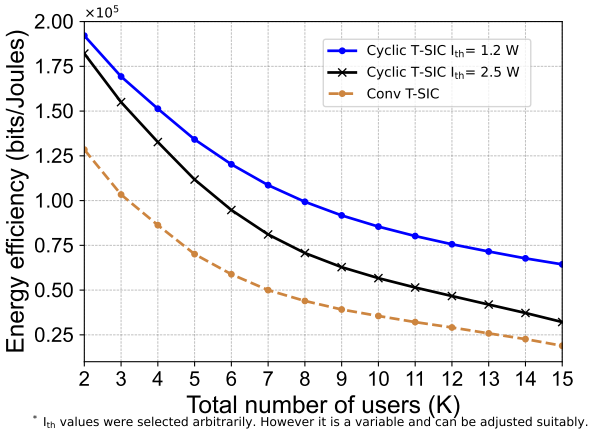

(b) EE vs total number of users under varying I_{th}. Parameters: ν = 5, ϕ= 50%.

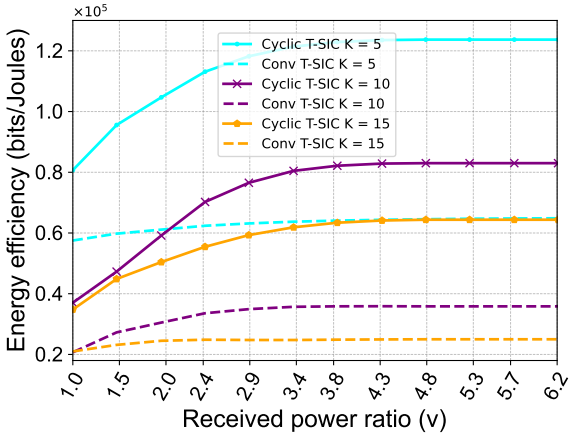

(c) Energy efficiency vs ν under varying number of users. Parameters: I_{th} = 1.2 W, ϕ= 50%.

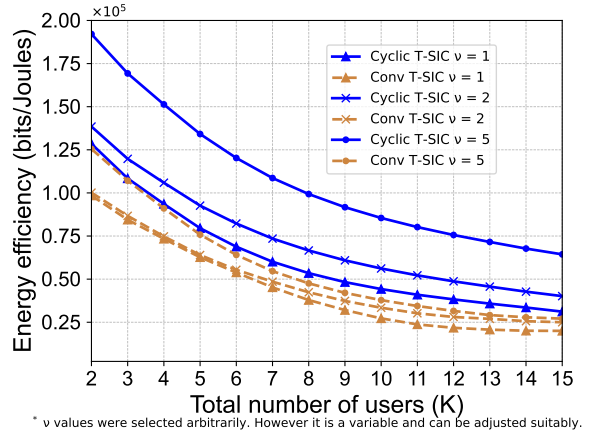

(d) EE vs total number of users. Parameters: I_{th} = 1.2 W, ϕ= 50 %, transmit SNR = 23 dBm.

Figure 3.4: EE performance under various scenarios.

Figure 3.4d illustrates the variation of EE against K under different ν values. Further, with the elevation in νs, an increment in EE of the Cyclic T-SIC is observed because $\boldsymbol{D_u}$ is derived optimally considering the significant gaps between each k users in terms of γ_k.

Further, it can be observed that consistent results are obtained in Figure. 3.4c and Figure. 3.4d. In Cyclic T-SIC, EE converges respectively under $\nu = 1, \nu = 2$ and $\nu = 5$, to 4×10^5, 6×10^4 and 8.3×10^4 bits per Joule at $K = 10$. Similarly, under Conv T-SIC, EE converges respectively under $\nu = 1, \nu = 2$ and $\nu = 5$, to $2 \times 10^4, 3.2 \times 10^4$ and 3.6×10^4 bits per Joule at $K = 10$.

Figure 3.5a depicts the average BER against K under Cyclic T-SIC and Conv T-SIC. The BER of both schemes increment against K since with a higher K, the γ_k difference among user data decreases. This lowers the accuracy of the received data detection, which impacts the decoding process. Moreover, the average BER in Cyclic T-SIC is lower than Conv T-SIC. The main reason behind this is that the Cyclic T-SIC scheme derives

the optimal k_{opt} to decode based on the $\boldsymbol{D_u}$ derived. The availability of distinct γ_k values between the user data decoded in the Cyclic T-SIC scheme increases the accuracy in decoding. Further, the Cyclic T-SIC decodes all K data over successive iterations by taking into consideration of the γ_k of each user data. Conversely, Conv T-SIC decodes such data in a single iteration, which increases the BER.

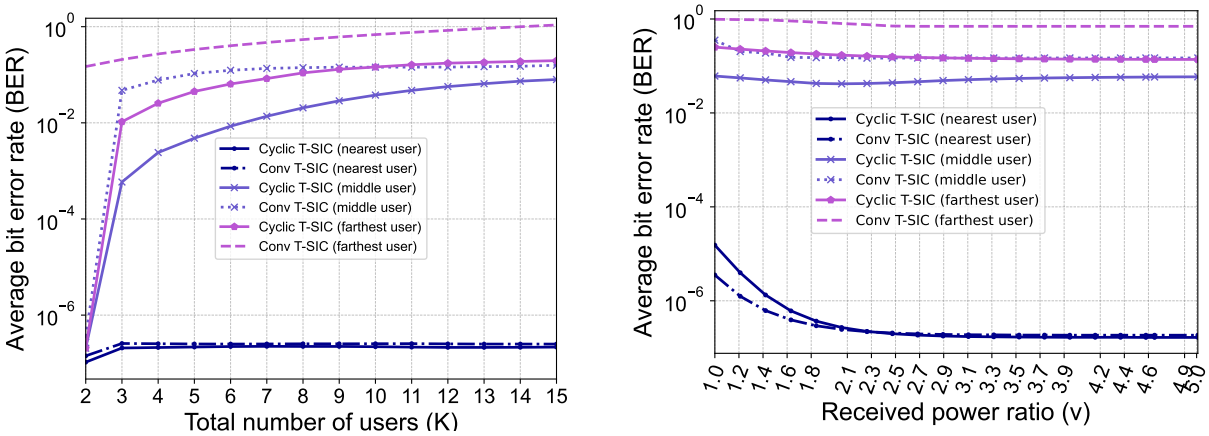

(a) BER vs number of users (K). (b) BER vs received power ratio (ν).

Figure 3.5: BER analysis of nearest, middle, and farthest users under Cyclic and Conv T-SIC schemes. Parameters: ν = 2, I_{th} = 1.2 W, transmit SNR = 23 dBm, $\phi = 50\%$, K = 10.

Figure 3.5b depicts the BER against the ν for the nearest user, middle user, and farthest user. A significant BER gap is seen between the nearest user and middle user. As ν increases, a comparable γ_k level difference is seen between the near user and far user. Hence, the decoding accuracy reduces as the γ_k gap increases between consecutive users. The highest γ_k level is received from the nearest user. Under $\nu < 2$, the Cyclic T-SIC has a higher BER than Conv T-SIC. The reason being that the when $\nu < 2$, the interference faced by the nearest user is higher than the estimated interference using Cyclic T-SIC. In the proposed optimal $\boldsymbol{D_u}$ of Cyclic T-SIC, only a set of selected users are decoded assuming that the interference from the remaining users is minimum. Hence, the decoding error is higher than Conv T-SIC. Meanwhile, as $\nu \gtrapprox 2$, the interference from the remaining users on the near user is less significant and hence the decoding accuracy is high and similar to Conv T-SIC. Furthermore, for the middle and farthest users' BER of Cyclic T-SIC is lesser compared to Conv T-SIC. In the middle and farthest user case, the γ_k of the consecutive users is minimum that Cyclic T-SIC decodes the user data during a successive iteration of Cyclic decoding utilizing the retransmissions from the transmitters. Thereby, the γ_k level of the received signals from the middle and farthest users are sufficiently high enough during the successive iteration since the stronger signals also do not interfere.

Figure 3.6a depicts the BER performance against the transmit SNR under the Cyclic T-SIC and Conv T-SIC schemes. BER in Cyclic T-SIC is lower than Conv T-SIC for the case where transmit SNR is < 23 dBm. The optimal $\boldsymbol{D_u}$ derivation depending on the γ_k levels

of each kth user and I_{th} constraint increases the accuracy of decoding. Meanwhile when the transmit SNR $\gtrapprox 23$ dBm, BER of Cylic T-SIC $>$ BER of Conv T-SIC. The difference between γ_k levels of each kth user is less significant when all users transmit at SNR $\gtrapprox 23$ dBm. Hence, The optimal $\boldsymbol{D_u}$ derivation is less accurate, thereby increasing the BER in Cyclic T-SIC.

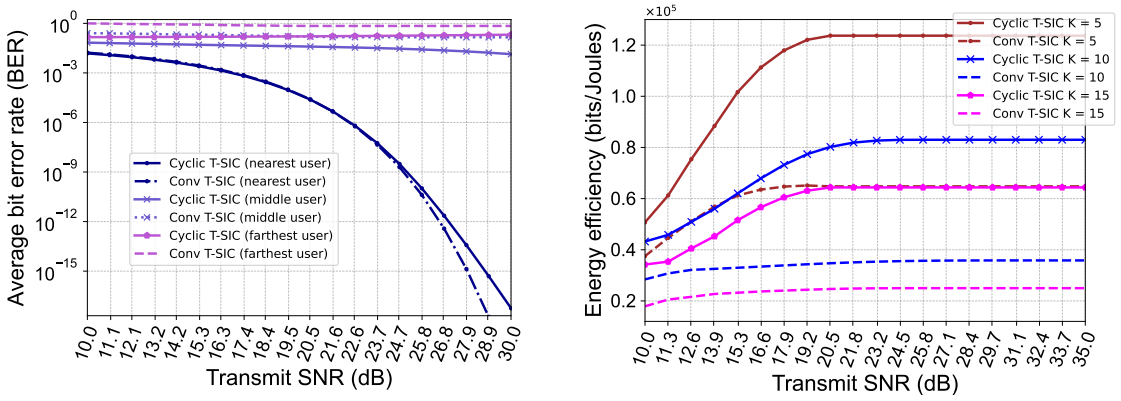

(a) BER vs transmit SNR for ν = 2.

(b) EE vs transmit SNR for ν = 5.

Figure 3.6: BER and EE analysis of the proposed Cyclic T-SIC. Parameters: I_{th} = 1.2 W, ϕ = 50%, K = 10.

Moreover, Figure 3.6b depicts that the EE of the proposed system is higher than Conv T-SIC, because the optimal $\boldsymbol{D_u}$ reduces the E_c per decoding iteration. Moreover, with a lower transmit SNR, a higher EE can be gained using Cyclic T-SIC compared to the Conv T-SIC scheme. Jointly considering the results obtained in Figure. 3.4d and Figure. 3.6b, following insights can be drawn. In Cyclic T-SIC, EE converges respectively under $K = 5, K = 10$ and $K = 15$, to 1.3×10^5, 8.3×10^4 and 6.4×10^4 bits per Joule at transmit SNR $= 23$ dBm. Similarly, under Conv T-SIC, EE converges respectively under $K = 5, K = 10$ and $K = 15$, to $7 \times 10^4, 3.6 \times 10^4$ and 2×10^4 bits per Joule at transmit SNR $= 23$ dBm.

Figure 3.7a represents the BER performance against the relative symbol time offset, ϕ, between users under Cyclic and Conv T-SIC schemes. The BER performance worsens with the increment in ϕ since the co-channel interference increases. However, the Cyclic T-SIC has a reduced BER because of deriving the optimal $\boldsymbol{D_u}$ to select n_{sym} decoded per iteration based on the I_{th}. Figure 3.7b, depicts that the EE of Cyclic T-SIC is higher than Conv T-SIC, although the co-channel interference between users increased with the ϕ. The optimization of number of user data decoded based on the I_{th} limits the k_{opt} decoded per iteration. This results in reducing the interference among the symbols which are decoded and improves the EE of Cyclic T-SIC compared to Conv T-SIC. Further, it is observed that a lower BER and higher EE can be obtained using the Cyclic T-SIC scheme, even if the ϕ increases the asynchrony among the received data signals. In addition, EE starts converging after the $\phi \gtrapprox 0.3$. BER converges since I_{th} and minimum rate thresholds are reached with the $K = 10$ and hence the same $\boldsymbol{D_u}$ is obtained, and the n_{sym} reaches a maximum limit.

In Cyclic T-SIC, EE converges respectively under $K = 5, K = 10$ and $K = 15$, to 1.3×10^5,

8.3×10^4 and 6.4×10^4 bits per Joule at transmit SNR $= 23$ dBm and $\phi = 50\%$, proving the consistency between results obtained in Figure. 3.6b and Figure. 3.7b. Similarly, under Conv T-SIC, EE converges respectively under $K = 5, K = 10$ and $K = 15$, to $7\times10^4, 3.6\times10^4$ and 2×10^4 bits per Joule at transmit SNR $= 23$ dBm and $\phi = 50\%$.

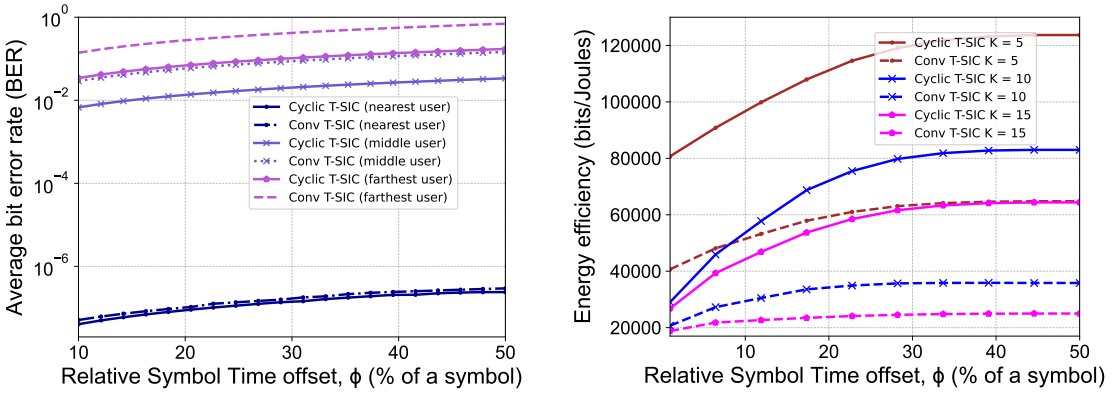

(a) BER vs ϕ for $\nu = 2$.

(b) EE vs ϕ for $\nu = 5$.

Figure 3.7: BER and EE analysis of the proposed Cyclic T-SIC against relative symbol time offset. Parameters: I_{th} = 1.2 W, ν = 5, transmit SNR = 23 dBm, K = 10.

Figure. 3.7a depicts the BER performance of nearest, middle, and farthest users against ϕ. In general, the BER performance worsens with the increment in ϕ since the co-channel interference increases. The BER of the nearest user of both Cyclic and Conv T-SIC schemes are nearly similar since, the nearest user data has a significant γ_k level in both schemes which increases the accuracy of decoding its data. Moreover, the Cyclic T-SIC of both middle and farthest users have significantly reduced BER compared to Conv T-SIC because of decoding their data in successive iterations of Cyclic T-SIC with the use of retransmissions. This leads to deriving the optimal $\boldsymbol{D_u}$ and selecting n_{sym} decoded per iteration based on the I_{th}.

Moreover, consistent results are obtained in Figure. 3.5a, Figure. 3.5b, Figure. 3.6a and Figure. 3.7a under $K = 10$, $\nu = 2$, transmit SNR $= 23$ dBm and $\phi = 50\%$. The BER value of respectively the nearest user, middle user, and farthest user converges to approximately 2.2×10^{-7}, 0.037 and 0.14 under Cyclic T-SIC. The BER value of respectively the nearest user, middle user, and farthest user converges approximately to 2.2×10^{-7}, 0.15 and 0.68 under Conv T-SIC.

Figure 3.8a depicts the theoretical computational complexity against K under Cyclic and Conv T-SIC schemes. The curve with the Cyclic T-SIC has a considerably lower complexity compared to the Conv T-SIC. In Cyclic T-SIC, the user data are decoded in sequential iterations, where only $k_{\text{opt}} \leq K$ data is decoded per iteration. In contrast, Conv T-SIC decodes the total K data in a single iteration. Hence, a complexity reduction of 56.14% by Cyclic T-SIC over Conv T-SIC is observed in this case.

Figure 3.8b depicts the total simulation delay against K under Cyclic T-SIC and the Conv T-SIC schemes. The average simulation delay in Cyclic T-SIC is lower than that of Conv T-SIC. As K increases, the decoding delay increases in Conv T-SIC decoding. In con-

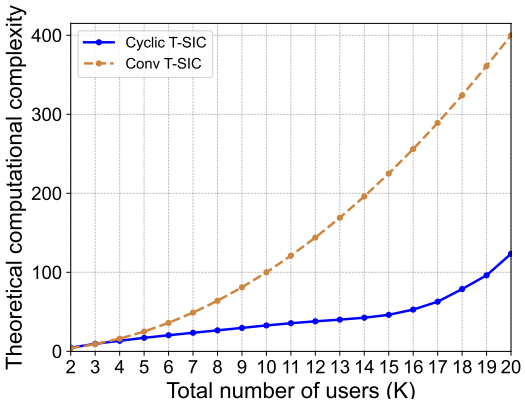

(a) Computational complexity vs K.
Parameters: I_{th} = 1.2 W, ν = 5, ϕ= 50%.

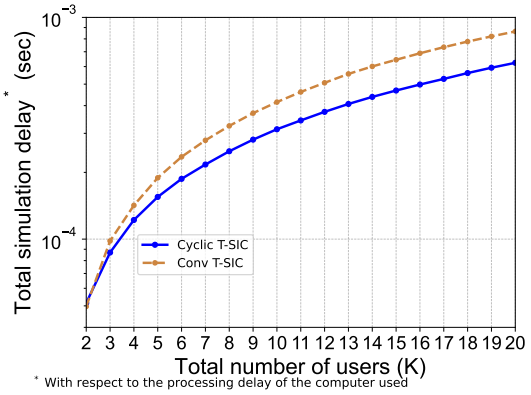

(b) Total simulation delay vs K.
Parameters: I_{th} = 1.2 W, ν = 5, ϕ= 50%.

Figure 3.8: Computational complexity and simulation delay of proposed Cyclic T-SIC.

trast, the delay is less in Cyclic T-SIC since $k_{opt} \leq K$ per decoding iteration. The delay decreases with the successive iterations as the k_{opt} data decoded in such iterations decreases. Also, the Cyclic T-SIC achieves a simulation delay reduction of 22.44% compared to Conv T-SIC in this case. Note that the complexity reduction of the proposed scheme is in Figure. 3.8a is significantly higher than the simulation delay in Figure. 3.8b. Complexity analysis is done under theoretical assumptions and in contrast simulation delay is measured with respect to the processing delay of the computer used. Hence, depending on the processing speed and other hardware delays, the corresponding decoding delay of the proposed scheme is varying as in Figure. 3.8b.

3.2/ Optimization of Secure Emergency Call Services in Asynchronous-NOMA D2D Network

Reliable emergency call services are required to save victims during catastrophes in a timely manner. The presence of jammers in disaster areas can impact the reliability of emergency call transmissions. The upcoming cellular networks with faster data rates are expected to facilitate reliable connectivity in various communications in autonomous driving, unmanned aerial vehicle (UAV) networks, remote monitoring, emergency communications [19]. However, an immensely increased number of devices and high usage of virtualization and the cloud will lead to many multifaceted security threats, hazards, and jamming attacks. Moreover, the industry should strive to maintain a high standard of 5G security to realize healthy and robust communication in the future.

Hence, enhancing the secrecy capacity of the wireless communication networks has become one of the research focuses in the B5G/6G networks [155]. Moreover, D2D-assisted multi-hop emergency protocols have been proposed for emergency call transmissions [152]. In D2D networks, due to the distributed locations of the transmitters, signals arrive at the receiving terminal with varying time offsets and hence, time-synchronous data

reception is not possible. In [98], an A-NOMA scheme is proposed for enhancing spectral efficiency and reducing the BER of the communication. Hence, in this work, a novel binary optimization problem is proposed for optimal data detection which will enhance the secrecy capacity of an A-NOMA-assisted D2D communication under the presence of jamming users. Further, the secrecy capacity of the proposed optimized scheme is compared with the conventional secrecy capacity values.

3.2.1/ System Model and Problem Formulation

3.2.1.1/ System Overview

We assume a multi-hop emergency call forwarding system for a network area under a disaster, where D2D uplink transmissions are occurring between a $k \leq K$ number of victim/relay nodes (e.g., Victim A, Victim B, etc), and $r \leq R$ number of receiving victim/relay nodes (e.g., Victim C, etc) as shown in Figure 3.9. However, such k transmitters can comprise an equal number of both $m \leq K$ legitimate users, and $e \leq K$ jamming users, and $m + e = K$. It is assumed that such e nodes (e.g. Jammer A, etc) send a noisy data signal toward the receiver nodes to deteriorate its decoding ability. Moreover, all users are geographically distributed within a small local neighborhood. Hence, the total K users share a single subcarrier out of a total of N subcarriers that are allocated to the D2D communication system. In addition, in the realistic channel conditions, we assume that the signals are affected through propagation delays, and hence, signals between transceivers are received asynchronously. Thus, an A-NOMA scheme is utilized to decode the received data signals.

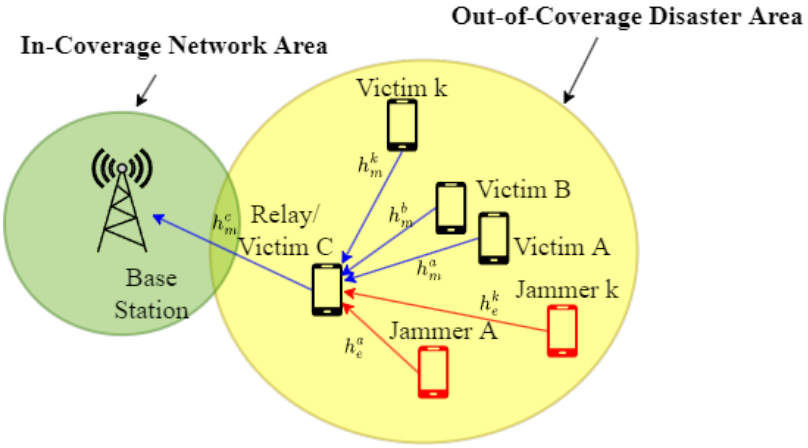

Figure 3.9: Asynchronous-NOMA uplink scheme for D2D Emergency Call Forwarding Services.

The received signal for the k^{th} user at sth symbol is given as,

$$y^k[s] = h^k . \sqrt{P^k} . x^k[s] + \eta_{k,i}^k[s] + n_0, \tag{3.40}$$

where $k \in \{\text{Victim } k, \text{Jammer } k\}$ and $x^k[s]$ denotes the sth symbol of the k^{th} user's data

which is complex and generated by a higher modulation M-ary QAM symbol mapper. P^k denotes the transmission power of k^{th} user, h^k denotes the k^{th} user CSI and $\eta^k_{k,i}[s]$ denotes the interference from other ith users on the desired k^{th} user's sth symbol. Additionally, the received SINR of the k^{th} user, γ^k, is formed as,

$$\gamma^k = \frac{P^k g^k}{\text{Var}(\eta^k_{k,i}) + \sigma^2}, \tag{3.41}$$

where the channel gain of k^{th} user, thermal noise variance are given by g^k, σ^2 respectively. The γ^k_m of the m^{th} user $\gamma^k_m = \frac{P^k_m g^k_m}{\text{Var}(\eta^k_{m,i})+\sigma^2}$. It is assumed that the receiver detects the presence of a jammer e during the post processing stage and the γ^k_e of such an e user $\gamma^k_e = \frac{P^k_e g^k_e}{\text{Var}(\eta^k_{e,i})+\sigma^2}$.

3.2.1.2/ Optimization

The objective is to detect the optimal combination of s symbols of each k user which maximizes number of decoded symbols, n_{sym}, of the A-NOMA transmissions under the presence of e users. Further, a binary decision vector of the optimal data symbols to be decoded is introduced as $\boldsymbol{D} = [D_k]_{k\in\mathcal{K}}$, where $D_k = 1$ if the data symbols of the k^{th} user are selected to be decoded, and $n_{sym} = \sum_{k=1}^{K} D_k(K-k+1)$. The number of symbols decoded per each k^{th} user is $(K-k+1)$ under the T-SIC decoding scheme proposed in [98] for A-NOMA schemes. Hence, an optimization problem is formed as, ,

$$\underset{\boldsymbol{D}}{\text{maximize}} \quad \sum_{k=1}^{K} D_k(K-k+1) \tag{3.42a}$$

$$\text{subject to} \quad c_r \geq 0, \tag{3.42b}$$

where,

$$c_r = D_k\left[\left\{B\log_2\left(1+\gamma^k_m\right) - R_{\text{min}}\right\} - \left\{R^e_{\text{max}} - B\log_2\left(1+\gamma^k_e\right)\right\}\right]^+, \tag{3.43}$$

here $[]^+$ represents a positive quantity, which means that (3.43) is valid is positive or $\gamma^k_m \geq \gamma^k_e$ and $R^e_{max} \geq R_{\text{min}}$. The solutions derived from such an optimization problem is used thereby to maximize the sum-secrecy capacity, C_s, of the communication system given as [155],

$$C_s = \sum_{k=1}^{K} D_k \log_2\left(\frac{1+\gamma^k_m}{1+\gamma^k_e}\right). \tag{3.44}$$

Further, k^{th} user data with $D_k = 1$ are decoded while the remaining users' data are decoded upon the reception of retransmissions from such users.

3.2.2/ Performance Analysis

The performance of the proposed algorithm is evaluated for a D2D A-NOMA transmission with three m users and three e users. For simplicity, a unit total bandwidth of 1 Hz, equal P_m^k for each m user and equal P_e^k for each e user, and a channel with Rayleigh fading is considered. In addition, $R_{\min}$ and R_{max} are set to 1 Hz and 10 Hz respectively. The distance gap between the transmitters and its associated receiver is uniformly distributed in [0m, 100m]. Further, the noise level of the channel n_0 is set to 0.1W.

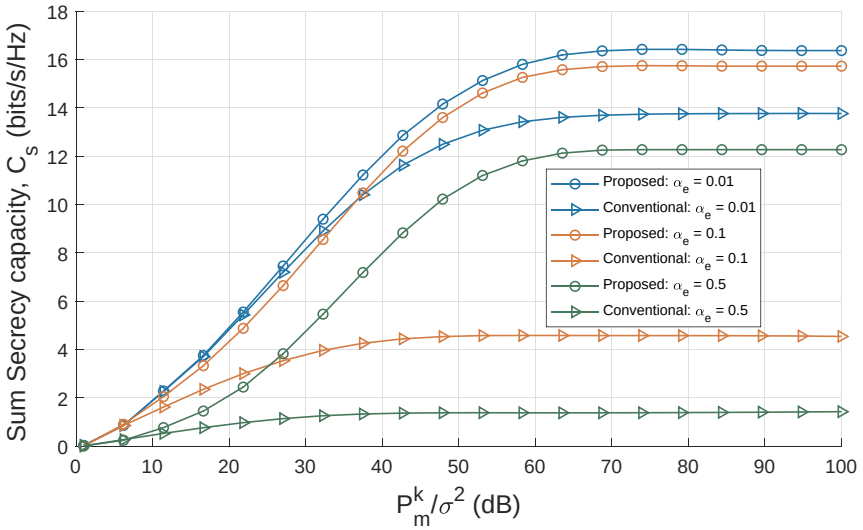

Figure 3.10: Sum secrecy capacity vs P_m^k/σ^2 in an A-NOMA assisted D2D uplink communication under different α_r values.

Figure 3.10 depicts the variation of C_s against the transmit SNR at the legitimate user, under different $\alpha_r = \frac{P_e^k}{P_m^k}$ values. Variation of C_s is considered under the proposed scheme and compared with the conventional C_s under $\alpha_r \in 0.01, 0.1, 0.5$. It is seen that as the α_r increases, the C_s decreases. The reason is that as jammer's γ_e^k increases, the $\log_2(1 + \gamma_e^k)$ increases and hence C_s decreases. Moreover, it is seen that the proposed scheme achieves a higher C_S value compared to the conventional C_s when the transmit SNR of the legitimate m user is increased. The $D_k = 0$ for the k^{th} user data with $\gamma_e^k > \gamma_m^k$, and hence such data are omitted from decoding and only the reliable data with $\gamma_e^k \leq \gamma_m^k$ are decoded. Meanwhile, in the conventional C_s, the k^{th} user data with $\gamma_e^k > \gamma_m^k$ result in $C_{s_k} \leq 0$. In addition, the achievable C_s converges as the optimal D_k vector is reached under the constraint imposed by c_r. To sum up, the proposed scheme C_s becomes higher than the conventional C_s and it was observed that the proposed scheme achieves a C_s gain of 30.7%, 75.4%, 84.0% under α_r values of 0.01, 0.1, and 0.5, than the conventional C_s.

3.3/ Conclusion

The first section of this Chapter introduced a Cyclic T-SIC scheme to improve the de-

coding complexity, energy consumption, and BER of a superimposed signal received in a massive D2D network using an A-NOMA system. The performance of the proposed scheme was evaluated through computer simulations and was seen to have significantly improved energy efficiency compared to the traditional Conv T-SIC scheme. The optimization algorithm in Cyclic T-SIC allowed the receiver to identify the optimal symbols to decode while taking into account co-channel interference and data rate constraints. Additionally, it was found that Cyclic T-SIC achieved lower BER and higher energy efficiency, even when the received data signals were asynchronous with a phase shift of $\phi \gtrapprox 0.3$. When the transmit signal-to-noise ratio (SNR) was ≥ 23 dBm and the parameter $\nu \geq 5.0$, there was also a convergence in energy efficiency and BER in Cyclic T-SIC due to the threshold in the optimization algorithm that limits the number of symbols decoded per iteration. Additionally, Cyclic T-SIC had lower decoding complexity and delay because it only decoded a maximum of $k_{opt} \leq K$ symbols per iteration. The second section of this chapter investigated the problem of improving the achievable capacity C_s in an A-NOMA-enabled D2D communication system in the presence of jammers during a disaster scenario. A binary optimization algorithm was proposed to reliably detect data at the receiver by considering the γ values of both legitimate users and jammers. The results showed that the proposed optimized scheme outperforms the conventional C_s with gains of 30.7%, 75.4%, and 84.0% under α_r values of 0.01, 0.1, and 0.5, respectively.

4

Outband D2D-assisted Multi-Hop Emergency Call Protocol Design

In the previous chapter, a new method called Cyclic T-SIC A-NOMA was proposed to improve the decoding complexity, energy consumption, and BER of a superimposed signal received in a massive D2D network. In this chapter, we introduce multi-hop communication protocols named M-HELP and 5G-SOS, which allow relaying of emergency calls using D2D in out-of-coverage, particularly after a disaster situation. The destruction of the cellular network infrastructure makes necessary the use of D2D communications extend the network coverage. Furthermore, during disaster situations, there is a rapid increase in network traffic as a result of emergency calls. As a solution, the Asynchronous NOMA D2D mode, which was explained in the previous chapter, is essential in guaranteeing the reliable decoding of the large amount of data that is received. In this chapter, we study the best way to guarantee the transfer of emergency calls to the network. In the next chapter, we discuss the victims' localization scheme using the data received over the proposed multi-hop protocols. During disasters such as earthquakes and floods, mobile networks are frequently used to ensure communication between potential victims and functional gNBs connected to the core network. However, in some cases, a fraction of gNBs in a particular network area may be entirely destroyed, leaving them with no access to other gNBs or the core network. To address this problem, a distributed emergency call protocol called M-HELP is proposed in this chapter, which is compatible with 3GPP standards and can be implemented in a completely distributed manner in 4/5G-enabled mobile networks. The protocol takes advantage of the high density of mobile devices and the progress in outband D2D communication to extend both mobile and network coverage. We assess the efficiency of M-HELP under various scenarios that represent different degrees of network destruction and different emergency call conditions. The results show that M-HELP has a significant impact on the transmission success rate, energy management, latency, and control traffic load.

4.1/ Related Work

In this section, we discuss the literature concerning cellular network resiliency and disaster mitigation. The resiliency of the cellular network refers to the ability of the system to resist the disaster effects without additional resources and using redundancies and topological features. Disaster mitigation refers to the actions envisaged after a disaster including the mobilization of additional devices.

Multiple works of the literature [21, 160, 169] address the resilience and self-adaptation of the mobile networks to face a disaster affecting the network infrastructure using various mechanisms. Table 4.1 presents the research works on recovery solutions for wireless networks. The extended architecture-based approaches complicate the 3GPP compatibility in communications and add extra infrastructure costs. In this case, external or movable physical units, such as satellite [158] or UAV [156, 157, 159, 170], are deployed to rapidly work as a stand-in for damaged network facilities.

Moreover, resilient architecture-based approaches are less disruptive to the 3GPP specifications. In [161], the authors proposed to relax the dependencies between UEs, gNBs, and the core network. The objective is to provide more resilience against link disruptions by using the virtualization/redundancy of the links and functionalities. Although this approach is efficient for localized perturbations, it remains inefficient when the disaster's impact is over a large geographical area. The application-based approaches try to manage the reliability and robustness issues on the service layer [162, 163]. The application has to detect the communication failure and has to adapt the transfer mode accordingly (use of other wireless technology, other coding schemes, data substitution, etc.).

The resilient protocol-based approach is widely discussed for ad-hoc networks [164, 165]. However, those protocols are incompatible with 5G network specifications. Some resilient-based protocols compatible with the 3GPP standard are proposed such as [166, 167]. Nevertheless, most of these protocols can not be used in an out-of-coverage situation when the disaster affects the network infrastructure.

Even if dealing with disaster situations is well studied in ad-hoc network literature [7–9], the projection of those solutions over 4/5G cellular standards is rarely studied and remains difficult. Furthermore, the UE or network nodes are not owned by the system itself, making the protocol possibilities more regulated and constrained than in private/community networks such as MANET and VANET systems [5, 6]. Moreover, the conception of emergency call service for 4/5G networks requires taking into account the strict and closed 3GPP recommendations specifying what could be done or not. Therefore, the emergency call protocol has to be as light as possible with less control and redundancy traffic.

Further, technologies such as PTT [27, 28] and D2D are dedicated to well-deployed local networks and hence are not adapted to a sudden surge in network demand due to a disaster or to a dysfunctional cellular network with large out-of-coverage areas. Few works of the literature dealt with the resilience and self-adaptation of mobile networks after a disaster that impacts the network infrastructure and causes a high amount of emergency calls. In [171], the authors proposed to reshape the mobile network architecture in order

Table 4.1: Existing works in the literature on wireless network recovery.

Related Work	**External architecture**	**Resilient architecture**	**Resilient application**	**Resilient protocol**	**3GPP compatible**	**Out-of-coverage**
UAV-Assisted Attack Prevention, Detection, and Recovery of 5G Networks [156]	x					x
Post-Disaster 4/5G Network Rehabilitation Using Drones: Solving Battery and Backhaul Issues [157]	x					x
Integration of satellite and LTE for disaster recovery [158]	x					x
UAV-Empowered Disaster-Resilient Edge Architecture for Delay-Sensitive Communication [159]	x					x
On the Disaster Resiliency within the Context of 5G Networks: The RECODIS Experience [160]		x			x	
Enabling Disaster Resilient 4G Mobile Communication Networks [161]		x			x	
Terrestrial Trunked Radio-Tetra: A Global Security Tool [162]			x		x	
Towards Failure Resiliency in 5G: Service Shifting [163]			x		x	
Ad-hoc network recovery after severe disaster [164]				x		x
A mobile ad-hoc network multi-path routing protocol based on biological attractor selection for disaster recovery communication [165]				x		x
D2D Multihop Energy-Efficient Routing and OFDMA Resource Allocation in 5G Networks [166]				x	x	
Assisted Routing Algorithm for D2D Communication in 5G Wireless Networks [167]				x	x	
FINDER: A D2D based critical communications framework for disaster management in 5G [44]				x	x	x
M-HELP (Our approach) [168]				x	x	x

to relax the dependencies between UEs, gNBs, and the core network. The objective of such works is to provide more resilience against link disruptions. This kind of approach, based on virtualization/redundancy of links and functionalities, is efficient for localized perturbations and is inefficient when the disaster impact is larger.

Other works such as [1] and [38] focus on the recovery aptitude of the networking system after a disaster. These approaches envisage the use of movable physical units to rapidly work as a stand-in for damaged network facilities. In [172], a satellite system in conjunction with a terrestrial mobile network is studied. In [173], the use of UAVs in disaster-hit areas is investigated. The main drawbacks of these approaches are linked to the cost of additional devices deployment and the time needed for their deployment (responsiveness issue).

Furthermore, in Figure 4.1, we summarize the different approaches to public safety service. We show by this figure that our method represents a mix of the two main approaches aiming to improve the network resiliency and use of D2D proximity protocols. The network resiliency approach tries to maintain the connectivity of users' terminals to the network while proximity service techniques try to provide local services without the need for the core network.

This chapter investigates an understudied way of using an enhanced D2D protocol to overcome network shortcomings. The idea is to use the terminal devices as relay stations for directing emergency calls to the fully functional gNBs.

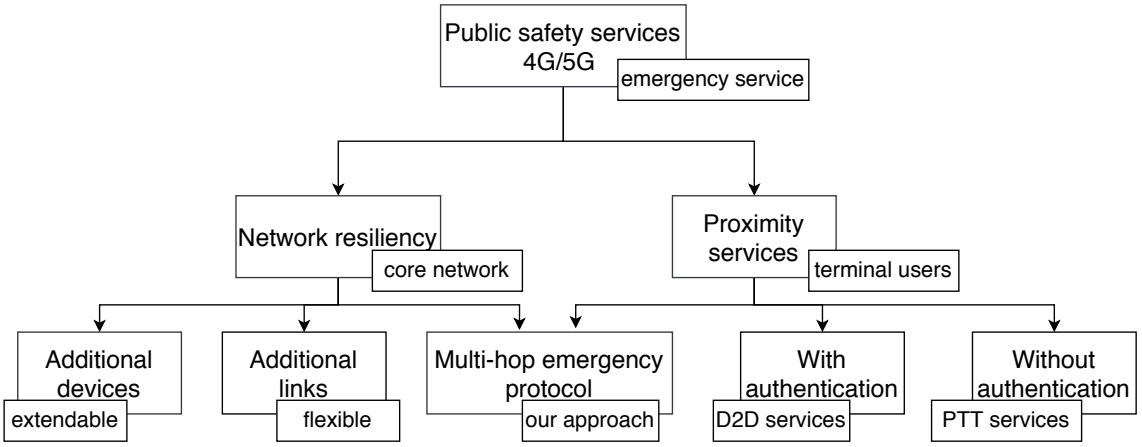

Figure 4.1: Taxonomy of public safety research works. Our approach proposes an enhanced D2D that also improves network resilience.

Amongst the rare works on the massive use of D2D mechanisms to overcome large disaster situations, mention may be made of FINDER protocol [47]. In FINDER algorithm, mobile devices organize themselves into hierarchical clusters and route emergency calls to working gNBs. Here the whole region under the out-of-coverage area is divided into different clusters. Each cluster has a cluster head (CH) selected by the members of the cluster. The mobile nodes, in each cluster, send the data to the CH and the CH aggregates the data and sends it to the nearest active gNB via multi-hop D2D communications, using a neighboring CH as a relay.

4.2/ System Model

An overview of the system model considered to design and implement the emergency call protocols for multi-hop relaying from out-of-coverage regions to network infrastructure is presented in this section. It is assumed that $m \in M_d$ are 4/5G emergency service-enabled UEs. In such a network area, each m can behave both as an emergency call initiator and relay. Since a disaster scenario is evaluated, it is assumed that each m is stationary and its location is fixed at the initial period just after the disaster. Furthermore, two modes of transmission, D2D and classical, are utilized to forward the emergency calls to the network infrastructure, as illustrated in Figure 4.2. In this example, three UEs (M_3, M_4, and M_5) are in an emergency and out of coverage due to the failure of the covering gNB.

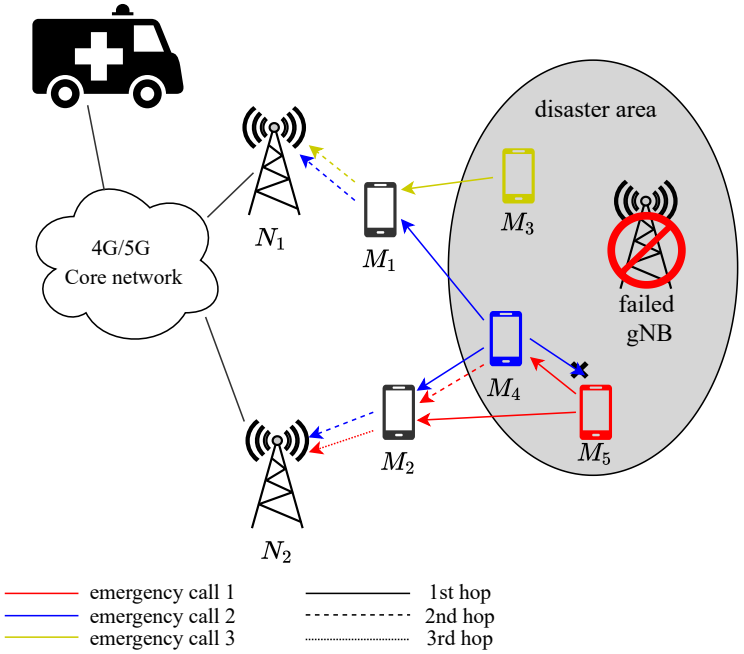

Figure 4.2: The proposed emergency call service architecture. Emergency UEs in the disaster area forward their calls in the direction of the functioning gNBs via relay UEs in the neighborhood. Distinct emergency calls generated by each emergency UE are represented by the color of the arrow. Solid lines indicate the D2D communication mode, while dashed lines indicate the classical communication between gNB and UE.

4.2.1/ Informational Model

Each device $m \in M_d$ is characterized by the following data:

- Current battery level (residual energy), $\text{SoC}_m \in [0, 100]$;
- Coverage status by at least one gNB, $\text{Ic}_m \in \{0, 1\}$:
  The coverage status is one if the UE has at least one direct communication link with a gNB $n \in N$. When a UE is out of coverage $\text{Ic}_m = 0$.

- GPS localization accuracy, $\text{LocAcc}_m \in [0.001, 1]$:
  Location information is obtained using GPS. It is assumed that the error in such a GPS measurement is represented by the distance between the actual position and the estimated position of m, $\delta_m \in [0..\infty]$ measured in meters. Hence, LocAcc_m is modeled as (4.1),

$$\text{LocAcc}_m = \frac{1}{\delta_m + 1} m^{-1}. \tag{4.1}$$

- RSSI detected, RSSI_m:
  The broadcast physical layer synchronization signals (PBCH) periodically transmitted by the operational gNBs enable the UEs to establish quality indicators, including RSSI, Reference Signal Received Power (RSRP), Reference Signal Received Quality (RSRQ), SINR, and Channel Quality Indicator (CQI) up to 75 km from the gNB [174, 175]. These measured indicators are useful in the selection of the best paths toward the nearest operational gNB.

  The RSSI indicator [176] is measured by each UE to estimate the strongest signal received from the surrounding operational stations $g \in N$ as shown in (4.2). The RSSI value depends on device location and more specifically on the signal path loss [176] between the gNBs and the device. Signals' path loss, namely $P_l(d, f)$, is varied due to the propagation parameters such as the distance between gNB and receiver UEs, height and location of UEs, transmission frequencies, terrain contours, and environment.

$$\text{RSSI} = \max_{n \in N} \left(\mathbb{E}\Big(\sum_{rb \in RB} P_t(n) - P_l(d, f) \Big) \right), \tag{4.2}$$

  where $P_t(n)$ is the power of the transmitted signal by a given station n. RB represents the set of radio resource blocks used to transmit the physical broadcast channel (PBCH) signals. RB corresponds to the set of OFDM symbols and sub-carriers on which the PBCH is transmitted. For each operational station, a UE computes the average received signal power [177] over all the symbols and sub-carriers, f of RB. Finally, the UE only considers the highest computed average as its RSSI value.

4.2.2/ Emergency Call Procedure

The emergency call procedure can be triggered either by human intervention or autonomously (e.g., after a car accident detection). Once the call is triggered, the emergency application starts incorporating the emergency data, i.e., voice, text, video message, UE id, emergency call id, indicators about the emergency degree (level), RSSI indicator, and location. If the emergency caller is within the coverage of a network gNB, then the call is directly sent to the gNB using the classical communication mode. However, if the caller is out of coverage, the call is locally diffused using the out-of-coverage D2D procedure.

Consider the example scenario given in Figure. 4.2. First, M_3 sends a broadcast D2D emergency call that is only received by M_1 and relayed in the classical mode to the op-

erational gNB, N_1. The emergency call of M_4 is sent in direct D2D mode and is received by M_1, M_2, and M_5. The two relays M_1 and M_2 transfer the emergency call to N_1 and N_2 working gNBs, while M_5 ignores the M_4's emergency call because its own RSSI is worse than M_4. The M_5 diffuses its emergency call to the M_4, which relays it to all neighboring UEs until the emergency call reaches N_2.

Once a relay receives an emergency call and decides to relay it, the relay adds its identifier, position, and RSSI value to the relayed message. The emergency source position and relay positions help the public safety center precisely localize the source of the emergency call. Further, once an emergency call is received by a given gNB, a notification is diffused to all the UEs under coverage, indicating the successful transmission of that emergency call with its specific ID. That way, redundant uplink transmissions of the same emergency call are reduced.

4.2.3/ Outband D2D Communication

When a device m is out of coverage, it follows a certain procedure for emergency call transmission. First, a control message is sent via the PSCCH. The PSCCH serves, implicitly, to synchronize the sender with the potential receivers. It is used by ProSe-enabled m devices to send the Sidelink Control Information (SCI) that informs the receivers about the data transmission parameters used during the next sidelink period: subframes and radio resource blocks [43]. More precisely, the PSCCH indicates the index of the used subframes (time), the used radio resource blocks (frequencies), the modulation and coding scheme, and the D2D group destination ID. Each UE listens continuously to the PSCCH channel to detect if another UE is transmitting in the current sidelink period. Once the PSCCH message is received, the relay node tunes to the corresponding resources in the PSSCH to receive the emergency data.

4.3/ Multi-Hop Emergency all Protocol (M-HELP)

Due to the specificity of emergency call service under large disaster conditions, we aim for an emergency call protocol that is as light as possible. M-HELP is a fully distributed protocol with zero control charge. «Zero control» means that all exchanged messages are related to the emergency calls themselves plus additional data used for victims localization. However, no operational networking layer messages such as acknowledgments or clustering requests are used. M-HELP aims to maximize the probability that all emergency calls reach at least one gNB with a minimum delay and with a reasonable number of exchanged messages.

M-HELP procedures used by an emergency device and relay device are summarized in Algorithm 6 and Algorithm 7 respectively. As detailed in Algorithm 6, when an emergency UE, E, generates an emergency call, the application layer constructs a data message including the emergency data, *DATA*, user ID, emergency class, eNB/gNB serving station ID, GPS localization, observed RSSI and a couple of values $DATA.srcID$

and $DATA.callID$. *DATA.srcID* corresponds to the identifier of E. $Data.callID$ is the internal identifier given by E to the emergency call using the function *callIDGenerator()*. $callIDGenerator$ means that whatever the two different emergency calls initiated by E are, they have different $callID$s. Every new attempt is considered a new emergency call by changing the *DATA.callID* identifier of the message.

If the emergency source mobile is under the coverage of a given gNB, then the emergency call is sent using the classical uplink communication (PRACH and PUSCH channels). Otherwise, a D2D communication procedure is started. First, a PSCCH message is sent announcing that emergency data will be sent during the next sidelink period. The parameters included in PSCCH inform the receivers about the subframes given by Transmission Resource Pattern (TRP) and frequencies given by Resource Indicator Value (RIV) used later to transmit the emergency data over the PSSCH channel. The PSCCH includes a destination group ID equal to "Any" to indicate that all the mobile phones are concerned. After sending the data over the PSSCH channel, E device counts the number of relay devices of its own message, during a period of T_0. If this number exceeds a given threshold RS_{th}, the E considers that the emergency call is sufficiently relayed, otherwise, the emergency call is resent until the maximum number of re-transmissions, n_0^u, is reached.

Once an emergency call is received, the relay device R checks if the message was already received and processed. If the emergency message is not already processed, R computes a waiting time, T_r, according to (4.3). During the period T_r, the device R counts the number of times that the newly received message is relayed by other devices. If this number, after T_r, is lower than RS_{th}, R relays the message after adding its own localization. Similar to E, the R checks its coverage status and transmits in either the classical or D2D mode.

$$T_r^{M-HELP} = \min\left(T_{\text{max}}, \frac{1}{\text{LocAcc}_r + \delta} \times \frac{1}{\text{Ic}_r + \delta} \times \frac{\text{SoC}_{\text{max}}}{\min\left(\text{SoC}_r, \text{SoC}_{\text{max}}\right)} \times \text{T}_{\text{cycle}}\right) \tag{4.3}$$

The computation of the waiting time T_r aims to prioritize the devices according to their current state. Devices with a lower State of Charge (SoC), out of coverage, or with lower localization accuracy wait longer before deciding to relay the received emergency call. Longer T_r allows the device to wait for the decisions of the neighboring devices with a better SoC. Therefore, a device relays an emergency call, only if the number of relay devices in a better state is not sufficient. To prevent a very long waiting time, a maximum waiting time T_{max} is defined. Moreover, in M-HELP the R UE can only serve one call at a time and will not respond to other incoming calls during that time.

4.3.1/ Simulation and Results

To assess the performance of the proposed multi-hop emergency call protocol service, we implemented M-HELP using AnyLogic® software [178]. We studied a covered area of $7.5\text{km} \times 10.5\text{km}$. Under normal conditions, the mobile network presents eight gNBs and hundred emergency service-enabled devices. For each scenario considered, hundred random runs were launched in the simulation results, changing the position of the UEs

Algorithm 6 Emergency call generation at Emergency device

Input data: my srcID, emergency data, GPS localization, RSSI, T_0, $RS_{\text{threshold}}$, I_{TRP}, RIV, MCS, n_0^u
DATA.content ∈ {emergency data, localization, RSSI} *Generation*
DATA.srcID = my srcID, DATA.callID = callIDGenerator()
my State = busy
if I am out of coverage **then**
  nbAttempts=0
  repeat
    send PSCCH with I_{TRP}, RIV, MCS
    send DATA by PSSCH channel
    start = now()
    while now()-start $< T_0$ **do**
      if I receive PSSCH **then**
        mess = received DATA
        if mess.srcID == my srcID **then**
          N_{RS} + +
        end if
      end if
    end while
    if $N_{RS} \geq RS_{\text{th}}$ **then**
      EXIT
    end if
    nbAttempts++
    DATA.callID = callIDGenerator()
  until nbAttempts $> n_0$
else
  send DATA using ordinary link (RACH + PUSCH)
  my State = idle
end if

and victims' devices. Finally, the average value of the outputs was obtained and plotted. Further, the emergency calls were generated at random time instances from a uniform distribution over the time interval considered. Due to the catastrophe, the gNBs get dysfunctional in numerical order from one to eight, as illustrated in Figure 5.8a. Further, the emergency D2D takes a time of T_{d2d} seconds for transmission.

4.3.1.1/ EXPERIMENTS

As depicted in Figure 5.8a, mobile devices are randomly distributed over the network area. The fixed parameters used for the simulation are presented in Table. 6.1. Further, the values for parameters such as distribution of UE spread, ETI were generated via a uniform distribution over the considered interval. The values of the waiting time threshold, T_{max}, the number of emergency call transmission, ($RS_{\text{threshold}}$), and the limit of emergency call regeneration (n_0^u) are chosen empirically. However, the singular impact of those parameters will be discussed in the Section 4.4.

Algorithm 7 Emergency call reception at Relay device

Input data: received data, LocAcc, SoC, $T_{\max}$, $RS_{\text{threshold}}$, I_{TRP}, RIV, MCS
toRelayMess=received data
if (not already relayed the message from toRelayMess.DATA.srcID) && (my State == idle) **then**
  compute T_r
  start=now()
  my State = busy
  while now()-start $< T_r$ **do**
    mess=received data
    if mess.DATA.srcID==toRelayMess.srcID **then**
      $N_{RS}++$
      if $N_{RS} \geq RS_{\text{threshold}}$ **then**
        EXIT
      end if
    end if
  end while
  if $N_{RS} < RS_{\text{threshold}}$ **then**
    if I am out of coverage **then**
      DATA.content = toRelayMess.DATA.content + myLocation
      DATA.srcID=toRelayMess.DATA.srcID
      send PSCCH with I_{TRP}, RIV, MCS
      send DATA on PSSCH channel
    else
      send DATA using ordinary link (RACH + PUSCH)
    end if
  end if
  my State = idle
end if

4.3.1.2/ Evaluation Criteria

The following metrics are considered to assess the protocol performance.

- **Success rate** represents the ratio between the number of emergency calls received successfully by at least one gNB/eNB and the total number of emergency calls given by (4.4).

$$\text{Success rate} = \frac{\text{number of successfully received emergency calls}}{\text{number of emergency calls}} \tag{4.4}$$

- **End-to-End Latency (EEL)** is the average delay between emergency call generation and its first successful reception by a gNB. EEL is measured in seconds and includes all the delays caused by processing, buffering, temporizing, and transmission times given by (4.5).

$$EEL = t_{\text{call}_{\text{reception}}} - t_{\text{call}_{\text{generation}}} \tag{4.5}$$

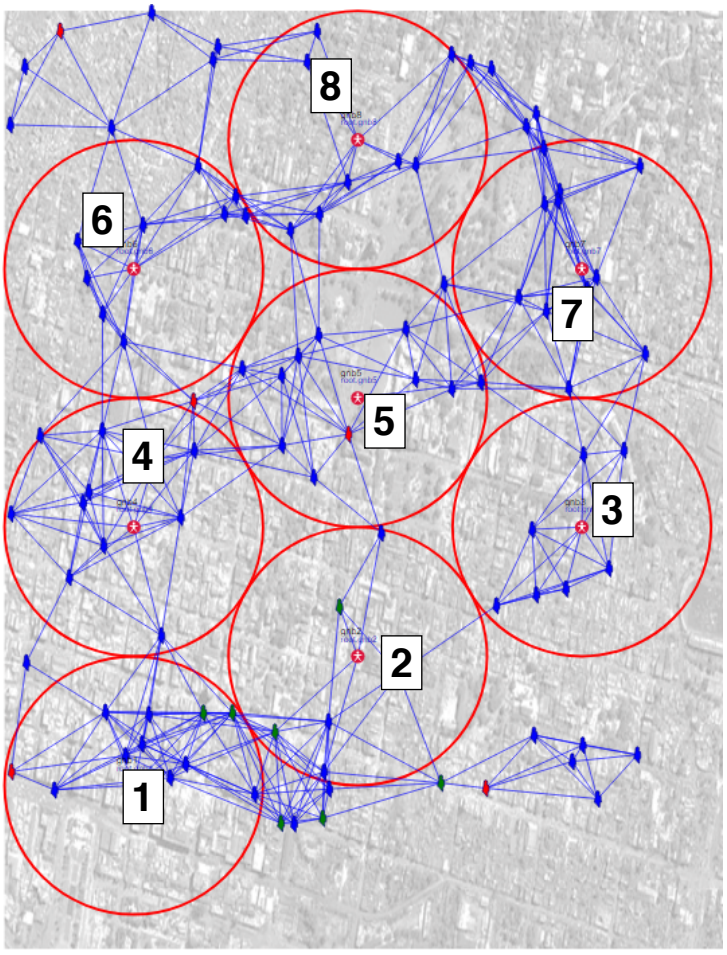

Figure 4.3: Screenshot of our anyLogic®simulator: studied scenario with 8 gNBs and 100 randomly distributed devices. Linked devices (resp. device-to-gNB links) represent D2D (resp. traditional) communication possibilities. Red circles represent the gNBs' covering areas.

- **Number of messages per node,** ϕ, represents the average number of relayed emergency messages per device given by (4.6).

$$\phi = \frac{\text{total number of relayed messages}}{\text{total number of network nodes}} \tag{4.6}$$

- **Energy consumption per node**, β, measures the average energy consumption per device as given by (4.7). This includes the energy consumed for the transmission and reception of emergency calls.

$$\beta = \frac{\text{total energy consumption of total nodes}}{\text{total number of network nodes}} \tag{4.7}$$

Table 4.2: Simulation parameters

Parameter	**Value**
Network area	7.5×10.5 km^2
gNB coverage	1.5 km
Total gNB number	8
Total UE number	100
UE's localization accuracy	RAND (0.001,1)
Initial UE's SoC	RAND(0,100) J
Maximum waiting time (T_{max})	120 sec (2 min)
Delay for emergency re-transmission, T_0	5 minutes
D2D link connection range	1.5 km
Data transfer delay per D2D link, T_{d2d}	60 sec (1 min)
Threshold of relaying UEs, $RS_{\text{threshold}}$	2
Upper limit of re-transmissions, n_0^u	3
Distribution of UE spread	RAND(7.5, 9.5) km^2
Number of emergency calls	variable
Emergency calls occurring interval, ETI	variable
Number of operational gNBs	variable [1..8]

4.3.1.3/ Performance Analysis

First, we studied the variation of the average number of sent messages per device and the success rate according to the number of operational gNBs. Figure 4.4a shows that when there is just one functional gNB, the success rate is above 50%. Furthermore, the success rate exceeds 85% when the number of functional gNBs is bigger than 4. Also, we observe that the average number of call forwarding per node increases when the number of available gNBs decreases. Indeed, emergency calls need more hops to reach the few remaining gNBs.

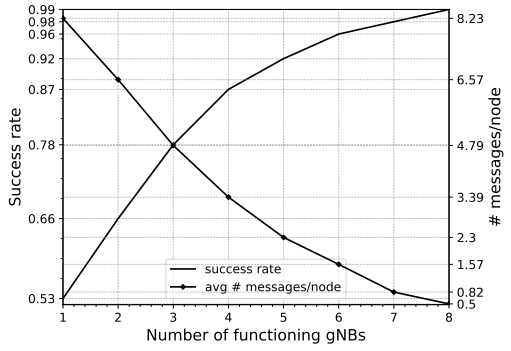

(a) Success rate and D2D message per node vs functioning gNBs.

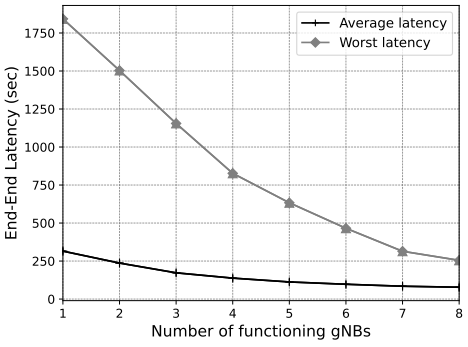

(b) Average latency against the number of functioning gNBs.

Figure 4.4: Variation of success rate, messages per node, and latency against the number of functioning gNBs. Parameters are: 50 emergency calls occurring during one hour.

Figure 4.4b shows the variation of worst and average latency for the same scenario as Figure 4.4a. According to the used $T_0 = 300s$ and $T_{\text{max}} = 120s$, the worst latency to reach the first gNB is around 25 minutes when only one gNB is working. The average latency reaches 13 minutes (800s) for the single working gNB case.

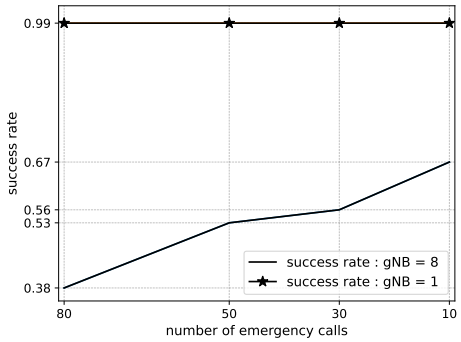

(a) Average success rate against NEC.

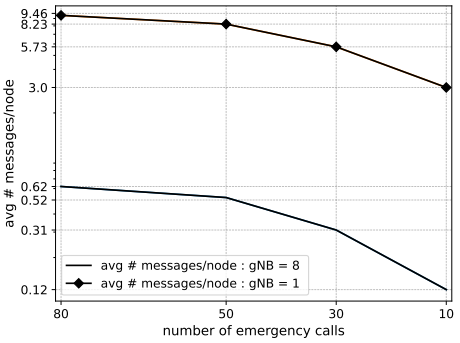

(b) Average number of D2D messages per node against NEC.

Figure 4.5: (a) Variation of the success rate and the average number of D2D messages per node according to the NEC occurring in 1 hour, under two cases: all gNBs are functional and only one gNB is functional.

Figure 4.5a shows the variation of the average number of sent messages per node and the success rate according to the number of emergency calls occurring in 1 hour. Two cases are tested: 1 functional gNB and 8 functional gNBs. As expected, the success rate is the highest when all the gNBs are working since the probability that the emergency source is close to a working station is high. This is reflected in the low number of sent D2D messages (less than 0.2 per node). However, for a single working gNB case, the success rate falls below 20% with 80 emergency calls. The success rate of M-HELP remains acceptable when the number of emergency calls is reasonable. We recall that devices are considered monotasking and during the processing of an emergency call, a device can not respond to another request. Therefore, the success rate of M-HELP protocol is highly underestimated, since current technological progress allows to manage several requests at the same time.

Figure 4.6a shows the variation of the average sent messages per node and the success rate according to the interval of time during which the emergency calls are generated. The number of generated emergency calls is fixed to 50 and the number of functional gNB is 2. Figure 4.6a shows that the success rate increases when emergency calls are spread over a longer interval period. Indeed, a relay device processes the first received emergency call and ignores the others until it finishes the algorithm 7. When the emergency calls' arrivals are concentrated in a short interval of time, the probability that an emergency call is ignored increases leading to a lower success rate. In Figure 4.6b, we observe that when the emergency calls are sufficiently spread over time, the risk that a relay device is in a busy state decreases, making the number of exchanged messages increases too. Furthermore, we observe that messages exchanging finishes by around 5 to 30 minutes after the generation of the last emergency call, due to the use of control thresholds,

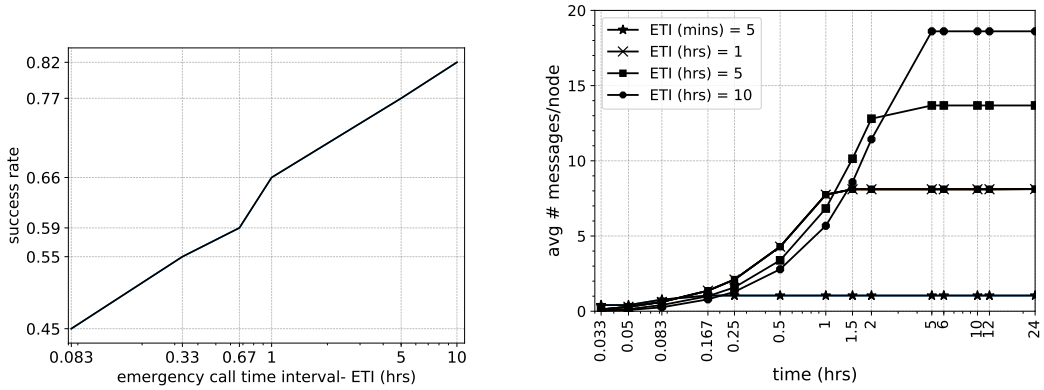

(a) Average success rate against ETI. (b) Average messages/node against time.

Figure 4.6: (a) Variation of the success rate according to the interval of time during which the emergency calls occur (ETI) and Progression over time of the average number of D2D messages per node. Parameters are: 2 operational gNBs and 50 emergency calls. On the abscissa, the time is displayed in logarithmic scale.

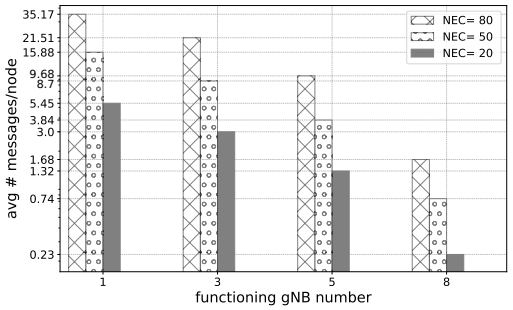

Figure 4.7: Average number of D2D messages per node after auto stabilization according to the number of operational gNBs. Parameters are: ETI is 5 hours, NEC = 20, 50 and 80.

$RS_{\text{threshold}}$ and n_0^u. The network traffic is kept controlled such that the average data traffic per node reaches a limit and remains constant with time.

Figure 4.7 shows the variation of the average number of sent messages per node according to the number of operational gNBs under 20, 50, and 80 emergency calls. When the network is not seriously damaged, D2D communication is rarely used. The intensive use of D2D communications appears when more than 50% of the network is damaged.

Moreover, to determine the notable efficiency of M-HELP, its performance was evaluated in comparison with an already existing protocol called FINDER. The results obtained are shown by Figures 4.8a, 4.8b and 4.8c. It is observed that M-HELP has a higher success rate and residual energy than the FINDER protocol and provides lower average messages per node. The reason is that devices, in FINDER protocol, relay the emergency call only to the CH. The CH aggregates the received data and sends it to nearby CHs. This results in a high traffic concentration on CHs and reduces the success rate. Furthermore, CHs

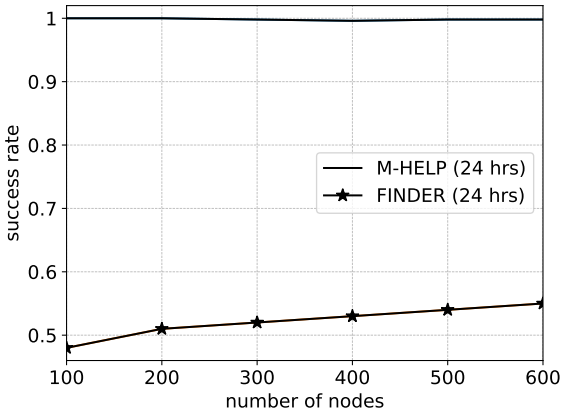

(a) Variation of success rate against number of nodes

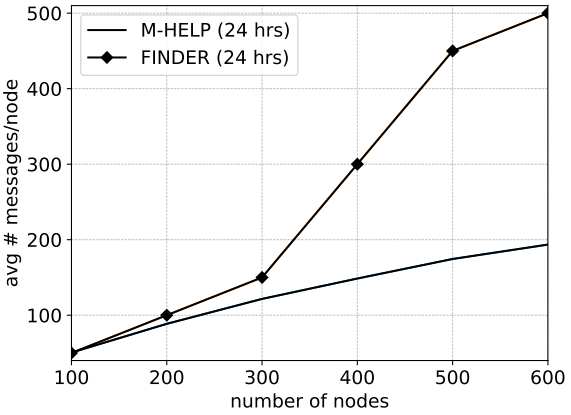

(b) Variation of the average number of sent messages against the number of nodes

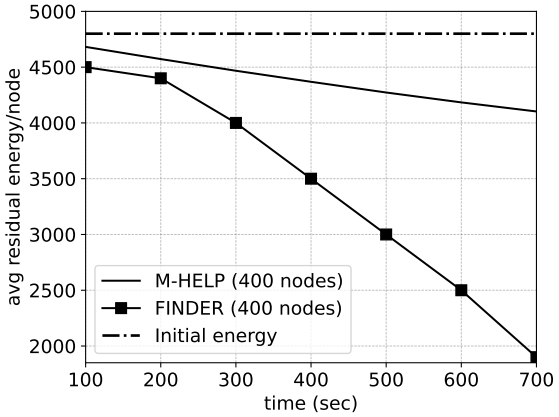

(c) Variation of residual energy against the number of nodes.

Figure 4.8: Comparison of M-HELP with FINDER protocol. Parameters are: 1 operational gNB, energy to transmit a message = 0.08 mJ, energy to receive a message = 0.05 mJ, and random number of calls occurring over 24 hours.

consume higher energy than ordinary devices.

Comparison to that, M-HELP adopts a massively distributed approach where there is no weight on a particular device to relay the emergency call to the gNB. Since the relay devices listen to the transmissions of the same emergency data, before transmitting it on their own, less traffic is generated in the network. Further, the stronger relay devices transfer the message before any other relay device in the neighborhood.

The computation of the waiting time T_r in (4.3) offers a dynamic and distributed way to select the stronger relay devices. This avoids high data congestion at one relay device, disperses the traffic among the network devices, and conserves the energy of the intermediate relay devices. Compared to FINDER, the lightness of the M-HELP protocol reduces the relay devices' charge. In addition, the prioritization of most available devices to transmit emergency calls is a significant advantage. A drawback of M-HELP is fixing

the value of maximum waiting time, T_{max}, which can affect the residual energy in the relays with low battery levels.

Numerical simulations demonstrate the that M-HELP provides several benefits over outband D2D multi-hop protocols such as FINDER, including high transmission reliability, reduced energy consumption, and reduced traffic redundancy. However, it is also noted that M-HELP has its limitations in terms of its adaptability to the disaster conditions such as emergency call loads, scale of the disaster, D2D transfer delays, and UE densities. Hence, we introduce a new protocol called 5G-SOS, in the following section, to address this issue of adaptability in ad-hoc out-of-coverage emergency call protocols.

4.4/ Adaptive Multi-Hop Emergency Call Protocol: 5G-SOS

A 5G-SOS protocol that enhances the performance of M-HELP in transmitting emergency calls reliably to the core network is discussed in this Section. In contrast to M-HELP, 5G-SOS can adapt its parameters based on the local emergency call congestion observed in the local neighborhood.

Similarly to M-HELP, in 5G-SOS the devices under gNB coverage transmits or relays an emergency call via a traditional 4/5G uplink channel, otherwise a D2D communication procedure is used for emergency call forwarding. Further, 5G-SOS enabled device follows the same procedure (Algorithm 6) to generate and transmit an emergency call. Moreover, the relay device R in 5G-SOS follows the same procedure given in Algorithm 7. However, 5G-SOS dynamically adjusts parameters such as T_r, RS_{th}, T_0, n_0^u depending on the observed local area network condition, in contrast to M-HELP. Moreover, 5G-SOS can queue multiple emergency calls in a buffer, allowing it to handle a larger volume of emergency callers compared to M-HELP.

4.4.1/ Adaptation of Parameter Values in 5G-SOS

4.4.1.1/ Waiting Time before Relaying: T_r

In the M-HELP the waiting time before relaying a received emergency call, T_r in (4.3), can not exceed a value T_{max}. T_{max} was fixed to a specific value, i.e., 2 mins. However, the value of T_{max} should be adapted according to many factors such as the rate of observed emergency calls and UEs density in the local neighborhood. Hence the computation of the T_r is adjusted in 5G-SOS as follows:

$$T_r^{5G-SOS} = \min\left(T_{\text{max}}(n_k, n_c),\ \frac{\text{RSSI}_{\text{tx}}}{\text{RSSI}_{\text{r}}} \times \frac{1}{\text{LocAcc}_r + \delta} \times \frac{1}{\text{Ic}_r + \delta} \times \frac{\text{SoC}_{\text{max}}}{\min\left(\text{SoC}_r, \text{SoC}_{\text{max}}\right)}\right). \tag{4.8}$$

Algorithm 8 On receiving an emergency call, DATA

if (!χ.contains(DATA.srcID, DATA.callID)) **then**
  χ.Push(DATA)
  if η_b.size() < 3 **then**
    Compute T_r
    DATA.deadline = T_r + now ()
    DATA.$N_{RS} = 0$
    η_b.Push(DATA)
  end if
else if $\exists$ waitingCall $\in$ η_b such as (DATA.srcID,DATA.callID) = (waitingCall.srcID,waitingCall.callID) **then**
  waitingCall.N_{RS} + +
  if waitingCall.$N_{RS} \geq RS_{\text{th}}$ **then**
    η_b.Remove(waiting call)
  end if
end if

Algorithm 9 Every one second

Input data: my srcID, GPS localization, RSSI
for all waitingCall $\in \eta_b$ **do**
  if now () $\geq$ waitingCall.deadline **and** my State is "idle" **then**
    my State ="busy"
    if I am out of coverage **then**
      DATA.content = waitingCall.DATA.content
      DATA.relay.add (GPS Localization, RSSI,my srcID)
      DATA.srcID = waitingCall.DATA.srcID
      send PSCCH with I_{TRP}, RIV, MCS
      send DATA on PSSCH channel
    else
      send DATA using ordinary link (RACH + PUSCH)
    end if
    η_b.Remove(waitingCall)
    myState = idle
  end if
end for

where T_{max} parameter is adapted as follow:

$$T_{\text{max}}(n_c, n_k) = \min(\max((a - n_c)^2 + b \times (n_k - {n_c}^2)^2, 0), u_b), \tag{4.9}$$

Similarly to M-HELP, 5G-SOS computes the waiting time T_r, using Ic_r, LocAcc_r, and SoC_r of a R device. However, 5G-SOS introduces the use of the RSSI ratio in addition to the use of the dynamic T_{max}. The new computation mechanism of T_r and T_{max} parameters is characterized by the following features:

- RSSI ratio:

  The ratio between the $RSSI_{\text{tx}}$ of the transmitter, and the $RSSI_r$ of the R itself

is used in the computation of T_r. This ratio is higher than one when the transmitter of the emergency call is in better radio conditions than the receiver. That means that the receiver is farther from the gNBs than the sender or the relay of the emergency call. In this case, the ratio contributes to increasing the value of T_r^{5G-SOS} in order to penalize the receiver in the decision of relaying the emergency call. Otherwise, when the ratio is less than one, the receiver is in better radio conditions (closer to the gNB), and the T_r^{5G-SOS} is decreased to give priority to the receiver.

Further, the RSSI ratio is used to improve the latency fairness between UEs. Indeed, a R device waits less time when the request is sent by a farther device than when the request is sent by a closer device, as depicted in Figure 4.9. Therefore, when two requests are received at the same time, the request of the farthest device from the gNB is transmitted first, which contributes to balancing the emergency call transfer delays.

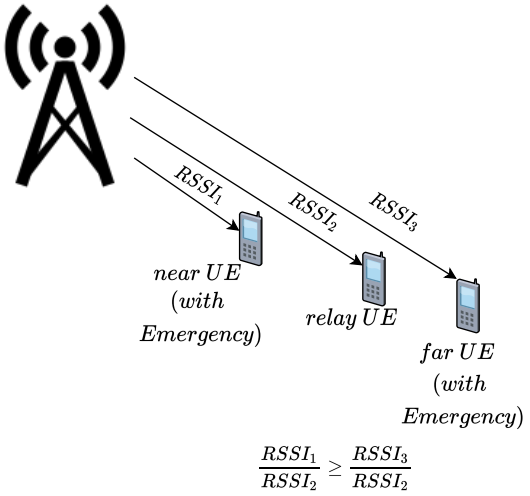

Figure 4.9: A relay UE gives higher priority for a far emergency UE than a near UE using the RSSI ratio. The RSSI ratio in (4.8) is lower for a far UE than a near UE. The relay UE waits a lesser time, hence relays faster the transmissions of the far UE emergency call in the direction of a functioning gNB.

- Dynamic T_{max}:

  In 5G-SOS, T_{max} is not a fixed value, in contrast to M-HELP. It is modeled using a modified Rosenbrock [179, 180] function as described in Equation 4.9. Where a and b are two parameters that govern the shape of the T_{max} curve.

  The Rosenbrock function allows increasing the sensitivity of the protocol to real-time local factors such as the number of emergency requests, n_k, and neighborhood congestion, n_c, detected in previous time intervals. More precisely, n_c represents the total number of received emergency requests, including multiple receptions during the last minute. Further, n_c is used to measure the level of congestion in the neighboring environment in the previous minute. On the other hand, n_k measures the total number of different emergency call requests received in the previous minute.

Rosenbrock function is used since it has a slope with the same behavior to $T_{\max}(n_c, n_k)$ given in Table 4.3). A low number of distinct emergency calls n_k with a high congestion level n_c expresses a low emergency load but with many relaying opportunities for each emergency request due to the network density. In this case, a high $T_{\max}$ value allows the selection of the relevant relays. However, if both n_k and n_c are low, the $T_{\max}$ value is decreased since there are not enough relay alternatives, i.e., a weakly dense network. Finally, when n_k is high, a lower $T_{\max}$ is preferable in order to quickly handle the newly received emergency requests. Further, if the number of neighboring relaying devices is low and such devices have a low battery level, the devices will assign themselves a relatively shorter $T_{\max}(n_c, n_k)$ by 5G-SOS considering the low neighborhood congestion. The curve of the original Rosenbrock function, f, is given in Figure 4.10. When x increases while y is fixed, $f(x, y)$ increases. However, when y is increased while keeping x fixed, $f(x, y)$ decreases gradually.

Table 4.3: Expected behavior of $T_{\max}$ with the total number of emergency calls including duplicates, n_c and distinct emergency calls, n_k, observed in the neighborhood.

n_k	n_c	$T_{\max}$
↓	↓	↓
↓	↑	↑
↑	↑	↓

4.4.1.2/ Waiting Time for Re-Transmission, T_0

As seen in Algorithm 11, the victim's device waits for T_0 to check if a sufficient number of devices have relayed its emergency call. The computation of the T_0 follows the same mechanism as T_{max} since the re-transmission delay must be aligned with T_{max} values of the neighboring devices to prevent premature re-transmission. Consequently, T_0 is computed as follows:

$$T_0 = T_{\max}(n_k, n_c). \tag{4.10}$$

4.4.1.3/ Emergency Call List

In both M-HELP and 5G-SOS, only one emergency call is transmitted at a time. Each device manages a state variable named "my State" given in Algorithms 6, 7, 9 initialized to "idle". When the device starts to transmit or relay an emergency call, the state is turned to "busy". However, in contrast to M-HELP, 5G-SOS can receive and queue multiple emergency call requests during the "busy" state. This mechanism aims to reduce the loss of calls during the periods when the device is waiting to take a decision on relaying an already-received emergency call. Thereby, two lists are introduced in 5G-SOS namely the pending calls list, η_b, and the received calls' identifiers list, χ.

First, the relay device checks if the (*DATA.srcID, DATA.callID*) of the received call *DATA* is

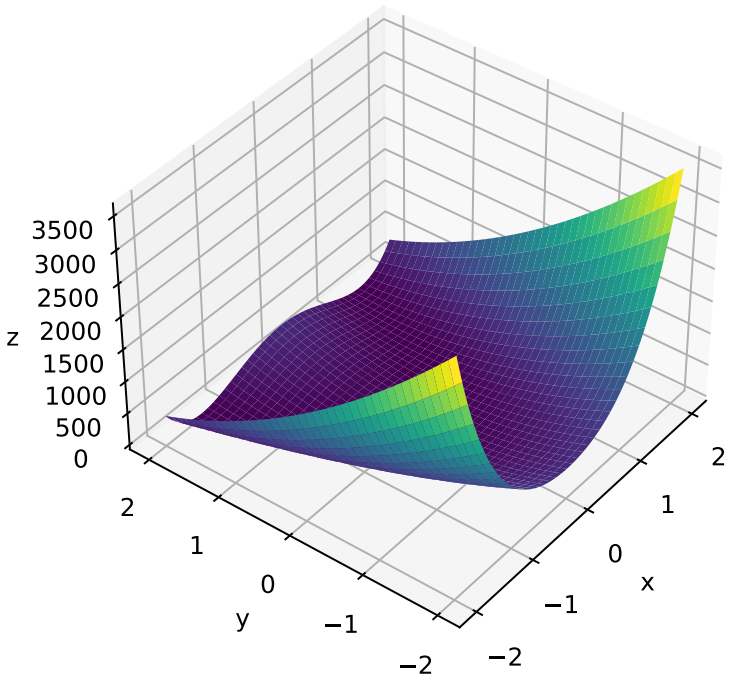

Figure 4.10: Illustration of the standard Rosenbrock function defined by two variables and given by $f(x,y) = (a-x)^2 + b(y-x^2)^2$. Here, we assume a = 1, b = 100, and the minimum value of zero is at (1,1). The adaptive T_{max} given in (4.9) is based on the Rosenbrock function.

in χ as described in Algorithm 8. If the received call is not in χ, the relay device stores the identifiers of the received call in χ and queues the call in η_b. To prevent the excessive increase of this list χ, the emergency calls are removed from χ after a fixed time, e.g. 30 minutes.

In the second list, η_b, the device stores the new emergency calls that need to be proceeded and eventually relayed. η_b allows managing a fixed number of emergency calls simultaneously. Each emergency call in η_b is associated with two fields: N_{RS} and $deadline$. N_{RS} is initialized to 0 and stores the number of times that the message *DATA* is relayed by other neighbors. The $deadline$ gives the time limit of the call in η_b. The $deadline$ is computed using T_r, as shown in line 5 of Algorithm 8. Every second, the relay device checks its η_b list as explained in Algorithm 9. If the *waitingCall.deadline* of a given call, $waitingCall$, is reached, the call is relayed after adding, in the $DATA.relay$ field, the relay's data, such as the RSSI, GPS location, and srcID, and all previous relays' data. A call is also removed from η_b when the call is sufficiently relayed ($N_{RS} >= RS_{\text{th}}$) by neighboring devices. The size of η_b is limited to a fixed value. If the limit size is reached, new emergency calls are ignored.

4.4.1.4/ Relaying Threshold, RS_{TH}

In 5G-SOS, in contrast to M-HELP, RS_{th} is updated according to the real-time conditions using the following expression:

$$RS_{\text{th}} = RS_{\text{th}}^{\text{max}} - \mid \eta_b \mid . \tag{4.11}$$

Based on the number of entries in η_b the RS_{th} is determined. Hence, the RS_{th} value of a device drops as the size of η_b increases. Thereby, as the number of emergency calls in the local neighborhood increases the RS_{th} is decreased to reduce losing emergency calls and relay them with less delay. To sum up, Table 4.7 presents a comparison between the features of M-HELP and 5G-SOS.

Table 4.4: Comparison between M-HELP and 5G-SOS

Feature	**M-HELP**	**5G-SOS**
T_{max}	Fixed	Adaptive
T_0	Fixed	Adaptive
RSSI ratio	Not included	Included
RS_{th}	Fixed	Adaptive
n_0^u	Fixed	Adaptive

4.5/ Simulation Results

4.5.1/ Test Environment

In order to investigate the performance of our protocol, we evaluated and compared 5G-SOS with M-HELP and FINDER [44] protocols under extreme emergency scenarios. Thereby, the testing environment, evaluation parameters, and performance analysis are presented in this section. The performance of the proposed 5G-SOS is assessed using AnyLogic®software. An emergency scenario in the Transverse city in Michigan, USA, with a number of devices varying between 5000 to 15,000 and seven working gNBs covering an area of $16.2 \times 21 \text{km}^2$ is considered. This scenario is illustrated in Figure 4.11.

4.5.1.1/ Propagation Pathloss Model and RSSI

In 4G/5G networks, operational gNBs periodically broadcast control signals, PBCH, over predefined resource blocks. The RSSI of such signals is computed using (4.2), where $P_l(d, f)$ represents the path loss of the signal due to environmental factors, i.e., buildings, mountains, etc. To compute the $P_l(d, f)$ in (4.2), the Cost231 propagation model for semi-urban areas, given in [181], is used. $P_l(d, f)$ of a signal transmitted by a working

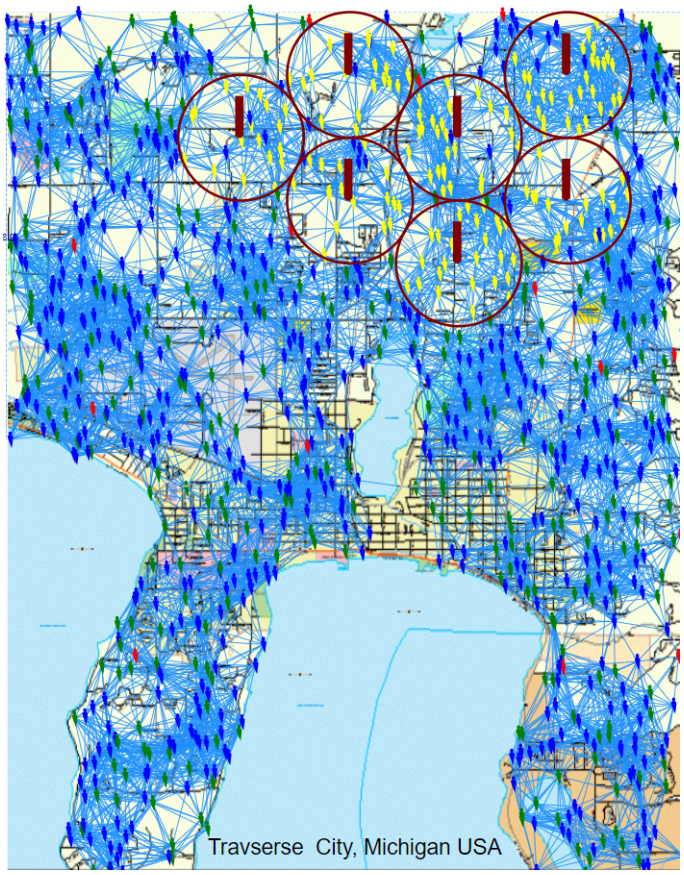

Figure 4.11: Studied network area of the Traverse city in Michigan, USA, with uniformly distributed 38 gNBs, with only 7 functioning, and 15,000 UEs in the AnyLogic software. Linked UEs (resp. UE-to-gNB links) represent D2D (resp. traditional) communication possibilities. Dark green circles represent the functioning gNBs' covering areas in which the gNBs are at the center. Non-functioning gNB coverage areas are indicated by red circles with dashes. Emergency devices, relay devices, in-coverage devices, and idle devices are represented respectively by the colors, red, green, yellow, and blue.

gNB varies according to the signal transmission frequency of the working gNB, f, and the distance between the working gNB and receiver UE, d, as given in (4.12). Further, h_g and h_m represent, respectively, the height of the gNB and receiver UE. C_m is a correction offset associated with the semi-urban environment. For the simulations, f is set to 885 MHz. $P_l(d, f)$ varies according to the used frequency, f, and the distance between a functioning gNB and a receiver UE, d, is modeled using (4.12) and (4.13). Further, the measured RSSI values are handled in Watts.

$$P_l(d, f) = 46.3 + 33.9 \log_{10}(f) - 13.82 \log_{10}(h_g) - a(h_m) + (44.9 - 6.55 \log_{10}(h_m)) \times \log_{10}(d) + C_m, \tag{4.12}$$

with:

$$a(h_m) = 3.2 \times log(11.75 h_m)^2 - 4.97. \tag{4.13}$$

4.5.1.2/ NEIGHBOR RELYING THRESHOLD: RS_{TH}

The maximum threshold for neighbor relaying, RS_{th}^{max}, is set to a constant and $|\eta|$ denoted the number of pending call requests in the UE buffer. The latter is used to estimate the number of different emergency calls being relayed in the neighboring area. Further, the maximum limit for $|\eta|$ is assumed to be a constant. Hence, when the value of $|\eta|$ changes from one to maximum, the RS_{th} adapts its value according to (4.11). In comparison, the value of RS_{th} is fixed in the M-HELP protocol.

4.5.1.3/ T_{MAX} PARAMETERS

The values of the parameters a, b of the Rosenbrock function (Equation 4.9) are continuously adjusted according to the observed n_c as shown in Table 4.5. We recall that n_c represents the number of different emergency calls received over the last minute. n_c and n_k (number of different emergency calls received) are used to compute the value of T_{max}. This value allows computing the wait times Tr^{5G-SOS} (time before relaying an emergency call) and T_0 (time before re-transmitting an original emergency call). Figure 4.12 shows the impact of the total emergency call request count including duplicates, n_c, and n_k factors on the value of T_{max}.

The minimum and maximum limits of n_c for different device density values such as 100, 1000, and 4000 are gathered and used as n_c limits to be observed by a UE given in Table 4.5.

Table 4.5: Adaptive T_{max} model parameters

n_c Limits	a	b
$0 \leq n_c \leq 10$	1	0.5
$10 \leq n_c \leq 200$	1	0.2
$200 \leq n_c$	1	0.1

4.5.2/ PERFORMANCE ANALYSIS

In this Section, the performance of 5G-SOS is studied and compared with M-HELP and FINDER [44] under multiple disaster configurations while 75% of the gNBs in the network area are out of operation. The emergency calls are randomly generated in a uniform distribution, over an emergency occurring time interval (ETI) of 30 min. Further, the performance is assessed by considering that all nodes are stationary. If the network nodes do not form a connected graph, emergency calls cannot reach the gNBs. Hence, the D2D communication range is set in order to maintain such a connected network. Furthermore, the number of UEs (NoU) and NEC satisfy the condition, Number of Emergency Calls (NEC) < Number of UEs (NoU). The provided results are all averaged over 100 random executions, which differ by the victims' devices and emergency arrival times. Table 6.1 summarizes the parameters used in the simulation scenarios. The emergency data

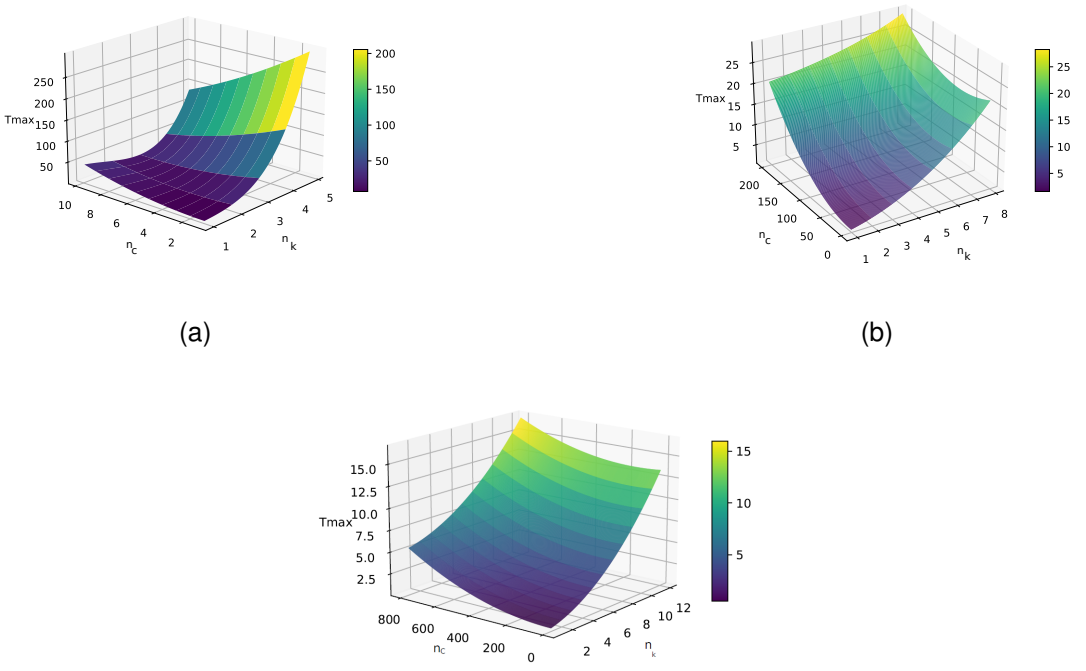

(a) (b)

(c)

Figure 4.12: Variation of T_{max} under three ranges of n_c. (**a**) Variation of T_{max} against n_c and n_k, when the n_c observed in the neighborhood is between 0 and 10. (**b**) Variation of T_{max} against n_k and n_c, when the n_c observed in the neighborhood is between 10 and 200. (**c**) Variation of T_{max} against n_k and n_c, when the n_c observed in the neighborhood is above 200.

transfer takes T_{d2d} seconds. During the emergency call transmission (D2D transmission or ordinary transmission) the UE cannot transmit other emergency requests.

4.5.2.1/ Scenarios and Tests

Extreme emergency scenarios are considered to assess the performance of 5G-SOS. In particular, the performance under extreme emergency scenarios under metrics such as success rate, EEL, ϕ, and β metrics, defined in Section 4.3.1.2, are studied.

4.5.2.2/ Impact of Emergency Calls Time Distribution

The impact of emergency call time distribution, ETI, on success rate and *EEL* is observed in Figures 4.13a and 4.13b. ETI defines the period during which the emergency calls are initiated. It is observed that when the emergency call arrivals are spread over a longer ETI, the amount of successful transmissions increases. As the relay nodes become over-charged due to a shorter ETI value, the probability that a node ignores an incoming

Table 4.6: Traverse city area emergency simulation parameters

Parameter	**Value**
Total network area	16.2×21 km^2
Amount of working gNBs	7
Total UE spread	RAND(16.2,21)
Initial T_{max}	120 s
Initial T_0	120 s
UE's GPS localization accuracy	RAND (0.001,1)
Initial UE's SoC	RAND(0,100) J
BS/gNB Link distance (d)	1.5 km
D2D link connection range	1.5 km
Data transfer delay by D2D mode, T_{d2d}	10 s
Data transfer delay by classical PUSCH mode	1 s
Maximum limit for RS_{th}, $RS_{\text{th}}^{\text{max}}$	5
Upper bound of waiting time, u_b	120 s
Upper limit of re-transmissions, n_0^u	4
Maximum number of messages in η_b	3
Transmit power of gNB, (P_g)	300.0 dBm
Signal transmission frequency of gNBs (f)	885 MHz
BS/gNB antenna effective height (h_g)	100 m
UE antenna effective height (h_m)	1.5 m
Constant offset of Cost231 Hata model (C_m)	0 dB
Number of UEs, NoU	Variable
Number of Emergency Calls, NEC	[0,15000]
Emergency calls occurring interval, ETI	variable
Energy to transmit	0.08 mJ [44]
Energy to receive	0.05 mJ [44]
Total Simulation running time	30 min

request, due to the buffer saturation, increases. In contrast, when the ETI is longer, the number of idle relay nodes available to cater to each relay request is higher.

Further, it is seen that with the increment in ETI, the success rate and *EEL* of 5G-SOS is significantly improved compared to M-HELP and FINDER. The adaptive parameters in 5G-SOS enhance the responsiveness to a large number of emergency calls occurring in a shorter ETI. The parameters, RS_{th} and T_{max}, are adaptive in 5G-SOS compared to M-HELP, where such parameters are fixed to a specific value. The success rate is lower in FINDER protocol due to the fact that devices relay the data only to the cluster head (CH). The CH aggregates the received data and sends them to nearby CHs. Such an aggregation results in a high traffic concentration on CHs and reduces the success rate. Moreover, under each protocol, the *EEL* increases against the duration of ETI. As the

emergency calls occur over a shorter ETI, the amount of idle relay nodes is low. Since relay nodes do not buffer the simultaneously received calls in M-HELP, only a few calls are successfully transferred to the gNB. Hence, initially, the corresponding latency in M-HELP is low. The *EEL* in 5G-SOS is initially higher than M-HELP since the success rate of calls is higher and hence, the corresponding latency increases. As the adaptive parameters in 5G-SOS allow the quick transferring of calls, the waiting time at the relays decreases which results in a lower *EEL* compared to both M-HELP and FINDER. In FINDER, the delay in selecting the cluster head and communicating calls via multiple cluster heads leads to higher *EEL*, when the amount of successful calls increases.

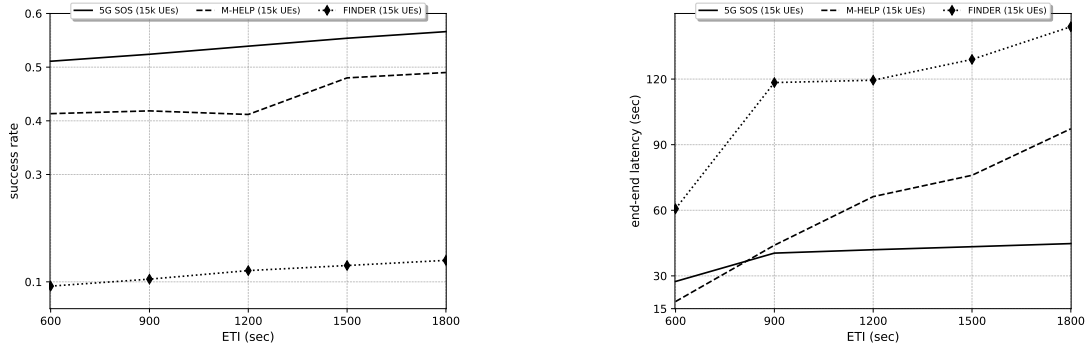

(a) Success rate against ETI.

(b) End-to-end latency against ETI.

Figure 4.13: Performance of 5G-SOS, M-HELP, and FINDER under the scenario-: ETI: 600–1800 s, NoU: 15,000, NEC: 5000.

4.5.2.3/ Impact of Device Density

In Figures 4.14a and 4.14b, we study the impact of the network density on the emergency call transfer under a fixed number of emergency calls and fixed emergency time interval. As observed in Figure 4.14a, the success rate increases with the increment in the number of UEs since it increases the availability of more idle nodes under all the protocols considered. A higher number of idle nodes increases the probability of serving a large number of emergency calls compared to a low device density network. As in the previous section, initially the *EEL* in 5G-SOS increases compared to M-HELP, since a higher latency is consumed to achieve a higher success rate under the constraints of increasing local congestion. It is reflected in Figure 4.13b where the *EEL* increases with the number of UEs due to the increase of the local congestion and thus the waiting times T_r in 5G-SOS. The increment in local congestion increases T_{max} and causes saturation in buffers, which results in lower relaying efficiency. However, the adaptive nature of 5G-SOS parameters allows faster relaying of calls compared to M-HELP and FINDER. It is observed that increasing the number of devices plays a positive role in the improvement of the success rate of 5G-SOS, M-HELP, and FINDER. The use of 5G-SOS significantly reduces the *EEL* compared to M-HELP and FINDER, since 5G-SOS uses the local congestion data, RSSI, and buffering to increase the relaying efficiency in an adaptive manner.

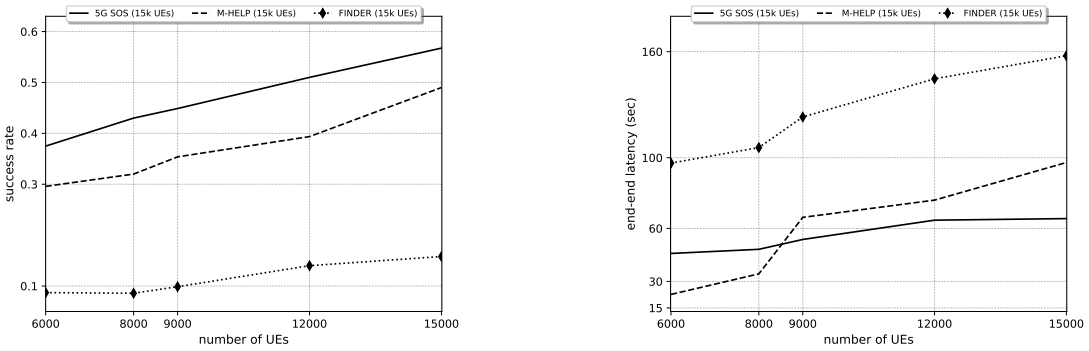

(a) Success rate against NoU.

(b) End-to-end latency against NoU.

Figure 4.14: Performance of 5G-SOS, M-HELP, and FINDER under the scenario-: NoU: 6000 to 15000, NEC: 5000, ETI: 1800 s (30 min).

4.5.2.4/ Impact of Emergency Data Size

The emergency data size depends on the type of sent data such as text, audio or video. The emergency data size increases respectively with text, audio, and video data types. Moreover, the emergency call data size is completely correlated with the transmission duration of the emergency call (D2D or classic mode). Hence, the impact of emergency data size on the performance of 5G-SOS is observed in Figures 4.15a and 4.15b, where emergency calls occur within a fixed ETI. As shown in Section 4.5.2.4, when the data size is low, the success rate is higher compared to transferring high-quality data. Hence, it is suitable to reduce the data size during broad disaster situations. As the duration for emergency call transfer increases, the number of busy nodes processing other emergency calls increases. This leads to a lower relaying efficiency and thus a drop in the overall number of successful transmissions. The *EEL* of 5G-SOS is lower than M-HELP and FINDER, since the T_{max} is low as the n_c and n_k are also low in the local region due to the impact of the emergency call transfer delay. M-HELP and FINDER have a higher *EEL* since the data transfer delay directly impacts the total delay at each relay.

4.5.2.5/ Impact of the Percentage of NEC over NoU

First, it is observed, in Figure 4.16a, that the success rate of 5G-SOS is nearly 100% when the number of emergency calls are less than 5% of the total devices. Further, when the percentage of NEC over NoU approaches 80%, i.e., almost all nodes generate an emergency call, around 37.4% of calls are relayed successfully against only 29.5% in M-HELP and 8.7% in FINDER. Moreover, when 5000 emergency calls occur within an ETI of 600 s (10 min), more than 50% of calls reache the core network, as observed in Figure 4.13a.

Figure 4.16d presents the *EEL* under varying NEC over NoU ratios. It is noted that 5G-SOS adapts the $T_{\max}$ parameter according to the n_k and n_c factors, as discussed in Section 4.4. Hence, when the ratio between the number NEC and NoU reaches 80%, the *EEL*

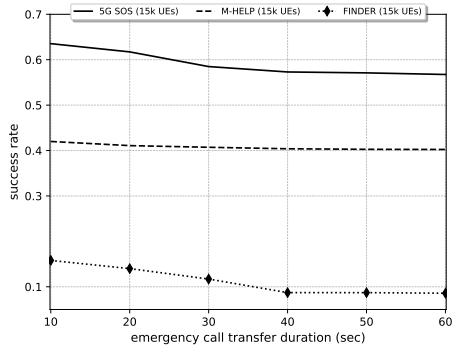

(a) Success rate against emergency call transfer duration.

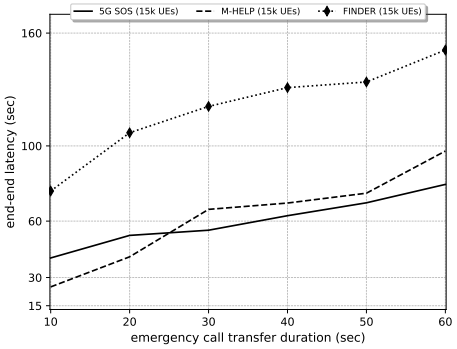

(b) End-to-end latency against emergency call transfer duration.

Figure 4.15: Performance of 5G-SOS, M-HELP, and FINDER under the scenario-: NoU: 15000, NEC: 5000, ETI: 1800s (30 min).

is further reduced by adapting parameters such as T_{max}, RS_{th}, to serve large amounts of emergency calls. Overall, we observe that the 5G-SOS protocol reduces latency compared to M-HELP and FINDER.

Additionally, as seen in Figure 4.16c, 5G-SOS provides a slightly higher average number of messages per node than M-HELP. The amount of emergency call requests served by 5G-SOS is higher than M-HELP due to calls' buffering. Hence, the average number of messages per node has increased against M-HELP. Furthermore, compared to FINDER, 5G-SOS and M-HELP adopt a massively distributed approach leading to charge balancing of emergency call relay over the devices. Since the relay devices detect the re-transmissions of the same emergency call before eventually transmitting it, less traffic is generated in the network. Furthermore, the most adapted relay devices transfer the message before any other relay device in the neighborhood.

In terms of residual energy, FINDER has a higher energy consumption compared to 5G-SOS and M-HELP, as seen in Figure 4.16d and CHs consume higher energy than cluster member devices. 5G-SOS consumes higher energy compared to M-HELP. Indeed, 5G-SOS buffers the multiple simultaneous calls received while M-HELP ignores such calls. The computation of the waiting time T_r in (4.8) offers a dynamic and distributed way to select the stronger relay devices and limit the maximum T_r based on the level of congestion detected in the local neighborhood. This avoids high data congestion at a particular relay device, disperses the traffic among the network devices, and conserves the energy of the intermediate relay devices. Furthermore, the use of the RS_{th} parameter prevents overloading the network with multiple copies of the same requests in a dense environment.

4.5.2.6/ Overall Analysis

The lightness of the protocols and the smart selection of adapted devices to relay emergency calls are the major contributions of 5G-SOS and M-HELP compared to FINDER. All

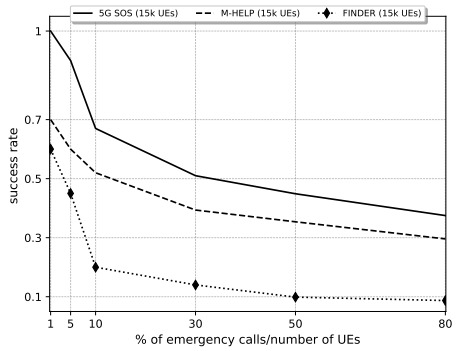

(a) Success rate against the ratio of NEC to NoU.

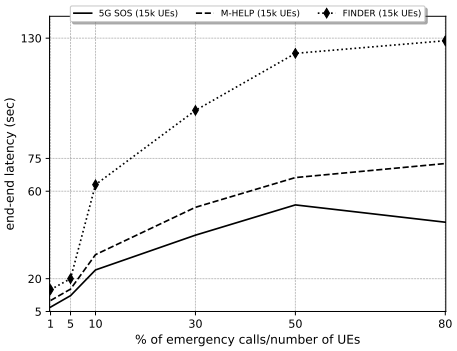

(b) End–end latency against the ratio of NEC to NoU.

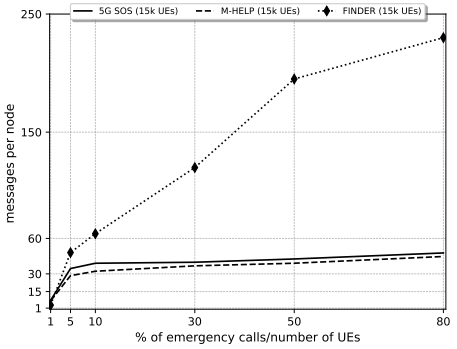

(c) Number of messages per node against the ratio of NEC to NoU.

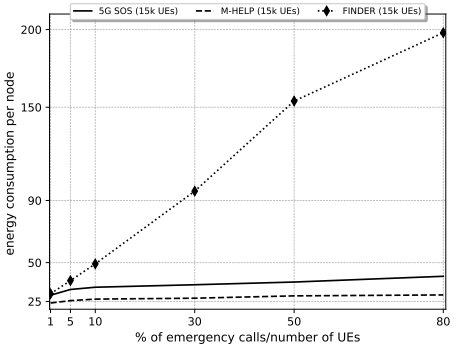

(d) Energy consumption per node against the ratio of NEC to NoU.

Figure 4.16: Performance of 5G-SOS, M-HELP, and FINDER under the scenario-: NoU: NEC: 1% of NoU to 80% of NoU, NoU: 15000 UEs, ETI: 1800s (30 min).

in all, 5G-SOS and M-HELP have improved performance compared to FINDER in terms of transmission success rate, *EEL*, energy consumption, and network congestion control.

The overall summary of the performance of 5G-SOS over M-HELP and FINDER is given in Table 4.7. The average improvement by 5G-SOS over all the considered scenarios is approximately 24.9% than M-HELP and 73.9% than FINDER in terms of success rate. Further, the reduction of the average end-to-end latency is 20.8% compared to M-HELP and 61.7% compared to FINDER. Moreover, 5G-SOS allows a reduction in the average energy consumption by 79.2% compared to FINDER. In contrast, 5G-SOS has a higher energy consumption than M-HELP by around 29.1%. On top of that, the average messages per node in 5G-SOS is lower than FINDER by around 81.3%, but higher than M-HELP by 6.2%.

4.6/ Conclusion

Simulation results using 5G-SOS over Traverse City of Michigan, USA, with a 15,000 population, demonstrated that 5G-SOS succeeds in transferring more than 80% of the emer-

Table 4.7: Summary of performance analysis.

Parameter	**Gain in 5G-SOS vs. M-HELP**	**Gain in 5G-SOS vs. FINDER**	**Comparison**
Success rate	24.9%	73.90%	Success rate$_{5G-SOS}$ > Success rate$_{M-HELP}$>Success rate$_{FINDER}$
EEL	−20.80%	−61.70%	EEL_{5G-SOS}<EEL_{M-HELP}<EEL_{FINDER}
ϕ	29.10%	−79.20%	ϕ_{M-HELP}<ϕ_{5G-SOS}<ϕ_{FINDER}
β	6.20%	−81.30%	β_{M-HELP}<β_{5G-SOS}<β_{FINDER}

gency calls when the victims represent <5% of the devices. Further, it was observed that 5G-SOS provided a higher success rate, higher average residual energy per node, and lower average number of sent messages per node than FINDER. 5G-SOS enhanced M-HELP performance in terms of success rate and end-to-end latency. In addition, 5G-SOS provided satisfactory performance (success rate of 50%) even when the number of simultaneous emergency calls became very high (5000 calls over 10 min). On average, 5G-SOS performed 24.9% better than M-HELP and 73.9% than FINDER in terms of success rate. Additionally, 5G-SOS reduced the average end-to-end latency of the emergency calls transfer by 20.8% compared to M-HELP and 61.7% compared to FINDER. The 5G-SOS protocol is characterized by adaptive behavior that uses locally available data provided by sidelink (from neighbors) and downlink (from gNBs) signals. This adaptation allowed adjusting the expected performance of the service (latency and success rate) to the current charge of the network. Limitations of 5G-SOS are having a higher energy consumption than M-HELP by around 29.1% and slightly higher average messages per node than M-HELP by 6.2%.

5

D2D Communications for Victims Localization in Post-Disaster Situation

The multi-hop D2D assisted protocols discussed in previous chapters are effective in transmitting emergency calls reliably to the network. However, once the emergency calls have been received, it is important to accurately and quickly locate the victims' devices in order to provide timely assistance. This can be especially challenging in out-of-coverage areas. In this Chapter, a system is proposed that uses radio measurements obtained through D2D multi-hop assisted emergency calls to locate both in-coverage and out-of-coverage devices. To account for the uncertainty of the measurements, a dynamic constraint satisfaction problem (DCSP) is formulated to localize victims in real time. It is assumed that the multi-hop relay devices' absolute positions are unknown. The performance of the proposed scheme, $MVLA_{all}$, is compared with an existing particle filtering-based localization algorithm called RSSI Monte Carlo boxed Localization (RSSI-MCL) under a varying number of emergency user devices and functioning gNBs. It is observed that $MVLA_{all}$, has a significant performance compared to RSSI-MCL regarding localization accuracy and delay. Proceeding further, in the next chapter, an emergency call service architecture is proposed to enable the localization of high congestion cluster centers during a pandemic such as Covid-19.

In classical localization, homogeneous or hybrid techniques are used under a fully operational radio network infrastructure, where the devices' signals received by the gNB are combined to extract the positions of the devices. However, under a large disaster situation impacting the network infrastructure, the device position is extracted using the ad-hoc D2D signals received by neighbor devices. Furthermore, Figure 5.1 shows the difference between these classical and ad-hoc localization approaches.

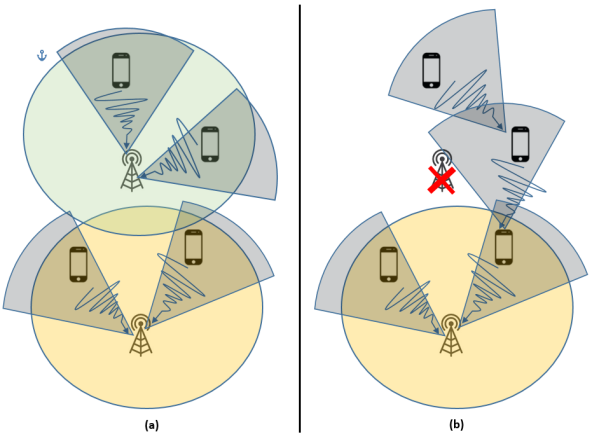

Figure 5.1: Comparison between (a) classical localization approach under operational network and (b) our localization approach under dysfunctional network. In the classical approach, the localization system uses the signals received by the base stations from the devices. In our case, the localization system uses mainly signals received by the devices from other devices. The sectors in the figure refer to the signal AoA estimation and the wavy arrows to the signal quality measured by the RSSI.

5.1/ Related Work

5.1.1/ Major Localization Algorithms

Localization measurement techniques such as RSSI, AoA, ToA, and GPS describe the used physical measurements and how these measurements are converted to geographical properties of the receiver: distance from the transmitter, orientation relatively to the transmitter or the coordinates. These estimated properties take the form of confidence interval rather than a scalar values. For example , the ToA technique provides a ring of varying thickness around the transmitter. Consequently, returned localisation techniques results need to continuously be combined, inferred and adjusted using methods such as Particle Filtering (PF) [185], Least Squares Error (LSE) [182], Kalman Filtering, and CSP. These algorithms process the geographical estimations returned by localization techniques over time to estimate the position of a device and improve the accuracy of the results.

Many research studies have used PF-based algorithms known as the Monte Carlo Localization (MCL) and Montecarlo Boxed Localization (MCB) [82, 187, 190–192]. However, the PF-based algorithm shows a high computational complexity that causes high memory usage and latency [185]. The Extended Kalman Filter (EKF) is another localization algorithm based on the Kalman filter principles and assumes Gaussian uncertainty in the measurements [192, 193]. However, due to the incomplete knowledge regarding the measurement process, the assumption that the errors follow a known probability distribution such as Gaussian is not proven and localizing techniques may lead to random errors. In addition, such assumptions lead to more biased computations in the presence of repeated or sequential location estimations [57]. For instance, in a situation involving a self-driving car, if the GPS measurement consistently lacks accuracy in a certain di-

Table 5.1: Comparison of Major Localization Algorithms

Related Work	**Progressive Positioning Propagation**	**Control traffic**	**Number of reference nodes**	**Data availability**	**Deployed Localization Algorithm**	**Required Measurements or data**
[182]	No	Yes	Medium	Fixed	Weighted Least Squares (WLS) assisted localization	RSSI+AoA
[183]	No	Yes	Medium	Fixed	EKF-based localization	RSSI+AoA
[184]	No	Yes	Medium	Fixed	MCL-assisted localization	RSSI
[185]	No	Yes	Medium	Fixed	PF-assisted localization	GPS+RSSI +AoA
[82]	No	Yes	Medium	Fixed	PF-assisted localization	GPS+RSSI
[186]	No	Yes	Medium	Fixed	MCB-assisted localization	GPS+RSSI
[187]	No	Yes	Medium	Fixed	MCB-assisted localization	GPS+RSSI
[117]	No	Yes	Medium	Fixed	CSP-assisted localization	GPS+AoA
[188]	No	Yes	Medium	Fixed	CSP-assisted localization	GPS+AoA
[189]	No	Yes	Low	Fixed	CSP-assisted localization	GPS+RSSI
[121]	No	Yes	Low	Fixed	CSP-assisted localization	GPS+AoA
Our approach	Yes	No	Very low (< 3)	Progressive	CSP-assisted localization	GPS+RSSI +ToA+AoA

rection, the vehicle may continuously make assumptions about its location that become

more biased over time. This results in an incorrect estimate that becomes progressively worse with each subsequent estimation.

CSP-based algorithms have been used for robots and radio device localization tasks in private ad hoc context [115–121, 188, 189]. Techniques such as priority ordering, filtering, and iterative min-conflict methods have been used to enhance the performance of CSP algorithms [122–124]. Moreover, in comparison to EKF, the only assumption in the CSP algorithm is to verify that the errors are bounded within maximum and minimum limits. Additionally, the minimum and maximum error limits can be determined by analyzing the tolerance levels of measurements obtained from experimental data. It is important to note that assuming errors are bounded is a crucial assumption. Still, if this assumption is found to be invalid, there are techniques to eliminate the outliers [57]. Further, the localization based on Gaussian uncertainty has been shown to be inconsistent in terms of localization error compared to a CSP method [117]. Consistency in estimations can be significantly crucial for localization in real-world circumstances.

In comparing the MCL and EKF algorithms, it is observed that MCL has shown better performance when compared to the EKF method in the literature [192]. Further, it should be noted that a variation of MCL known as RSSI-based Monte-Carlo Boxed Localization (*RSSI-MCL*) has shown better performance than MCL in [187]. Both MCL and MCB use the technique of Monte Carlo which is based on random sampling, to determine the position of a target device. It is to be noted that the main difference in MCB localization from MCL is due to using a bounded area as the search space for the target node's position.

Moreover, comparing MCL and CSP algorithms shows that CSP improves localization accuracy [115, 194]. CSP-based localization can apply constraints on the solution space to ensure that the estimated position is physically plausible and consistent with the available measurements. This allows CSP-based localization to produce more accurate and reliable results than MCL which is based on random sampling. Nevertheless, the existing CSP algorithms have mainly focused on the use of anchor nodes whose actual locations are known with high confidence. Moreover, the existing localization systems often rely on control signals that provide information for the localization of target devices. Additionally, they have not taken into account a sequential localization method in which multiple devices are localized one after another and the estimated positions of previous devices affect the localization of subsequent devices.

5.2/ Victims Localization under Partially Non-operational 5G Network

5.2.1/ System Overview

Consider a network area in which $m \in M$ is a set of emergency service-enabled cellular devices whose location coordinates (x_m, y_m) are unknown. In addition, there is a set of operational base stations, represented as *gNB* $\in G$, whose positions are known. In the event of an emergency call made from device m, it employs a multi-hop protocol to forward the call to the network infrastructure. Further, m incorporates its GPS location into the data it transmits to neighboring devices. These neighboring devices then add their own GPS information and measurements obtained from the signals they received from the transmitting device, including RSSI, AoA, and ToA.

Furthermore, this process of adding data and forwarding it to the next device is repeated through multiple hops until it reaches the emergency platform. Each device involved in the multi-hop transmission includes its own device ID and call ID in the data it transmits. Upon receiving the emergency call transmission, the emergency platform can decode the data and determine the number of participating devices by analyzing the unique device IDs associated with a specific Call ID. The platform then employs the location information gathered by each device and a Multi Victim Localization Algorithm (*MVLA*) to determine the location of the emergency device and update it to the rescue teams. The *MVLA* consists of several steps including constraint generation, dynamic localization mode selection, constraint linearization, and constraint satisfaction to determine the location of devices. Figure 5.2 illustrates the overall working scheme of the emergency call service.

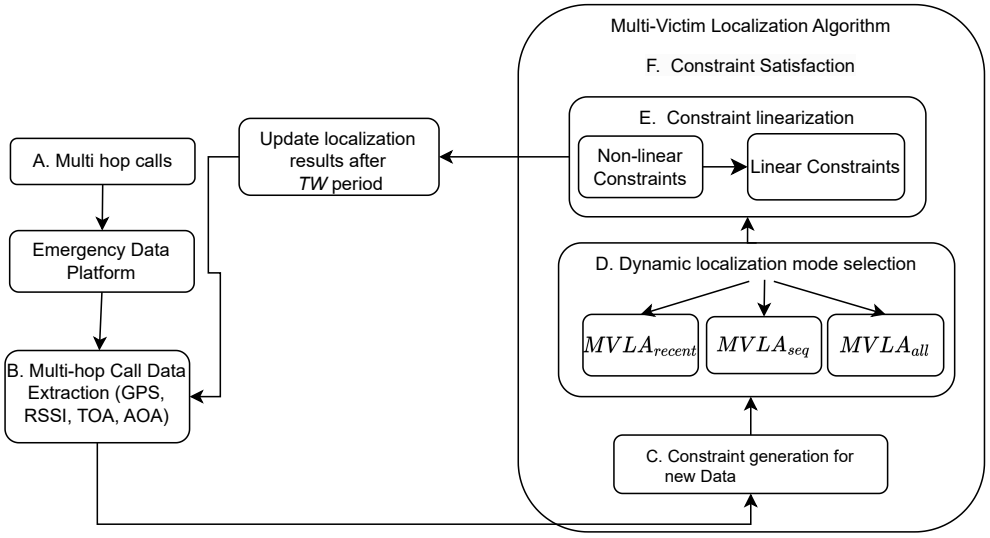

Figure 5.2: Emergency localization service working scheme.

5.2.2/ Multi-Hop Data Extraction

Once an emergency call, represented as C_{m_0}, is initiated, it follows a specific path, $P_{C_{m_0}} =< m_0, m_1, ..., m_k, gNB >$, where $m_0 \in M$ is the device that initiates the call, $m_1, ..., m_k$ are the devices the call passes through before reaching *gNB*. Once the emergency call is received by the emergency platform, the radio measurements inserted by the devices in the path are extracted. The RSSI of the device m_i as computed by its successor m_j in the path $P_{C_{m_0}}$ is represented as $RSSI(m_i, m_j)$. The GPS coordinates provided by the device m_i are represented as $GPS(m_i)$. The AoA of m_i as estimated by its successor m_j is represented as $\Theta(m_i, m_j)$. The ToA of m_i as computed by *gNB* is represented as $ToA(m_i, gNB)$.

5.2.3/ Constraints Generation

The extracted data $RSSI(m_i)$, $GPS(m_i)$, *AoA*(m_i, m_j) and *ToA*(m_k, gNB), are converted into constraints by the emergency platform localization system. Figure 5.4 illustrates a scenario in which the location of a victim device can be determined by combining the constraints generated from GPS, RSSI, ToA, and AoA measurements.

5.2.3.1/ GPS Constraint

Each $GPS(m_i)$ data is converted into a constraint on the coordinates of the device m_i. The real position of the device m_i, (x_{m_i}, y_{m_i}), is assumed to be within a given range (r_i) around the coordinates provided by $GPS(m_i)$, i.e., $(x_{GPS(m_i)}, y_{GPS(m_i)})$. More formally, the GPS constraint is written as:

$$\sqrt{(x_{m_i} - x_{GPS(m_i)})^2 + (y_{m_i} - y_{GPS(m_i)})^2} \leq r_i. \tag{5.1}$$

This constraint states that the actual location of device m_i is within a circular region, with the GPS coordinates of the device $(x_{GPS(m_i)}, y_{GPS(m_i)})$, as its center and a radius of r_i. The radius, r_i, is determined by the minimum and maximum GPS radius bounds, R^g_{max}, and R^g_{min}, and is calculated based on the location accuracy parameter in the GPS data for the device given by ϕ_i. The ϕ_i is a value between 0.1 and 1, where a higher value corresponds to a more accurate GPS reading and, therefore, a smaller r_i. Next, r_i used in (5.1) is defined as $r_i = \frac{a}{b^{\phi_i}}$, where a and b are constants that assume that r_i varies exponentially with respect to ϕ_i. The minimum and maximum bounds for r_i, R^g_{max} and R^g_{min}, are determined by relating ϕ_i values of 0.1 and 1 to their corresponding r_i values. The minimum value of r_i, R^g_{min}, is defined as, $R^g_{min} = \frac{a}{b^1}$. The maximum value of r_i, R^g_{max}, is defined as, $R^g_{max} = \frac{a}{b^{0.1}}$. The values of a and b can be determined once the minimum and maximum limits of r_i, represented by R^g_{min} and R^g_{max}, are established through practical experiments and prior assumptions that take into account the specific scenario.

5.2.3.2/ RSSI CONSTRAINT

The RSSI data between two devices, m_i and m_j, is converted into two constraints on the distance between them. The equation (5.2) expresses the lower bound and equation (5.3) expresses the upper bound of the distance. Thereby, the RSSI constraint is given as:

$$\sqrt{\left(x_{m_i} - x_{m_j}\right)^2 + \left(y_{m_i} - y_{m_j}\right)^2} \geq d_{rssi}(m_i, m_j)(1 - \alpha_{rssi}), \tag{5.2}$$

$$\sqrt{\left(x_{m_i} - x_{m_j}\right)^2 + \left(y_{m_i} - y_{m_j}\right)^2} \leq d_{rssi}(m_i, m_j)(1 + \alpha_{rssi}), \tag{5.3}$$

where α_{rssi} denotes the ratio of uncertainty on the RSSI distance measurement. Moreover, the distance is estimated using the reverse log-distance path loss model, as given in $d_{rssi}(m_i, m_j) = d_0 \times 10^{\left(\frac{P_0 - P_r}{10 \times n_p}\right)}$, where p_r, p_0, and n_p are respectively, the measured RSSI power, the nominal transmission signal power of a cellular device received at a reference distance d_0, and the path loss exponent. The d_0 is usually taken as 1 m and n_p is determined based on the environment [82]. This model is more accurate than the free space pathloss model in densely populated areas as it incorporates the impact of non-line-of-sight path loss [195].

5.2.3.3/ AOA CONSTRAINT

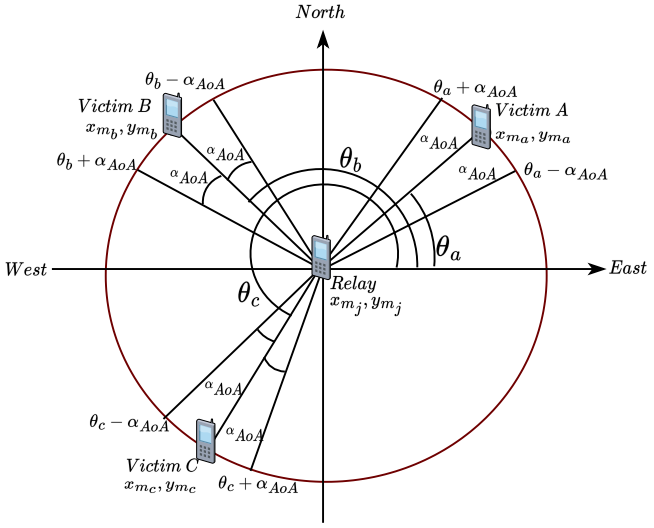

Figure 5.3: Angle of Arrival (AoA) estimation of Victim devices A, B, C with respect to the Relay device. The angle is measured in the anticlockwise direction with respect to the East.

The estimated orientation of device m_i in relation to device m_j, is denoted $AoA(m_i, m_j)$ and

is converted into the following two constraints:

$$\widehat{\theta} m_i, m_j \leq \mathit{AoA}(m_i, m_j) + \alpha AoA, \tag{5.4}$$

$$\widehat{\theta} m_i, m_j \geq \mathit{AoA}(m_i, m_j) - \alpha AoA, \tag{5.5}$$

where α_{AoA} represents the error margin of the estimated AoA. The AoA corresponds to the angle at m_j, in the anti-clockwise direction, formed by the latitude line (East-West) and the line connecting m_i and m_j, denoted as $\widehat{\theta}_{m_i,m_j}$. The constraints in (5.4) and (5.5) are combined in (5.6) using the coordinates of m_i and m_j. Furthermore, the constraints in (5.6) considers three different cases depending on the position of m_i relative to m_j, as depicted in Figure 5.3, where the devices are located in either the first or fourth quadrant, the second quadrant, or the third quadrant.

$$\begin{aligned}
&\text{if } (-\pi < AoA(m_i, m_j) - \alpha_{AoA}) \text{ and } (AoA(m_i, m_j) + \alpha_{AoA} \leq \pi): \\
&\qquad \tan^{-1}\left(\frac{y_{m_i} - y_{m_j}}{x_{m_i} - x_{m_j}}\right) \geq AoA(m_i, m_j) - \alpha_{AoA}, \\
&\qquad \tan^{-1}\left(\frac{y_{m_i} - y_{m_j}}{x_{m_i} - x_{m_j}}\right) \leq AoA(m_i, m_j) + \alpha_{AoA}, \\
&\qquad \text{if } (AoA(m_i, m_j) - \alpha_{AoA} \leq -\pi): \\
&\qquad\qquad x_{m_i} - x_{m_j} < 0, \\
&\qquad\qquad \frac{y_{m_i} - y_{m_j}}{d(m_i, m_j)} \leq \sin(2\pi - AoA(m_i, m_j) - \alpha_{AoA}), \\
&\qquad\qquad \frac{y_{m_i} - y_{m_j}}{d(m_i, m_j)} \geq \sin(AoA(m_i, m_j) + \alpha_{AoA}), \\
&\qquad \text{if } (AoA(m_i, m_j) + \alpha_{AoA} > \pi): \\
&\qquad\qquad x_{m_i} - x_{m_j} < 0, \\
&\qquad\qquad \frac{y_{m_i} - y_{m_j}}{d(m_i, m_j)} \geq \sin(AoA(m_i, m_j) + \alpha_{AoA} - 2\pi), \\
&\qquad\qquad \frac{y_{m_i} - y_{m_j}}{d(m_i, m_j)} \leq \sin(AoA(m_i, m_j) - \alpha_{AoA}),
\end{aligned} \tag{5.6}$$

where $d(m_i, m_j) = \sqrt{\left(x_{m_i} - x_{m_j}\right)^2 + \left(y_{m_i} - y_{m_j}\right)^2}$.

5.2.3.4/ ToA Constraint

The connection between the final cellular phone, m_k, and *gNB* is a typical 5G duplex communication. As a result, before forwarding the received call to the emergency platform, the *gNB* includes the information, $\mathit{ToA}(m_k, gNB)$, which represents the time difference between the transmission of the message from m_k and its reception at *gNB*. Thus, $\mathit{ToA}(m_k, gNB)$ can be converted into an estimation of the distance between m_k and *gNB* by using as $d_{toa}(\mathit{ToA}(m_k, gNB)) = \mathit{ToA}(m_k, gNB) \times 3 \times 10^8$. Emergency service platform con-

verts $ToA(m_k, gNB)$ data into two constraints:

$$\sqrt{\left(x_{m_k} - x_{gNB}\right)^2 + \left(y_{m_k} - y_{gNB}\right)^2} \geq d_{toa}(m_k, gNB)(1 - \alpha_{toa}), \tag{5.7}$$

$$\sqrt{\left(x_{m_k} - x_{gNB}\right)^2 + \left(y_{m_k} - y_{gNB}\right)^2} \leq d_{toa}(m_k, gNB)(1 + \alpha_{toa}), \tag{5.8}$$

where α_{toa} is the ratio of uncertainty on the ToA based distance measurement. Moreover, as the distance between a transmitting device (m_i) and a receiving device (m_j) gets larger, the values of α_{toa} and α_{rssi} will also increase as the error in distance estimation increases. Additionally, after a list of constraints for a particular device is compiled, it is combined to calculate the potential location of the device. An example of this process can be seen in Figure 5.4, which shows how a constraint satisfaction algorithm can be used to find the location of a device when GPS, RSSI, ToA, and AoA measurements are available.

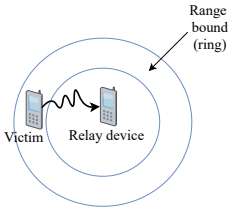

(a) Range constraint: RSSI or ToA

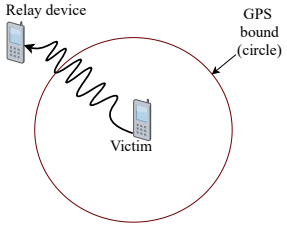

(b) GPS constraint

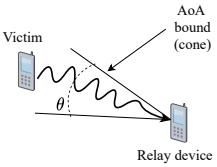

(c) AoA constraint

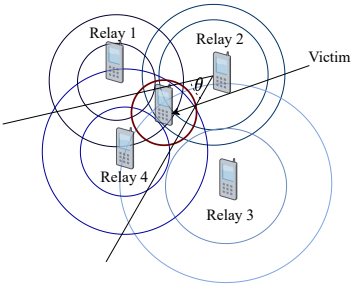

(d) GPS, AoA and n range constraints (e.g., RSSI, ToA)

Figure 5.4: Victim localization with GPS, AoA and n range measurements (e.g., RSSI, ToA)

5.2.4/ Dynamic Localization Mode Selection

In this section, the proposed multi-victim localization algorithm and its working scheme is presented. This algorithm extracts radio data such as RSSI, GPS, AoA, ToA from emergency calls and generate constraints as explained in the Sections 5.2.2 and 5.2.3. Such constraint generation is done during each time interval of *TW* and localization results are given at the end of *TW*. Thus, during each *TW*, a Dynamic Constraint Satisfaction Problem (DCSP) is formed which corresponds to a varying set of constraints on devices' coordinates. Further, the set of constraints used in the DCSP is dependent on the chosen mode of the Multiple Victims' Localization Algorithm (*MVLA*). Such *MVLA* modes are as

follows:

- *MVLA*$_{recent}$: Only the most recent data received during the past time window, *TW*, is taken into account. Data from previous emergency calls are ignored and only the sources of the calls received during the last *TW* period are localized.
- *MVLA*$_{seq}$: Instead of ignoring the received data before *TW*, the result of previous CSP resolutions is added to the list of newly generated constraints. The previous CSP resolutions are denoted for a device m_i as $x_{m_i} \leq x_{max_i}; x_{m_i} \geq x_{min_i}$ and $y_{m_i} \leq y_{max_i}; y_{m_i} \geq y_{min_i}$.
- *MVLA*$_{all}$: In each *TW*, the entire problem, including all previously generated constraints and the latest ones, is considered in the CSP.

Furthermore, the order in which devices are to be localized during a certain time interval is done based on a priority ordering mechanism. Thereby, the cellular phones participating in each multi-hop call are ordered based on a priority value, $P(m_i)$, assigned to each phone. This priority value is determined using the following equation:

$$P(m_i) = 3 \times \phi_i + 5 \times \frac{1}{d_{gNB_i}} + NC_i, \tag{5.9}$$

where $\phi_i \in [0.1, 1]$ represents the estimated GPS accuracy provided by the mobile device m_i (see Section 5.2.3.1). The distance (d_{gNB_i}) between m_i and its nearest *gNB* is calculated based on the *gNB* coordinates (x_{gNB}, y_{gNB}) and the GPS coordinates of the device ($x_{GPS(m_i)}$,$y_{GPS(m_i)}$). However, this distance estimate can be a less imprecise approximation due to the lack of accuracy in the GPS coordinates. NC_i is the number of received calls where m_i appears as a source or relay device. The factors ϕ_i, $dgNB$ and *NC* were chosen as they can determine the localization accuracy of a device. Further, the devices involved in a multi-hop call are localized in decreasing order of priority. The weights of the three factors ϕ_i, $\frac{1}{d_{gNB_i}}$, NC_i were set based on the expected localization accuracy from each technique gNB, GPS and constraints inference. We assumed that $\frac{1}{d_{gNB}}$ is the most significant factor since the gNB provides localization information by taking the combination of both the cellular and satellite signal measurements. Relegated to second place, we assumed that the *GPS* technique provides accurate localization when the conditions are favorable (number and visibility of the satellites). Finally, *NC* was given the least weight since the reliability of the location estimation from newly received calls can be volatile over time. Also, further study is needed to fully understand the impact of each weight on the algorithm's performance.

5.2.5/ Constraints Linearization

After completing the priority ordering step, the selection of constraints to be satisfied is based on the *MVLA* mode. Next, the non-linear constraints in the selected set are transformed into a set of linear constraints using the SLP algorithm [196]. Figure 5.5 illustrates the victim localization process using the SLP-assisted constraint satisfaction method [196]. This algorithm transforms each non-linear constraint into a group of linear

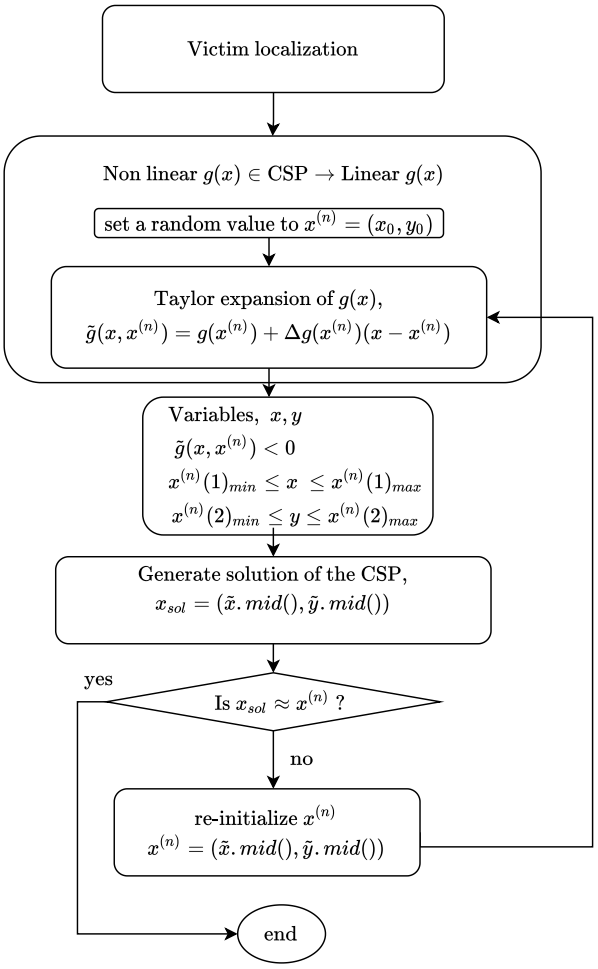

Figure 5.5: Victim Localization Procedure based on a SLP and Constraint Satisfaction approach.

constraints that approximate the region where the constraint is satisfied. The transformation is achieved through the use of a first-order Taylor series approximation. For example, the GPS constraint in (5.1) is converted to four linear constraints of the form:

$$x_{m_i} \geq x_{GPS(m_i)} - r_i, \tag{5.10a}$$

$$x_{m_i} \leq x_{GPS(m_i)} + r_i, \tag{5.10b}$$

$$y_{m_i} \geq y_{GPS(m_i)} - r_i, \tag{5.10c}$$

$$y_{m_i} \leq y_{GPS(m_i)} + r_i. \tag{5.10d}$$

The RSSI constraint in the form (5.2) and (5.3) is transformed into five linear constraints as (5.11a), (5.11b), (5.11c), (5.11d), (8.12e). In the case of ToA constraints, its approximation can be performed in a similar manner as the RSSI constraints.

$$x_{m_i} \leq x_{m_j} + d_{rssi}(m_i, m_j)(1 + \alpha_{rssi}), \tag{5.11a}$$

$$x_{m_i} \geq x_{m_j} - d_{rssi}(m_i, m_j)(1 + \alpha_{rssi}), \tag{5.11b}$$

$$y_{m_i} \leq x_{m_j} + d_{rssi}(m_i, m_j)(1 + \alpha_{rssi}), \tag{5.11c}$$

$$y_{m_i} \geq x_{m_j} - d_{rssi}(m_i, m_j)(1 + \alpha_{rssi}), \tag{5.11d}$$

$$x_{m_i} \geq x_{m_j} + d_{rssi}(m_i, m_j)(1 - \alpha_{rssi})cos(\pi/4) \vee x_{m_i} \leq x_{m_j} - d_{rssi}(m_i, m_j)(1 - \alpha_{rssi})cos(\pi/4) \vee$$
$$y_{m_i} \geq y_{m_j} + d_{rssi}(m_i, m_j)(1 - \alpha_{rssi})sin(\pi/4) \vee y_{m_i} \leq y_{m_j} - d_{rssi}(m_i, m_j)(1 - \alpha_{rssi})sin(\pi/4). \quad (8.12e)$$

In addition, when AoA constraints are present, the AoA constraint expressed as $AoA(m_i, m_j) - \alpha_{AoA} \leq tan^{-1}(y_{m_i} - y_{m_j}, x_{m_i} - x_{m_j}) \leq AoA(m_i, m_j) + \alpha_{AoA}$ in (5.6) is converted into two linear constraints:

$$(x_{m_j} - x_{m_i})cos(AoA(m_i, m_j) - \alpha_{AoA}) + (y_{m_j} - y_{m_i})sin(AoA(m_i, m_j) - \alpha_{AoA}) \geq 0, \quad (8.12a)$$

$$(x_{m_j} - x_{m_i})cos(AoA(m_i, m_j) + \alpha_{AoA}) + (y_{m_j} - y_{m_i})sin(AoA(m_i, m_j) + \alpha_{AoA}) \leq 0. \quad (8.12b)$$

Figure 5.6 schematizes the effect of the linearization of constraints. The figure shows that constraint linearization causes a relaxation of the initial constraint leading to the enlargement of the feasible area (set of positions that satisfy the constraint). However, no feasible solution is excluded by the constraints' conversion. Figure 5.6 also shows that AoA conversion keeps the feasible area intact without any relaxation.

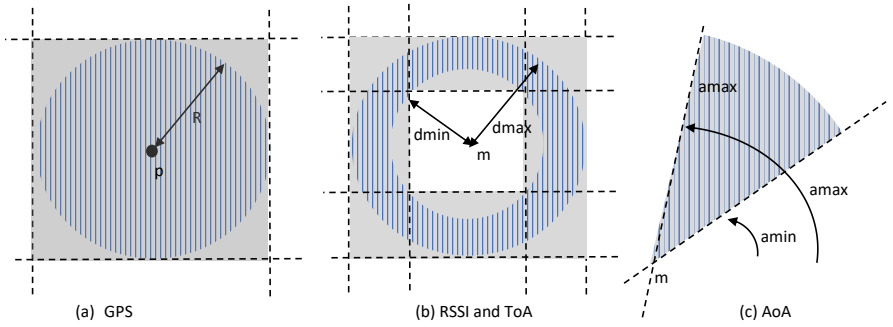

Figure 5.6: Conversion scheme of the non-linear constraints. The hatched area represents the initial feasible area, dotted lines represent the linear constraints obtained after the conversion, and the gray area represents the approximated feasible area obtained by the relaxation.

5.2.6/ CONSTRAINTS SATISFACTION

The batch of linear inequalities generated with regard to the list of devices in received calls is solved using an SLP-assisted DCSP. Algorithm 10 gives how the constraints are prepared for the CSP that works every TW cycle. The Algorithm 10 requires the following inputs: the list of devices in the received calls (Dev), the new constraints generated by the recent calls (*new_Cst*), previously generated constraints (*old_Cst*), previously estimated bounds for devices' locations (*slv_Cst*), and the selected dynamic localization mode, *MODE*. If the $MVLA_{recent}$ mode is selected, the constraints which are generated using the received calls in the last *TW* period are considered for localization. Next, if the mode is $MVLA_{all}$, the total constraints generated until the current *TW* are considered for localization. Next, if the mode is set to $MVLA_{seq}$, the current location bounds of the devices are updated using constraints generated from the received calls in the last *TW* period, and any previous *slv_Cst* available. Further, such a CSP is continued for a certain number of iterations until the solution for the victim localization is converged to a fixed point as given in Figure 5.5. The converged solutions provide the locations of the devices considered for localization.

Algorithm 10 Cyclical procedure of victim localization service.

Inputs
Dev; *new_Cst*; *old_Cst*; *slv_Cst*; *MODE*
Outputs: *slv_Cst*
Dev=*Dev* $\bigcup$ extractDevices(*new_Cst*)
Compute the priority of $d \in$ *Dev*
if MODE==$MVLA_{recent}$ **then**
  slv_Cst=*slv_Cst* $\bigcup$ SLP(*new_Cst*)
end
if MODE==$MVLA_{all}$ **then**
  slv_Cst=*slv_Cst*$\bigcup$ SLP(*new_Cst*, *old_Cst*)
end
if MODE==$MVLA_{seq}$ **then**
  slv_Cst=*slv_Cst*$\bigcup$ SLP(*new_Cst*, *slv_Cst*)
end
return *slv_Cst*

Additionally, to illustrate the process of device localization using the proposed methods, one example is provided using the $MVLA_{recent}$. Consider an example scenario involving three cellular phones m_1, m_2, and m_3 with computed priorities of 10, 12, and 8 respectively. In this scenario, it is assumed that m_1, m_2, and m_3 are located at coordinates (5, 5), (1, 3), and (10, 0) respectively, and their r_i values are 1, 2, and 1. The calls from these devices are received by the only functional gNB located at (0, 0).

Consider the case where the emergency service receives two emergency calls from the same original caller m_3. The first call follows the path $< m_3, m_1, m_2, gNB >$ and the second call follows the path $< m_3, m_2, gNB >$. This example is illustrated in Figure 5.7. The GPS and RSSI measurements included in the two received calls are used to generate constraints that give the following inequalities:

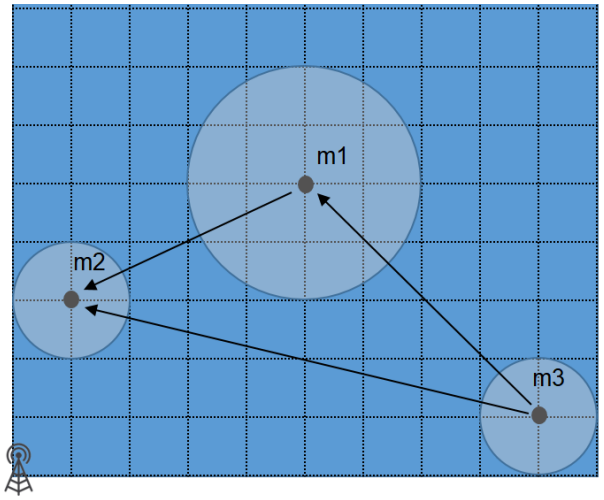

Figure 5.7: Example with three cellular phones m_1, m_2, m_3. The victim m_3 sends an emergency call that follows two paths. The depicted positions of the phones correspond to the provided GPS positions. The circle around the position depicts the GPS accuracy.

$$
\begin{aligned}
&1)\ \sqrt{(x_{m_3}-10)^2+(y_{m_3}-0)^2} \le 1,\\
&2)\ \sqrt{(x_{m_1}-5)^2+(y_{m_1}-5)^2} \le 2,\\
&3)\ \sqrt{(x_{m_2}-1)^2+(y_{m_2}-3)^2} \le 1,\\
&4)\ 4 \le \sqrt{(x_{m_1}-x_{m_3})^2+(y_{m_1}-y_{m_3})^2} \le 7,\\
&5)\ 3 \le \sqrt{(x_{m_2}-x_{m_1})^2+(y_{m_2}-y_{m_1})^2} \le 5,\\
&6)\ 7 \le \sqrt{(x_{m_2}-x_{m_3})^2+(y_{m_2}-y_{m_3})^2} \le 10.
\end{aligned}
\tag{5.12}
$$

The process of locating the victim starts with the highest priority cellular phone, m_2. In the first step, only the constraints related to a single phone (Constraints 1, 2, and 3) and those involving m_2 are considered. The non-linear constraints in 1, 2, 3, 5, and 6 are transformed into linear constraints, as outlined in Section 5.2.5. Next, the localization of m_2 is achieved using the CSP method. The method produces results by confining the x coordinate to within the range of [0.015, 2] and the y coordinate to within [2.27, 3.67]. The positions of the remaining devices are then estimated using the localized m_2. Moreover, the expected location of m_2 given by (5.13) is added to the inequalities system:

$$
\begin{aligned}
&7)\ 0.015 \le x_{m_2} \le 2,\\
&8)\ 2.27 \le y_{m_2} \le 3.67.
\end{aligned}
\tag{5.13}
$$

Subsequently, the constraints involving m_1 and the constraints related to a single cellular phone (Constraints 1, 2, 3, 4, 5, 7, 8) are resolved, resulting in the localization of the x coordinate of m_1 within the range [3.53, 5.39] and the y coordinate within [3.49, 6.37] as

given in (5.14).

$$\begin{aligned} &9)\ 3.53 \leq x_{m_1} \leq 5.39, \\ &10)\ 3.49 \leq y_{m_1} \leq 6.37. \end{aligned} \tag{5.14}$$

The predicted bounds of m_1 are then added to the inequalities system to locate the final cellular phone, m_3. By solving the inequalities system that encompasses constraints 1, 2, 3, 4, 6, 7, 8, 9, and 10, m_3 is localized with its x coordinate in the range [9.3, 10.66] and y coordinate in [1.96, 2]. Moreover, if the selected localization mode is $MVLA_{seq}$, the estimated positions of m_1, and m_2, and m_3 will be used as constraints in the next localization cycle. In contrast, $MVLA_{all}$ takes into account all received constraints and determines the location of the unknown device.

5.3/ Performance Analysis

The simulation environment comprised two key components: the first part was the arrival of emergency calls from out-of-coverage areas to the 4/5G network via M-HELP in 4.2, while the second part involved extracting data from the received emergency calls to determine the location of victims. The simulation considered a 4/5G network with a suburban area of 16.2×21 km^2 and 15,000 cellular devices, with only 7 out of 33 gNBs functioning after a disaster. The total cellular devices are uniformly distributed in the network area and the number of emergency devices are varied from 100 to 3000. Out of the total number of devices, 25% of them are in-coverage devices. Note that any device in the network can function as an emergency, a relay, or an idle device at any given time. Further details on the network and M-HELP parameters are outlined in Table 5.2. Moreover, the distribution of the in-coverage or out-coverage devices in the network area is depicted in Figure 5.8a. The network simulation was done using AnyLogic software, while the emergency center simulation was implemented using the Tubex Python library [197] and executed on the Google Colab platform [198]. The devices were localized using three different modes: $MVLA_{all}$, $MVLA_{recent}$, and $MVLA_{seq}$.

Also, the uncertainty parameters for each measurement type are expressed in Table 5.3. The possible range of r_i, can vary from a few meters to several tens of meters in ideal conditions but can drop to several tens or even hundreds of meters in challenging situations such as disasters. The R^g_{min}, and R^g_{max} were determined as given in Table 5.3. This is based on practical experiments that demonstrate an average minimum GPS accuracy of 2 m. Moreover, the R^g_{max} is set to 1000 m, considering worst-case scenarios of GPS accuracy during a scenario with no line of sight view of the satellites. Furthermore, in our scenarios, we took into account that the devices have various techniques with varying degrees of accuracy, and the accuracy level reflects the precision of the technology. For example, when the AoA is measured, the resulting estimate of the angle will have a specific level of precision. We assume that this precision falls within the previously established limits for the system, based on past practical experiments conducted in this area.

The accuracy of RSSI, ToA, and AoA measurements were determined through experiments evaluating their precision for localization. Data from these experiments showed

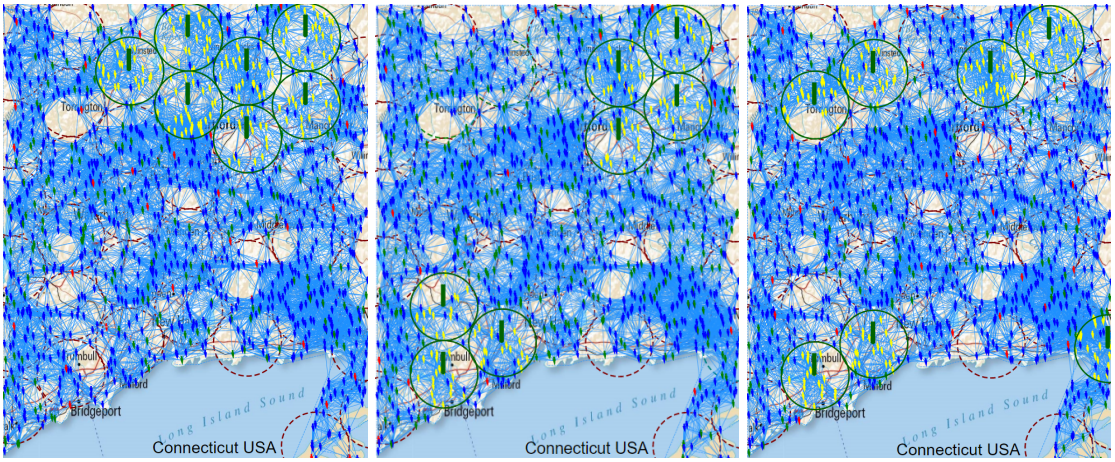

(a) Scenario 1: all operational gNBs are located in the same region.

(b) Scenario 2: operational gNBs are located in two different regions.

(c) Scenario 3: operational gNBs are located in four different regions.

Figure 5.8: Uniformly distributed 39 gNBs, with only 7 functioning, and 15,000 UEs in the AnyLogic® software. Linked UEs (resp. UE-to-gNB links) represent D2D (resp. traditional) communication possibilities. Dark green circles represent the functioning gNBs according to three scenarios. Non-functioning gNB coverage areas are indicated by red circles with dashes. Emergency devices, relay devices, in-coverage devices, and idle devices are represented respectively by the colors, red, green, yellow, and blue.

the minimum and maximum error margins for each measurement type in different environments, allowing for calculating the error of a target node. AoA measurement is found to have a total error range of $\pi/18 - \pi/3$ [69, 70], and in this study, its error margin is estimated as $\pi/6$ on each side of the central axis. The accuracy of RSSI distance estimation can be affected by various factors such as wireless channel conditions, interference, noise, and frequency band. It is estimated to fluctuate by up to 80% in a chaotic disaster environment. ToA-based distance estimation, on the other hand, is expected to have an error margin of 20%, since ToA is considered for devices under coverage. The values for accuracy parameters are given in Table 5.3.

Table 5.2: Sub-urban area emergency simulation parameters.

Parameter	**Value**
Update time interval, TW	120 sec
Total network area	16.2×21 km^2
gNB coverage	1.5 km
Total gNB number	39
Amount of working gNBs	7
Amount of broken gNBs	32
Total UE spread	RAND (16.2,21)
Total Simulation running time	45 minutes

Table 5.3: Parameters that define the error in each type of measurement.

Parameter	**Value**
Radius: GPS, R^g_{min}	2 m
Radius: GPS, R^g_{max}	1000 m
Range: RSSI, α_{RSSI}	0.8
Angle: AoA, α_{AoA}	$\pi/6$
Range: ToA (in-coverage), α_{ToA}	0.2

5.3.1/ Performance Study of MVLA Algorithms

The proposed *MVLA* modes are evaluated and compared to an existing *RSSI-MCL* scheme using three metrics: Average Distance Error (ADE), computing delay, and algorithm complexity. ADE denotes the difference between the real position, x_{rm_i}, y_{rm_i}, and the estimated position, x_{em_i}, y_{em_i} of a given cellular phone m_i given as $ADE = \frac{\sum_{i=1}^{n} \sqrt{\left(x_{em_i} - x_{rm_i}\right)^2 + \left(y_{em_i} - y_{rm_i}\right)^2}}{n}$, where n is the total number of localized victims. Moreover, computing delay is the time difference between receiving emergency data and updating the estimated victim location bounds. Next, algorithm complexity (ϵ) is the computational burden of the algorithm in terms of the number of iterations run to compute the total victim locations given as $\epsilon = \frac{\eta_{iter}}{TW}$, where η_{iter} is the number of iterations runs per TW.

First, Figure 5.9a depicts the ADE obtained from various combinations of the radio measurements. The obtained results show that the approach with *GPS+RSSI+AoA+ToA* resulted in the greatest reduction of the localization error. Indeed, when the number of constraints increases, the localization area that satisfies all the constraints becomes lesser. It is noted that the localization error decreased rapidly in the initial stages, as the emergency calls came successively from nearby locations. Over time, the ADE gradually increased due to the receipt of emergency calls from devices located at farther distances and hence longer paths. This is because the information about the farther devices is reduced. Eventually, the ADE stabilized as it became impossible to further converge the localization estimations of the devices.

Figure 5.9b depicts a comparison between the three proposed modes $MVLA_{all}$, $MVLA_{seq}$, and $MVLA_{recent}$. It is observed that $MVLA_{seq}$ and $MVLA_{recent}$ has a higher ADE than $MVLA_{all}$. This is attributed to the reduction in the number of constraints considered in each cycle by $MVLA_{seq}$ and $MVLA_{recent}$, which impacts their performance. These modes generate constraints only using data collected within the previous *TW* interval. The rapid increase in the ADE in $MVLA_{seq}$ and $MVLA_{recent}$ over time is observed due to the limited data and hence fewer constraints generated for victim devices located at far off locations. However, $MVLA_{seq}$ performs slightly better than $MVLA_{recent}$ as it took into account previously estimated localization results in determining the next bound for localization. Nevertheless, in situations where low complexity algorithms are needed during large emergency data scenarios, $MVLA_{seq}$ and $MVLA_{recent}$ modes can serve as suitable alternatives to the $MVLA_{all}$ mode.

Figure 5.9c depicts the obtained ADE according to the precision of the employed radio

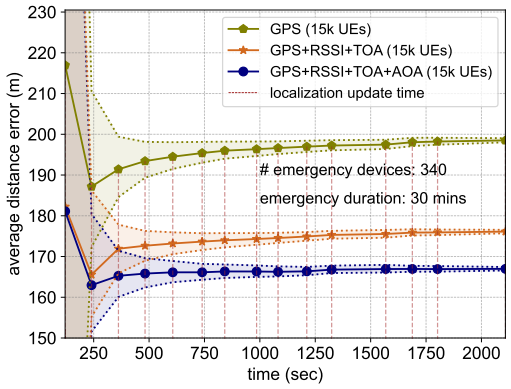

(a) Variation in ADE against time with *MVLA*$_{all}$ mode under different combinations of GPS, RSSI, ToA, and AoA.

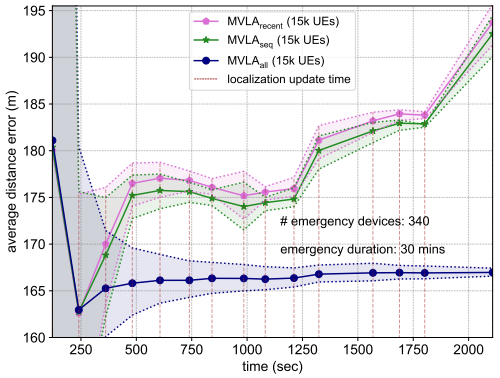

(b) Comparison of ADE against time under *MVLA*$_{recent}$, *MVLA*$_{recent\text{-}seq}$ and *MVLA*$_{all}$. Localization scheme: GPS+RSSI+AoA+ToA.

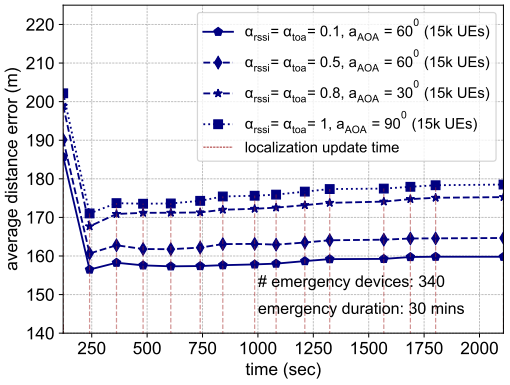

(c) Comparison of ADE against time under different $\alpha_{RSSI}, \alpha_{ToA}, \alpha_{AoA}$ values in *MVLA*$_{all}$ mode. Localization scheme: GPS+RSSI+AoA+ToA.

Figure 5.9: Performance analysis of proposed *MVLA* modes under a varying number of radio measurements, constraint size, and error limits. The total number of emergency devices localized = 340, emergency calls occurring duration = 30 minutes. The minimum and maximum error limits of each combination are denoted by the upper and lower bounds of the filled region with its distinct color.

measurements: $\alpha_{rssi}, \alpha_{toa}$ and α_{AoA}. It is observed that the lowest ADE is achieved when measurements with higher precision are combined. An increase in precision leads to a smaller geographical area that meets the constraints as the accuracy of measurements is improved.

Figure 5.10 illustrates the resulting ADE under different distributions of functioning gNBs across the network area. Furthermore, The results indicate that when the functioning gNBs are concentrated in one corner of the network, the ADE is worse than in scenarios where the operational gNBs are scattered across the network area. In Scenarios 2 and 3 of Figures 5.8b and 5.8c, there is a higher availability of functioning gNBs in close proximity. Therefore the number of hops required to reach such a gNB decreases. This

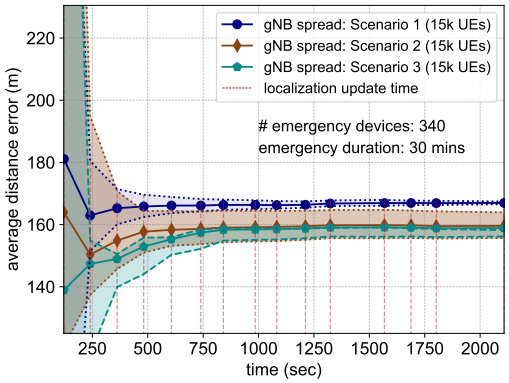

Figure 5.10: Impact of the functioning gNBs distribution over the average distance error (ADE) with $MVLA_{all}$ mode.

leads to a situation where emergency calls are routed through fewer intermediate relay devices. Hence the propagation of positioning uncertainty is reduced when gNBs are distributed as in Scenario 2 or even more as in Scenario 3. Conversely, the ADE is higher when gNBs are clustered together as in Scenario 1.

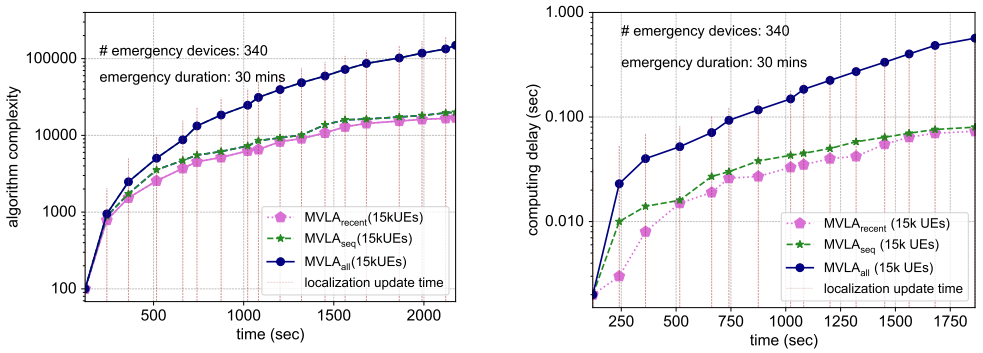

(a) Comparison of algorithm complexity against time.

(b) Comparison of computing delay against time.

Figure 5.11: Computational complexity and delay under the $MVLA_{recent}$, $MVLA_{recent\text{-}seq}$ and $MVLA_{all}$ schemes. Localization scheme used: GPS+RSSI+AoA+ToA. Parameters: R^g_{min} = 2 m, R^g_{max} = 1000 m, α_{RSSI} = 0.8, α_{ToA} = 0.2, $\alpha_{AoA} = 30^0$. Total number of emergency devices localized = 340, emergency calls occurring duration = 30 minutes.

Figure 5.11a depicts the algorithm complexity against time. It is seen that the $MVLA_{all}$ has a higher complexity than $MVLA_{seq}$ and $MVLA_{ord}$, due to handling a larger number of constraints, as given by the Algorithm 10. Figure 5.11b depicts the computing delay of the *MVLA* modes. The computing delay of localization estimation is also influenced by the number of constraints handled by the localization mode. Thereby, it is seen that $MVLA_{all}$ has a higher delay than the two other modes. It is observed that $MVLA_{all}$ still maintains a fast response time of 1 second for a scenario with 340 victims and 15000 devices. However, in scenarios with an increased number of victims and a denser cellular

network, the response time is likely to be higher.

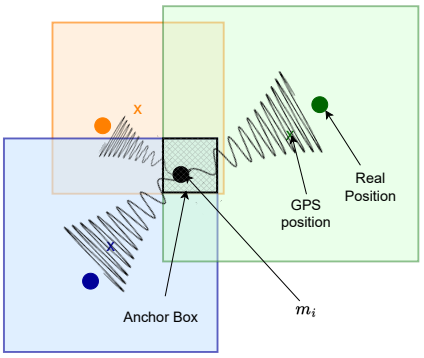

(a) Anchor box computation in *RSSI-MCL* method.

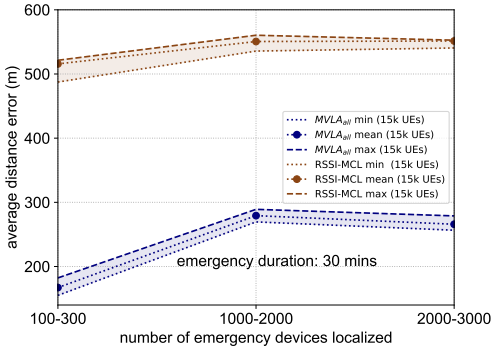

(b) Comparison of ADE achieved under *MVLA*$_{\text{all}}$ and *RSSI-MCL* against the number of victims.

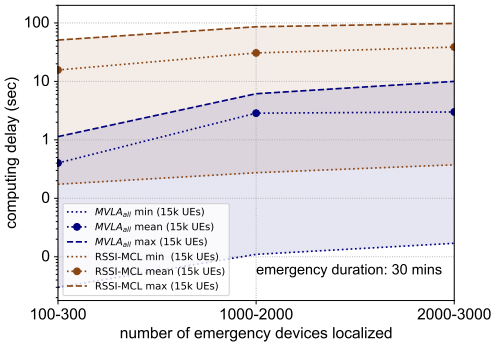

(c) Comparison of computing delay under *MVLA*$_{\text{all}}$ and *RSSI-MCL* against the number of victims.

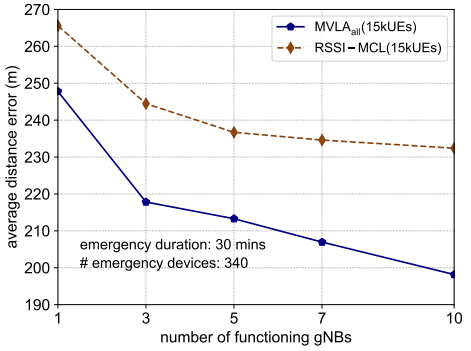

(d) Comparison of ADE under *MVLA*$_{\text{all}}$ and *RSSI-MCL* against the number of functioning gNBs. Total number of gNBs in the area (including broken gNBs) = 33.

Figure 5.12: Comparison of *MVLA*$_{all}$ against *RSSI-MCL*. Parameters: R^g_{min} = 2 m, R^g_{max} = 1000 m, α_{RSSI} = 0.8, α_{ToA} = 0.2, α_{AoA} = 30^0. Localization approach: GPS+RSSI+AoA+ToA. Emergency calls occurring duration = 30 minutes. The minimum and maximum error limits of each scheme are denoted by the upper and lower bounds of the filled region with its distinct color.

Next, the performance of *MVLA*$_{all}$ mode is compared with the *RSSI-MCL* [186]. *RSSI-MCL* uses a combination of particle filtering and RSSI-based distance constraints to localize the nodes. For each cellular phone, m_i, the emergency service platform extracts the couples of data of the type *RSSI*(m_j, m_i) and *GPS*(m_j). Each couple of data *RSSI*(m_j, m_i) and *GPS*(m_j) is used to compute a box area $\Gamma(m_j, m_i)$ where m_i is expected to be (see Figure 5.12a). The intersections of all the $\Gamma(m_j, m_i)$ boxes for a given cellular phone, m_i, is called anchor box $\Gamma(m_i)$. Then 50 particles uniformly distributed in the anchor box $\Gamma(m_i)$ are generated. Ultimately, only the particles that meet the RSSI constraints are used to determine the target location. The mean of these particles is considered as the estimated position of m_i.

In Figure 5.12b, the ADE obtained using *MVLA*$_{all}$ and *RSSI-MCL* is presented. It is

noted that the lower accuracy in *RSSI-MCL* is due to the utilization of smaller number of radio measurements than $MVLA_{all}$. Furthermore, the *RSSI-MCL* method fails to exploit the complete potential of the particle filtering method as it distributes particles uniformly over the anchor box when localizing static devices. Moreover, in contrast to $MVLA_{all}$, *RSSI-MCL* does not take into account the position uncertainty in relay devices, which is particularly relevant in emergency scenarios. The localization error of intermediate relay devices impacts significantly on the overall localization accuracy due to the propagation of localization along multi-hop devices. Next, it is noted that the accuracy in RSSI and GPS measurements can significantly deteriorate due to high levels of interference leading to inaccuracies. Additionally, GPS can introduce considerable errors when devices do not have direct Line of Sight (LOS) link with satellites. $MVLA_{all}$ method incorporates RSSI and GPS, but also AoA and ToA to reinforce the resultant localization accuracy. Thereby, $MVLA_{all}$ method has the potential to perform well in terms of accuracy during emergency situations. As a result, $MVLA_{all}$ demonstrates a reduction of ADE by 55.97% compared to *RSSI-MCL*.

Furthermore, the time response of *RSSI-MCL* and $MVLA_{all}$ according to the number of emergency devices is presented in Figure 5.12c. On average, *RSSI-MCL* took more time than $MVLA_{all}$. Indeed, the computation of the anchor boxes and extracting the particle positions that satisfy the constraints slowed down the *RSSI-MCL* method. Also, it is observed that in $MVLA_{all}$, the time response reaches 10 seconds when the number of victims is between 2000 to 3000 with 15000 available devices. The time response is expected to reach up to several minutes under large network scenarios (10^5 devices with 10^4 emergency calls). In such a case, the use of lighter modes, $MVLA_{seq}$ and $MVLA_{recent}$, is preferred.

Moreover, the impact of functioning gNBs on the ADE is seen in Figure 5.12d. The average localization estimation error declines with the increase in the number of functioning gNBs. The number of users under coverage increases and hence the location estimation accuracy in such devices increases. Hence, the sequential relay devices' location estimations are improved and victim location estimation accuracy is increased. The, *RSSI-MCL* has a lower decrement than $MVLA_{all}$ in localization error since only two types of radio measurements and particle filter algorithm are used. In contrast, $MVLA_{all}$ uses the dynamic constraint satisfaction algorithm with the combination of four radio measurement types.

5.3.2/ Devices' Mobility and Victims' Localization

Mobility of both victims' and relay devices is an intrinsic characteristic in the victims' localization process. The mobility feature must be considered at the two stages of the disaster management process, i.e., the victims' assessment and the localization. During the victims' assessment stage, protocols such as M-HELP presented in 4.2 or 5G-SOS in 4.4 allow forwarding emergency calls to the safety service platform. Therefore, it is important to improve the emergency call relay protocols to automatically resend the localization-related data when the victim's location significantly changes compared to the

last reported position.

In order to localize the victim, it's important to consider constraints related to the respective data reception time periods as the victim or relay devices involved are not in the same position. The satisfaction of these constraints may be then impossible since some constraints are outdated. To allow the progressive consideration of the automatic re-sending of the emergency call when victims move, the localization procedure must be launched periodically and the recent constraints (generated from recently received emergency calls) should be prioritized against the previously extracted constraints. This prioritization may take the form of penalties or weights assigned to the constraints according to the freshness of the used data. The possible unfeasibility of the generated system leads to the adoption of a new optimization approach where the objective is to reduce the weighted sum of unsatisfied constraints rather than satisfying all the constraints. To tackle this scenario, various techniques such as Meta-heuristics [**?**] (Genetic Algorithms, Simulated Annealing, Tabu Search, etc.) or Decision Tree exploration-based methods [**?**] such as Branch and Bound or Branch and Cut can be used.

5.4/ CONCLUSION

This chapter presented the localization mechanism of victims using data received over multi-hop emergency calls from in-coverage and out-of-coverage areas during a disaster. Hence, real-time multi-emergency device localization modes based on dynamic constraints satisfaction method were proposed. The simulations demonstrated that the $MVLA_{all}$ approach allowed to localize up to around 2500 victims in less than 10 seconds and improved localization accuracy by 55.9% compared to *RSSI-MCL*. In a more dense city with a higher number of victims, two alternative modes, called $MVLA_{seq}$ and $MVLA_{recent}$, can be used to reduce response delay with a trade-off of lower localization accuracy than $MVLA_{all}$. One of the major advantages provided by our approach is the management of the trade-off between localization accuracy and system responsiveness. It is then interesting to study how the constraints linearization improvement may impact the localization accuracy without increasing the CSP complexity. Currently, GPS, RSSI and ToA constraints are approximated using square areas. The study of other polygonal shapes that reduces the feasible area extension is one of the first steps in the improvement of the method. Additionally, the localization of moving devices using the proposed approach can be an interesting area for future research, which requires considering constraints related to the reception time of data, as the victim or relay devices involved are not in the same position. In such scenarios, optimization approaches like Meta-heuristics or Decision Tree exploration-based methods should be used to prioritize constraints based on their freshness. Furthermore, methods such as particle filtering are suitable for localizing multiple mobile victims due to its ability to track continuous position changes.

6

Enhanced Convex Hull-based Clustering for High Population Density Avoidance under D2D Enabled Network

The previous chapter of this thesis proposed a localization scheme for finding and aiding victims in disaster areas. However, in the current climate with pandemics like Covid-19, it is also necessary to locate areas of high population congestion in order to mitigate the impact of such disasters. Therefore, this chapter presents a proposed emergency call service architecture that can be used to identify these population congestion centers.

Global pandemics such as Covid-19 in 2020 have led to massive loss of human lives and strict lockdown measures worldwide. To return to a certain level of normalcy, community awareness on avoiding high population density areas is significantly important for infection prevention and control. With the availability of new telecommunication technologies, it is possible to provide highly informative population clustering data back to people using Wireless Aerial Agents (WAAs) placed in a local area. In this chapter, a service architecture that allows users to access the localization of population clusters is proposed. Thereby, a convex hull-based clustering method, Enhanced Population Clustering (*E-PC*), is proposed. This method refined the result of conventional clustering methods such as *K-means* and *Gaussian Mixture Model (GMM)*. Moreover, the potential in *E-PC* to achieve the same or higher results compared to the original *K-means* and *GMM*, while consuming lesser data points, is demonstrated. On average, *E-PC* improved the cluster detection performance in both *K-means* and *GMM* by 18.93% under different environments such as remote, rural, suburban, and urban in terms of silhouette score. Further, *E-PC* allows a 15% data reduction which results in decreasing the computational cost and energy consumption of the WAAs.

6.1/ Related Work

Crowd monitoring is an active research area that is used for different applications such as behavior analysis, intelligent surveillance systems, public riots detection, and congestion avoidance [199]. High population congestion is one of the main reasons for infectious diseases such as Covid-19 to spread fast and over a large geographical area [200]. Physical distancing has been argued as one of the effective means to combat the spread of such pandemics before vaccines or therapeutic drugs becomes available. Thus, the knowledge on population cluster centers in local areas, e.g., small cities, shopping complexes, schools, is important in avoiding overcrowded areas and preparing for current and future pandemics [201]. A variety of wireless communication and positioning technologies, including drones, cellular positioning systems, and GPS, can be used to monitor crowd gatherings outdoors [202]. Thus, D2D sidelink communication technology allows WAAs to reach UEs in the network edge or out of coverage areas, which may not be captured under the cellular network infrastructure [203, 204].

Techniques used for crowd monitoring could be mainly classified into supervised or unsupervised approaches. Supervised learning methods are used for applications such as behavior detection, density estimation, etc. Unsupervised learning methods are used for crowd clustering where clusters are detected via distance-based algorithms [205]. Meanwhile, recent trends in convex hull based methods for clustering have paved the way to simplify and enhance the performance in clustering algorithms [206].

Clustering is a data processing algorithm that classifies a set of entities based on proximity between cluster members, the concentration zones of the data, and their statistical distributions [207]. The purpose of clustering is both to minimize the intra-cluster distance and to maximize the inter-cluster distance. *K-means* and *GMM* are two of the most conventional clustering methods [208]. *K-means* approach groups data into clusters by minimizing the distances between data points and their cluster's centroid [209]. To that end, in an iterative way, k initial points (k is an input parameter of *K-means* method) from the dataset are randomly selected as cluster centers. Then the other dataset points are assigned to the closest cluster center. The sum of the intra-cluster distance is then computed. The process is repeated a given number of iterations to minimize the sum of intra-cluster variations.

In contrast, *GMM* identifies clusters using an Expectation-Maximization (EM) algorithm assuming that all data points are generated from a mixture of a finite number of Gaussian distributions. Further, it has been shown that *GMM* is a complex classification method and has a higher computation time compared to *K-means* [210]. Hence, *GMM* may be less energy efficient, limiting its use for low computing capacity in WAAs.

The unawareness of the number of clusters in the input data represents one of the issues with the unsupervised learning clustering approaches. Several techniques such as elbow method, silhouette method and gap statistics method have been proposed to compute the optimal number of clusters in the data [211].

Comparative studies show that *gap statistics method* provides better performance concerning the identification of the optimal number of clusters [212]. In *gap statistics method*

different values for the number of clusters, k are evaluated. For each k value, the clustering algorithm is run, then the sum of intra-cluster variation, W_k, over the generated clusters is computed. Thereafter, a set B of uniformly distributed points are generated and clustered. Finally, sum of intra-cluster variation over clusters of the set B, W_k^*, is computed and compared with W_k [213]. Hence, gap statistics for a particular k, is mathematically defined as:

$$Gap_k = log(W_k^*) - log(W_k), \tag{6.1}$$

Finally, the k value that maximizes Gap_k is selected as the optimal k.

Meanwhile, research works in [206, 214] have proposed methods to incorporate convex hull principles to improve performance in clustering algorithms. Convex hull of a planar set of points P is the smallest convex set enclosing P [215]. The convex hull is obtained in practice using facet enumeration techniques. Quickhull algorithm is such a facet enumeration method, which is considered an efficient and practical method for convex hull computation [216].

The Quickhull algorithm is based on the divide-and-conquer algorithm that divides the input data into subsets and recursively evaluate such subsets [217]. It is started by first computing the maximum and minimum points of P. Secondly, the horizontal and vertical lines passing through these points are found to form a bounding rectangle, which forms the initial hull. Next, the points lying within such a quadrilateral are eliminated from further consideration. Finally, as the algorithm executes, a convex hull is formed once the set of points outside each edge of the polygon is zero [216]. In addition, by adopting the Maximum Volume Inscribed Ellipse in a convex hull (MVIE) principle [218] in unsupervised learning, an understudied method of population clustering in a local D2D network is proposed.

6.2/ METHODOLOGY

In this Section, a novel method for population cluster detection called *E-PC* under a local D2D network, where users' phones reside within the coverage range of the WAA, is proposed. A MVIE based *K-means* clustering is used in *E-PC* to identify more than one cluster. Let M be a set of 4/5G D2D enabled UEs that have subscribed to the population clustering service provided by a WAA, namely u_a, which is hovering above a specific height in the local area (Figure. 6.1). Each $m \in M$ utilizes a PSCCH and a PSSCH to establish a D2D link with u_a. Two D2D modes are distinguished according to the coverage status of the user device and WAA [219]. In in-coverage D2D communication mode, one of the two devices is under the coverage of a given gNB station. However, in out-of-coverage mode [41], the synchronization of the two devices is made using the Primary Synchronization Signals (PSSs) and Secondary Synchronization Signals (SSSs).

Once a D2D link is established with the u_a, the device $m \in M$ transmits its location information to u_a every T_w period. The u_a stores the received location data for a maximum

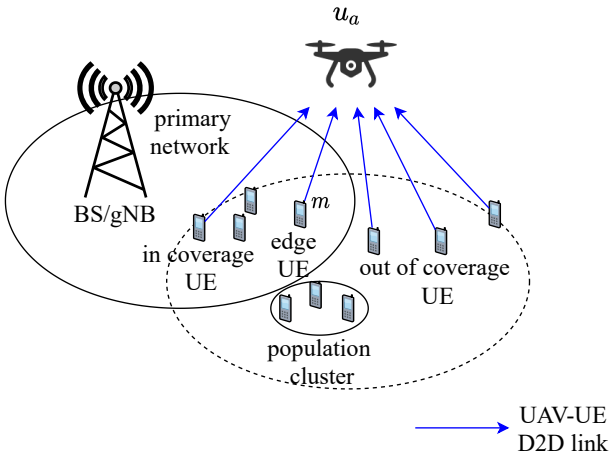

Figure 6.1: WAA u_a collecting location data from N_l number of UEs in a local region to identify the population clusters using the proposed algorithm.

time period $T_0 > T_w$. If the location data of a given mobile m is not updated after the T_0 period (e.g. the mobile switches off), the location data of the mobile is removed. The u_a works in two modes according to the clustering requests rate. The u_a counts the number of requests received each T_w. In each period T_M, the u_a computes the average number of requests per T_w during the last T_M period, RR. If this average exceeds 1, then the u_a switches to the *periodic clustering mode*. While if the requests rate RR is lower than 1, the u_a uses the *on-demand clustering mode*.

In the *periodic clustering mode*, the u_a computes the cluster centers in each T_w. Once a clusters' localization request is received, u_a sends the coordinates of the last computed cluster centers. Since the number RR is higher than 1, the *periodic mode* allows to limit the amount of energy consumed by u_a. In contrast, in *on-demand mode*, the clusters are only computed when a new request is received. Consequently, the u_a does not waste energy by computing the clusters when there is no request. To compute the cluster centers c_c, u_a uses the last received location data, N_l, from M during the last T_0 period. The mobile device localization is referenced by its geographical coordinates: longitude and latitude. Once a clusters' centers request is received, the response is sent to the user device m through the D2D sidelink channels. The clustering procedure in both *on-demand mode* and *periodic mode*, involves three main steps: convex hull computation, maximum volume inscribed ellipse optimization, and cluster centers computation.

6.3/ Convex Hull Computation

The convex hull of the set N_l is computed by calling a facet enumeration algorithm called Quickhull algorithm [216]. The convex hull of a set of points corresponds to the smallest convex 2D area that covers the set of points (see Figure 6.3).

Formally, the convex hull area of N_l, χ_c, contains the set of points, $\mathbf{x}$, respecting the following p inequalities:

$$\chi = \{\mathbf{x} \in \mathbb{R}^2 \mid \boldsymbol{a}_i^{\boldsymbol{T}}\mathbf{x} \leq \boldsymbol{b}_i,\ i = 1, ..., p\}, \tag{6.2}$$

Each equation $a_{i,1} \times x + a_{i,2} \times y = b_i$ corresponds to a line segment forming the convex hull boundary of N_l, where $a \in \mathbb{R}^{2\times p}$, $b \in \mathbb{R}^p$.

6.3.1/ Maximum Volume Inscribed Ellipse Optimization

During the second step of the clustering procedure, u_a computes the ellipse included in the convex hull with the maximum volume. Let's assume that the maximum volume inscribed ellipse, inside χ_c (Figure 6.3) contains the major part of the localized mobiles M. Therefore, regions outside the ellipse while being inside the convex hull represent negligible clustering areas. The area inside an ellipse ε could be defined as follows:

$$\varepsilon = \{\mathbf{x} \mid \mathbf{x} = \mathcal{B}\boldsymbol{u} + \boldsymbol{d}, \boldsymbol{u} \in \mathbb{R}^2, \|\boldsymbol{u}\|_2 \leq 1\}, \tag{6.3}$$

$\mathcal{B} \in \mathbb{R}^{2\times 2}$ is a symmetric positive definite matrix that represents the deformation matrix from a unit circle to an ellipse and $\boldsymbol{d} \in \mathbb{R}^2$ is the vector that gives the orientation of the ellipse. Maximum volume inscribed ellipse ε^* is obtained by determining the ellipse parameters, B and d, that maximizes the ellipse volume given in (6.5), and ensures that the ellipse is included in the convex hull ($\varepsilon^* \subseteq \chi$). Such constraint can be represented as the set of inequalities provided in (6.4).

$$\|\mathcal{B}\boldsymbol{a}_i\| + \boldsymbol{a}_i^T\boldsymbol{d} \leq \boldsymbol{b}_i,\ i = 0, ..., p. \tag{6.4}$$

The volume of an ellipse with parameters B and d is given by:

$$Vol(\mathcal{B}, \boldsymbol{d}) = \rho_2 \sqrt{det(\mathcal{B}^T\mathcal{B})}, \tag{6.5}$$

where ρ_2 gives the volume of a planar unit circle [218]. Hence, the maximum volume inscribed ellipse optimization is formulated as follows:

$$\begin{aligned} \min_{\mathcal{B},\boldsymbol{d}} \quad & -\sqrt{det(\mathcal{B}^T\mathcal{B})} \\ \text{s.t.} \quad & \|\mathcal{B}\boldsymbol{a}_i\| + \boldsymbol{a}_i^T\boldsymbol{d} \leq \boldsymbol{b}_i,\ i = 0, ..., p, \\ & \mathcal{B} \succeq 0. \end{aligned} \tag{6.6}$$

Noting that the objective function $det(\mathcal{B}^T\mathcal{B})$ in (6.6) is a non-convex function. The non convexity of the objective function leads to some problem of optimization convergence. To overcome this problem, the maximum volume inscribed ellipse is reformulated as a negative log determinant maximization problem [215, 218]. Log of determinant is used to ensure convexity of the objective function. This new problem is formulated as follows:

$$\begin{aligned} \min_{\mathcal{B},\boldsymbol{d}} \quad & -\log\det(\mathcal{B}) \\ \text{s.t.} \quad & \|\mathcal{B}\boldsymbol{a}_i\| + \boldsymbol{a}_i^T\boldsymbol{d} \leq \boldsymbol{b}_i,\ i = 0, ..., p \\ & \mathcal{B} \geq 0. \end{aligned} \tag{6.7}$$

In this work, CVXOPT solver was used to solve the MVIE optimization problem given in (6.7). CVXOPT is a convex optimization solver based on the Python programming language.

6.3.2/ Cluster Centers Computation

The goal is to detect cluster centers formed by the UEs and consequently avoid dense zones. It was assumed that UEs form clusters around the cluster centers following a Gaussian multivariate density function [220] with a μ 2D mean vector, and Σ^2 covariance matrix, given by (6.8). The graphical representation of UE locations following such a Gaussian density function is illustrated in Figure. 6.2.

$$f(x|\mu,\Sigma) = \frac{1}{\sqrt{(2\pi)|\boldsymbol{\Sigma}|}} \exp\left(-\frac{1}{2}(x-\mu)^T\boldsymbol{\Sigma}^{-1}(x-\mu)\right), \tag{6.8}$$

where x denote the coordinates of the UE locations.

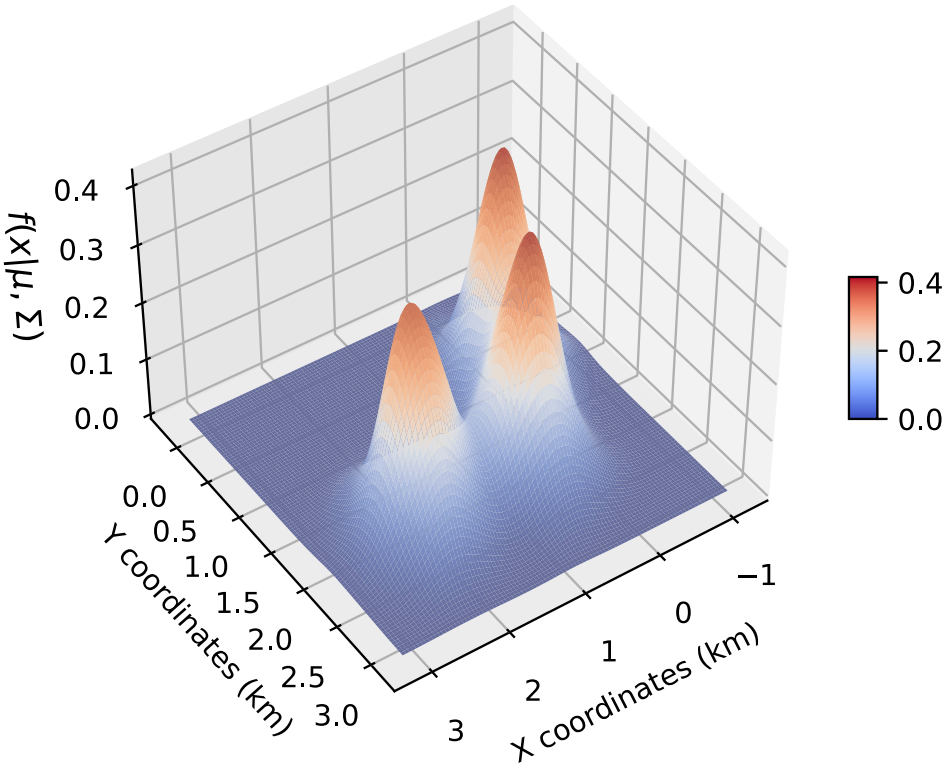

Figure 6.2: UEs forming clusters around three centers following a Gaussian multivariate density function, given in (6.8), each with a cluster variance of 0.3.

The UEs with a location outside the maximum volume inscribed ellipse ε^*, are more sparse and may decrease the clustering performance. Hence, in our proposed method, *K-means* is applied only on the locations inside ε^*. The optimal number of clusters K_{opt} inside ε^* are computed using the gap statistics method [213] discussed in the *related works* section. K_{opt} corresponds then to the cluster number which has the highest gap statistic value. Finally, the set of the K_{opt} cluster centers c_c are detected as shown in Figure 6.3. The location of c_c of each cluster is computed by the arithmetic mean of all data points that belong to that cluster [221].

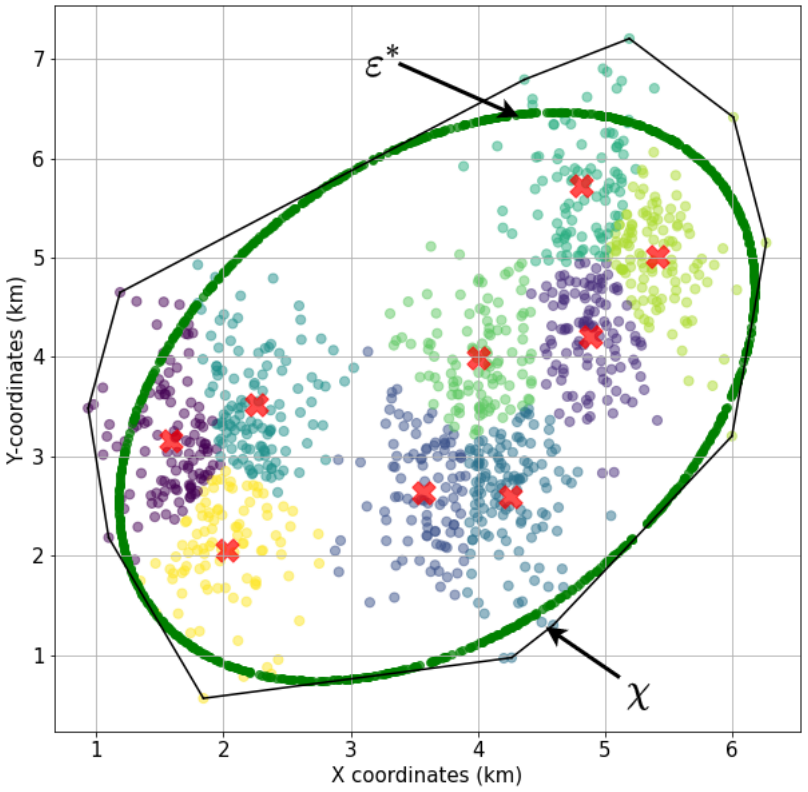

Figure 6.3: Proposed method: First, the optimal number of clusters, K_{opt}, in the UE locations inside the maximum volume inscribed ellipse ε^* is computed. Next, a conventional clustering method is used to detect K_{opt} in the total UE locations in the network area. Distinct colors represent the different clusters. The red crosses denote the cluster center locations, c_c.

Once a request is received, u_a sends the set of coordinates of the c_c to the corresponding mobile. The procedure followed by u_a for computing the cluster centers is summarized in Algorithms 11, 12 and 13.

6.4/ Performance Analysis

6.4.1/ Numerical Simulations

The proposed algorithm was implemented in the Google Colab online platform [222].

Algorithm 11 Procedure run every T_w on u_a

Input UE locations N_l
Output cluster centers c_c
if $RR >= 1$ **then**
  for every T_w period **do**
    Compute convex hull boundary of N_l, χ_c, locations
    Selecting the locations inside ε^* from N_l
    Determine K_{opt} using gap statistics method
    Use a conventional clustering method to find c_c
  end
end

Algorithm 12 Procedure run every T_M on u_a

Input list of received requests
Output average number of requests per T_w during the last T_M period, RR
Compute the average number of requests per T_w

Algorithm 13 Procedure run on reception of new request

Input mobile sender m, UE locations N_l
Output cluster centers c_c
if $RR < 1$ **then**
  Compute convex hull boundary of N_l, χ_c, locations
  Selecting the locations inside ε^* from N_l
  Determine K_{opt} using gap statistics method
  Use a conventional clustering method to find c_c
else
  Use the last computed c_c in Algorithm 11
end
Communication of c_c to m

The simulation parameters used are presented in Table 6.1. For each scenario, a sample dataset was generated containing n_{a_c} isotropic Gaussian clusters with the same variance S^2 using the *make blobs* Python function [223].

The clustering procedure on the generated dataset was started by calculating the convex hull, χ_c, of the points. Then using the optimization tool, CVXPY [224], the maximum volume inscribed ellipse, ε^*, was computed. Next, the gap statistics method was applied to determine the optimal number of clusters K^*_{opt}. Indeed, since that gap statistics method is not deterministic (see Section 6.1), the obtained K_{opt} can change on different runs. Hence, *gap statistics method* was applied for a given number of iterations, r_{km}, and the obtained K_{opt} with the highest gap statistics was selected as the most suitable K^*_{opt}. It should be noted, that the gap statistics method was applied only on points of the dataset that are inside the ε^*s. Once K^*_{opt} was computed, a conventional clustering method, i.e., *K-means*, *GMM*, was applied on the N_l points to determine the cluster centers c_c.

To ensure the relevance of the comparison, every method was run r_d times using the same simulation parameters but with different datasets. The results shown below correspond to the average evaluation of the method for each scenario.

‘

Table 6.1: Simulation parameters

Parameter	**Value**
Number of clusters in original data, n_{a_c}	3
Variance of each cluster	0.12
Network area	7×7 km^2
Minimum and maximum limits of K_{opt}	[2,...,15]
Total UE number (cluster points), N_l	variable $[10^2, 10^3, 10^4, 10^5]$
Number of iterations, r_{km}	10
Number of different data sets, r_d	3

6.4.2/ Evaluation Parameters

Silhouette score and data size reduction were used to evaluate the clustering in proposed and baseline approaches. The cluster detection performance was evaluated using the silhouette score [225]. Such a score was computed to study the separation distance between the resulting clusters [226]. Silhouette value of one data point, p, is defined as:

$$S(p) = \frac{(b(p) - a(p))}{\max(a(p), b(p))}, \tag{6.9}$$

where $a(p)$ is the mean distance between p and all other data points in the same cluster called mean intra-cluster distance, and $b(p)$ is the mean distance between p and all the points of the nearest cluster, called mean nearest-cluster distance [227]. Silhouette score computation returns a value between -1 and 1 that measures the quality of the clusters. More specifically, the higher the silhouette score, the better the cluster detection [225].

The data size reduction, d_r, was computed as:

$$d_r = d_{in} - d_{\varepsilon^*}, \tag{6.10}$$

where $d_{in}, d_{\varepsilon^*}$ denotes respectively, the total number of data points in the dataset of UE locations and the number of data points that are inside the ε^*.

6.4.3/ Results

The performance of the proposed approach *E-PC* applied on conventional clustering methods, was compared with two conventional methods: *K-means* and *GMM* clustering. The difference in the approaches is that, in the conventional clustering, the gap statistics method is applied on the total UE locations dataset, whereas in *E-PC*, the gap statistics

method is applied only on points of the dataset that are inside the ε^*.

Figures 6.4 and 6.5 present the silhouette score against the variance, S^2, of the generated clusters. It can be seen that, when the cluster variance $S^2 = 0.12$, silhouette score improvement is not significant with *E-PC* compared to only *GMM*. In this instance, the percentage of data reduction is 21.5% of the initial 10^4 data points. Since the sparsity of the data points is low, the impact of the data points situated outside the ellipse is considerable. Hence, when the data points are less sparsely scattered and the data size reduction exceeds more than 15%, the optimal number of data points required for the proposed approach has not been met as described in detail in Section 6.4.4.

In general, *E-PC* has achieved the same or higher performance compared to the conventional clustering methods while considering only the data inside ε^* to compute K_{opt}. Such performance can also be seen in Figures 6.7 and 6.8, where the silhouette score variation against the number of generated clusters is presented. As the number of clusters increase, the existence of clusters inside ε^* has increased and enabled *E-PC* to detect clusters notably.

The average silhouette scores achieved for different population sizes with original *K-means*, *GMM*, and after applying *E-PC* on such approaches are presented respectively in Figures. 6.10 and 6.11. On average, *E-PC* has provided a silhouette score performance improvement by 18.93% compared to using only *K-means* and *GMM*. The ability of cluster detection has increased when the UE locations outside the ε^* are excluded from consideration. The presence of clusters has become higher inside the ε^*. The selection of UE locations inside the ε^* in *E-PC* has enabled achieving the same or improved cluster detection using a reduced data size.

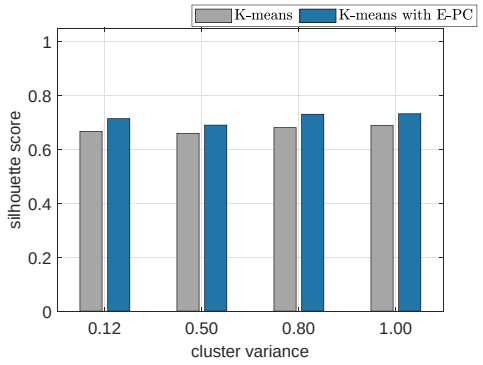

Figure 6.4: Silhouette score under K-means and K-means with E-PC.

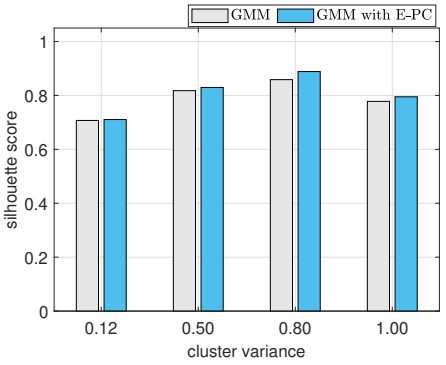

Figure 6.5: Silhouette score under GMM and GMM with E-PC.

Figure 6.6: Silhouette score under several cluster variances in a sub-urban region with 10,000 UEs.

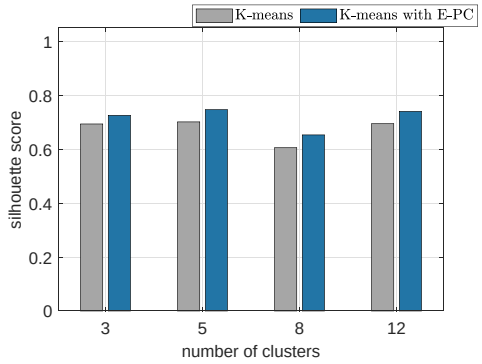

Figure 6.7: Silhouette score under K-means and K-means with E-PC.

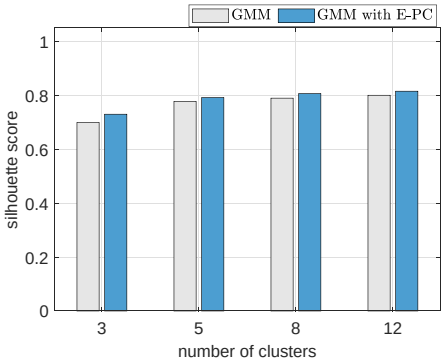

Figure 6.8: Silhouette score under GMM and GMM with E-PC.

Figure 6.9: Silhouette score under the number of clusters in a sub-urban region with 10,000 UEs.

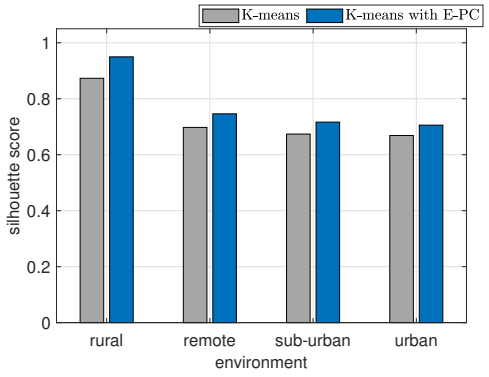

Figure 6.10: Silhouette score under K-means and K-means with E-PC.

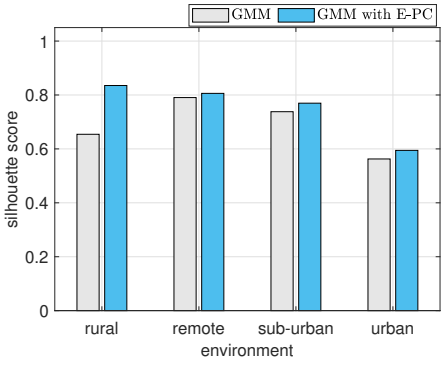

Figure 6.11: Silhouette score under GMM and GMM with E-PC.

Figure 6.12: Silhouette score under environment types, i.e. rural, remote, sub-urban, urban. It is considered that respectively, rural, remote, sub-urban and urban regions contain $10^2, 10^3, 10^4, 10^5$ UEs.

6.4.4/ Data Size and Silhouette Score Trade off

The maximum data size reduction possible (d_{r_m}), which withholds the performance of *E-PC*, under different environment types are given in Table. 6.2. On average, concerning all the environment types, the highest possible data reduction while maintaining the proposed approach performance above the baseline methods was 15% out of the total data points. It should be noted that energy consumption is directly proportional to the data size [228]. Hence, the proposed method improves the energy efficiency at u_a significantly, since the data volume used by the proposed approach was lesser than the baseline approaches.

Table 6.2: Data size reduction

Environment	d_{r_m}
Rural (100 UEs)	30.33%
Remote (1000 UEs)	24.70%
Sub-urban (10^4 UEs)	25.37
Urban (10^5 UEs)	15.24%

6.5/ CONCLUSION

With global pandemics such as Covid-19, awareness of population clusters has increased. In this chapter, a service architecture that allows users to access the localization of clusters was proposed. The proposed service works under two different modes: periodic and on-demand mode according to the service load. The objective was to preserve the energy of the WAA and to increase the system responsiveness. Also, a convex hull-based clustering method in local D2D networks was proposed, for population cluster detection. The proposed algorithm considered the region inside the ε^*, to obtain the same or higher performance in cluster detection compared to conventional methods such as *K-means* and *GMM* methods while considering lesser data points than such conventional methods. This clustering algorithm was performed at the WAA that covered the studied local region. The results showed that the proposed method outperformed the original *K-means* and *GMM* clustering performance by 18.93% under different environments such as remote, rural, suburban, and urban in terms of silhouette score. Moreover, the proposed approach allowed a 15% data reduction, thereby reducing the computational cost and energy consumption of the WAA. On the other hand, in the proposed method, UE locations within a cluster followed a Gaussian distribution. Hence, the performance of the proposed method for other distributions of UE locations corresponding to non-open areas, i.e., streets, indoor areas, remains to be evaluated. In addition, our approach is less efficient when the number of points outside ε^* exceeds a threshold of 15% of the total data. Therefore, the approach can be enhanced by switching to the conventional clustering methods in such a situation.

7

Conclusion and Future Directions

7.1/ Conclusion

In this Chapter, we conclude the thesis and provide several future directions in view of upcoming mobile standards for emergency call communications. The purpose of this thesis is to propose an array of distributed solutions for the problem of designing feasible, reliable and efficient 5G emergency communication service that can deal with a wide disaster situation under low cellular coverage. First, an in-depth overview of the previous research and existing work related to areas such as out-of-coverage D2D networks, multi-hop protocols, asynchronous NOMA multiple access scheme, localization, and optimization techniques was conducted. Next, Chapters 3-7 proposed new techniques for the data link, network, and application layers to increase the capacity of the 5G network and handle a high volume of emergency calls by improving its ability to receive, transfer, and locate emergency calls. Indeed, under a catastrophe affecting both citizens and network infrastructure, a massive amount of out-of-coverage emergency calls occur in limited laps of time. The efficiency of the 5G network lies then in its capacity to manage a huge number of D2D communications by reducing interference, packet loss and energy consumption.

In Chapter 3, a new decoding method for A-NOMA named Cyclic T-SIC was proposed to improve the capacity of massive D2D networks. This new Cyclic T-SIC technique is proposed to decode multiple superimposed signals received asynchronously. In Cyclic T-SIC, the receiver uses an optimization algorithm in sequential iterations to decode symbols effectively, even under co-channel interference and data rate constraints. The results showed that the proposed Cyclic T-SIC had a lower BER and higher energy efficiency, compared to the Conventional T-SIC method. The decoding complexity and delay were also reduced as the number of decoded symbols per iteration was limited in the proposed scheme. Furthermore, the improvement of the achievable D2D sum secrecy capacity C_s, with Cyclic T-SIC under limited coverage scenarios in the presence of jammers was studied. A binary optimization algorithm was introduced to enhance reliable data detection at the receiver by considering the γ values of both the legitimate users and jammers. The results showed that the optimized scheme significantly outperforms the conventional C_s.

Chapter 4 proposes a solution for connecting victims during a disaster scenario when the 4/5G network infrastructure is partially damaged. The proposed protocol named M-HELP transfers emergency calls from out-of-coverage areas to gNBs using device-to-multi-device sidelink communications. M-HELP has been specifically designed to eliminate the necessity for extra control traffic, such as acknowledgments, advertising, and clustering. Therefore, the impact of the protocol on the private devices used to relay emergency calls is reduced. In addition, the protocol is fully compatible with 5G specifications in order to simplify its operational integration. The experiments show that M-HELP provides a high success rate with low energy consumption, and M-HELP outperforms an existing D2D multi-hop emergency call protocol called FINDER.

Then, in Chapter 5, a self-adaptive network protocol named 5G-SOS was proposed to address the lack of adaptability in M-HELP. 5G-SOS is adaptive and uses locally available data from sidelink and uplink signals to adjust its performance to the current network charge. Simulation results in a city with a population of 15,000 showed that 5G-SOS was able to transfer over 80% of emergency calls when the victims made up less than 5% of the devices. 5G-SOS had a higher success rate, higher average residual energy per node, and lower average number of sent messages per node compared to FINDER and improved the performance of M-HELP in terms of success rate and end-to-end latency. However, 5G-SOS slightly increases energy consumption compared to M-HELP. This is due to the need for more messages in order to improve the emergency call success rate.

Chapter 5 addresses the problem of locating disaster victims through data received from multi-hop emergency calls from both in-coverage and out-of-coverage areas. Thereby, a real-time Multi-Victim Localization Algorithm *MVLA* based on dynamic constraint satisfaction is proposed. The simulation results show that the proposed localization algorithm was able to locate up to around 2500 victims in less than 10 seconds, with an improvement in localization accuracy of 55.9% compared to an existing method, *RSSI-MCL*, which has shown improved localization accuracy compared to methods such as EKF, and standalone MCL localization. Moreover, the proposed localization algorithm offer a significant benefit by effectively balancing localization accuracy and computational delay.

Chapter 6 focuses on the problem of detecting population congestion clusters during global pandemics such as Covid-19. A service architecture was proposed to allow users to access the localization of clusters, working in either periodic or on-demand mode. A convex hull-based clustering method was also proposed for population cluster detection and performed at a wireless aerial agent that covers the studied region. The results showed that the proposed method outperforms the conventional methods such as k-means and Gaussian Mixture Model by 18.93% in terms of silhouette score, while also allowing a reduction of 15% in the required data for congestion prediction. Furthermore, the proposed method enabled a reduction in computational cost and energy consumption of the wireless aerial agent. However, the performance of the proposed method for other distributions of user locations remains to be evaluated, and the approach may be less efficient when the number of data points outside a certain region exceeds a threshold of 15%.

7.2/ FUTURE DIRECTIONS

The objective of this thesis was to improve conventional emergency communication systems and create optimal systems for emergency situations in disasters where network coverage is limited. Therefore, the implementation of innovative D2D-assisted multi-hop communication protocols, advanced multiple access decoding techniques, and novel localization algorithms during emergencies were proposed. Moreover, the following areas could be the focus of future works:

- Investigating the performance of the proposed emergency communication schemes under 5G Ultra Reliable Low Latency Communication (URLLC) requirements. Hence, to ensure their practical performance, the proposed mechanisms must meet URLLC requirements by considering finite block-length transmissions.
- Studying the impact of increasing the linear constraints in the localization algorithm on its accuracy, while simultaneously maintaining an optimal equilibrium between localization accuracy and algorithmic complexity.
- Studying the localization of moving devices based on the proposed victim localization approach in Chapter 7, where a minimum conflict algorithm could be used to optimize the freshness of received data and locate dynamic devices.
- Conducting practical simulations of the proposed schemes using both private 5G network tool-kits and open 5G network platforms to evaluate their performance.

BIBLIOGRAPHY

[1] T. standardization sector of ITU, "Itu-t focus group on disaster relief systems, network resilience and recovery," 2014. version 1.0.

[2] R. A. Usman, F. Olorunfemi, G. Awotayo, A. Tunde, and B. Usman, "Disaster risk management and social impact assessment: Understanding preparedness, response and recovery in community projects," in *Environmental Change and Sustainability* (S. Silvern and S. Young, eds.), ch. 10, Rijeka: IntechOpen, 2013.

[3] S. Goshal, "How 5g enables resiliency and supports a resolute society.cdr." https://www.tcs.com/content/dam/tcs/pdf/perspectives/covid-19/How-5G-Enables-Resiliency-and-Supports-a-Resolute-Society.pdf, March 2020.

[4] V. Basnayake, H. Mabed, P. Canalda, and D. N. K. Jayakody, "Enhanced convex hull based clustering for high population density avoidance under d2d enabled network," in *2021 IEEE 94th Vehicular Technology Conference (VTC2021-Fall)*, pp. 1–7, 2021.

[5] A. Singh, D. M. Kumar, R. Rishi, and D. k. Madan, "A relative study of manet and vanet: Its applications, broadcasting approaches and challenging issues," vol. 132, pp. 627–632, 01 2011.

[6] S. Anjum, R. Md. Noor, and H. Anisi, "Review on manet based communication for search and rescue operations," *Wireless Personal Communications*, vol. 94, 05 2017.

[7] D. Gutiérrez, S. Toral, F. Barrero, N. Bessis, and E. Asimakopoulou, "Evaluation of ad hoc networks in disaster scenarios," pp. 759–764, 11 2011.

[8] V. Menon, J. Pathrose, and J. Priya, "Ensuring reliable communication in disaster recovery operations with reliable routing technique," *Mobile Information Systems*, vol. 2016, pp. 1–10, 02 2016.

[9] D. Gutiérrez, M. Askalani, S. Toral, F. Barrero, E. Asimakopoulou, and N. Bessis, "A survey on multihop ad hoc networks for disaster response scenarios," *International Journal of Distributed Sensor Networks*, vol. 2015, 05 2015.

[10] U. Samaratunge, D. N. Jayakody, S. Biswash, and R. Dinis, "Recent advances and future research challenges in non-orthogonal multiple access for 5g networks," 05 2018.

[11] R. Shankar, "Examination of a non-orthogonal multiple access scheme for next generation wireless networks," *The Journal of Defense Modeling and Simulation*, vol. 19, no. 3, pp. 453–465, 2022.

[12] A. Zafar, M. Shaqfeh, M.-S. Alouini, and H. Alnuweiri, "On multiple users scheduling using superposition coding over rayleigh fading channels," *Communications Letters, IEEE*, vol. 17, pp. 733–736, 04 2013.

[13] H. Baek, W. J. Yun, S. Jung, J. Park, M. Ji, J. Kim, and M. Bennis, "Communication and energy efficient slimmable federated learning via superposition coding and successive decoding," *CoRR*, vol. abs/2112.03267, 2021.

[14] X. Chen, L. Pu, L. Gao, W. Wu, and D. Wu, "Exploiting massive d2d collaboration for energy-efficient mobile edge computing," *IEEE Wireless Communications*, vol. 24, no. 4, pp. 64–71, 2017.

[15] C. N. Tadros, M. R. Rizk, and B. M. Mokhtar, "Software defined network-based management for enhanced 5g network services," *IEEE Access*, vol. 8, pp. 53997–54008, 2020.

[16] S. Wijethilaka and M. Liyanage, "Survey on network slicing for internet of things realization in 5g networks," *IEEE Communications Surveys & Tutorials*, vol. 23, no. 2, pp. 957–994, 2021.

[17] C. N. Tadros, M. R. Rizk, and B. M. Mokhtar, "Software defined network-based management for enhanced 5g network services," *IEEE Access*, vol. 8, pp. 53997–54008, 2020.

[18] W. J. Alonso, C. Schuck-Paim, and G. R. Asrar, "Global health and natural disaster alerts: preparing mobile phones to endure the unthinkable," *Earth Perspectives*, vol. 1, p. 24, Jul 2014.

[19] D. N. K. Jayakody, K. Srinivasan, and V. Sharma, *5G Enabled Secure Wireless Networks*. Springer, 2019.

[20] L. Carlà, R. Fantacci, F. Gei, D. Marabissi, and L. Micciullo, "Lte enhancements for public safety and security communications to support group multimedia communications," *IEEE Network*, vol. 30, 01 2015.

[21] R. Favraud, A. Apostolaras, N. Nikaein, and T. Korakis, "Toward moving public safety networks," *IEEE Communications Magazine*, vol. 54, pp. 14–20, 03 2016.

[22] R. L. D. C. M. C. W. J. Merkel, "Lte for public safety networks," 2015.

[23] B. Shang, L. Zhao, and K.-C. Chen, "Enabling device-to-device communications in lte-unlicensed spectrum," pp. 1–6, 05 2017.

[24] E. Dahlman, S. Parkvall, and J. Sköld, *Device-to-Device Connectivity:*, pp. 461–486. 12 2016.

[25] L. Carlà, R. Fantacci, F. Gei, D. Marabissi, and L. Micciullo, "Lte enhancements for public safety and security communications to support group multimedia communications," *IEEE Network*, vol. 30, 01 2015.

[26] A. Sanchoyerto Martinez, R. Solozabal, B. Blanco, and F. Liberal, "Analysis of the impact of the evolution towards 5g architectures on mission critical push-to-talk services," *IEEE Access*, vol. PP, pp. 1–1, 07 2019.

[27] 3GPP, "Universal Mobile Telecommunications System (UMTS) LTE Proximity-based services (ProSe) Stage 2 (3GPP TS 23.303)," Technical Specification version 14.1.0 Release 14 23.303, 3rd Generation Partnership Project (3GPP), 05 2017.

[28] S. Lien, C. Chien, G. S. Liu, H. Tsai, R. Li, and Y. J. Wang, "Enhanced lte device-to-device proximity services," *IEEE Communications Magazine*, vol. 54, pp. 174–182, December 2016.

[29] D. Astely, E. Dahlman, G. Fodor, S. Parkvall, and J. Sachs, "Lte release 12 and beyond [accepted from open call]," *IEEE Communications Magazine*, vol. 51, pp. 154–160, July 2013.

[30] J. Roessler, "Lte-advanced (3gpp rel. 12) technology introduction white paper," *Rohde & Shwarz*, 2015.

[31] G. Araniti, A. Raschellà, A. Orsino, L. Militano, and M. Condoluci, *Device-to-Device Communications over 5G Systems: Standardization, Challenges and Open Issues*. 09 2016.

[32] M. Tehrani and M. Uysal, "Device-to-device communication in 5g cellular networks: Challenges, solutions, and future directions," *Communications Magazine, IEEE*, vol. 52, pp. 86–92, 05 2014.

[33] K. Mikhaylov, J. Petajajarvi, J. Haapola, and A. Pouttu, "D2d communications in lorawan low power wide area network: From idea to empirical validation," 05 2017.

[34] L. Militano, G. Araniti, M. Condoluci, I. Farris, and A. Iera, "Device-to-device communications for 5g internet of things," *EAI Endorsed Transactions on Internet of Things*, vol. 15, 10 2015.

[35] J. Roessler, "Lte-advanced (3gpp rel. 12) technology introduction white paper," *Rohde & Shwarz*, 2015.

[36] M. Gundlach, "Overview of d2d proximity services standardization in 3gpp lte," 06 2014.

[37] R. L. D. C. M. C. W. J. Merkel, "Lte for public safety networks," pp. 77–83, 2015.

[38] R. Favraud, A. Apostolaras, N. Nikaein, and T. Korakis, "Toward moving public safety networks," *IEEE Communications Magazine*, vol. 54, pp. 14–20, 03 2016.

[39] R. L. D. C. M. C. W. J. Merkel, "Lte for public safety networks," 2015.

[40] D. W. Griffith, F. J. Cintrón, and R. A. Rouil, "Physical sidelink control channel (pscch) in mode 2: Performance analysis," in *2017 IEEE International Conference on Communications (ICC)*, pp. 1–7, 2017.

[41] R. Rouil, F. Cintrón, A. Ben Mosbah, and S. Gamboa, "Implementation and validation of an lte d2d model for ns-3," pp. 55–62, 06 2017.

[42] 3GPP, "Technical specification group radio access network; evolved universal terrestrial radio access (e-utra); physical layer procedures; ts 36.213. technical report.," 10 2016.

[43] D. W. Griffith, F. J. Cintrón, and R. A. Rouil, "Physical sidelink control channel (pscch) in mode 2: Performance analysis," in *2017 IEEE International Conference on Communications (ICC)*, pp. 1–7, 2017.

[44] A. Thomas and G. Raja, "Finder: A d2d based critical communications framework for disaster management in 5g," *Peer-to-Peer Networking and Applications*, vol. 12, pp. 912–923, 06 2019.

[45] L. Babun, A. Yurekli, and I. Guvenc, "Multi-hop and d2d communications for extending coverage in public safety scenarios," pp. 912–919, 10 2015.

[46] M. Schmittner, A. Asadi, and M. Hollick, "Semud: Secure multi-hop device-to-device communication for 5g public safety networks," in *2017 IFIP Networking Conference (IFIP Networking) and Workshops*, pp. 1–9, 2017.

[47] A. Thomas and G. Raja, "Finder: A d2d based critical communications framework for disaster management in 5g," *Peer-to-Peer Networking and Applications*, vol. 12, pp. 912–923, 06 2019.

[48] G. Steri, G. Baldini, I. N. Fovino, R. Neisse, and L. Goratti, "A novel multi-hop secure lte-d2d communication protocol for iot scenarios," in *2016 23rd International Conference on Telecommunications (ICT)*, pp. 1–6, 2016.

[49] G. Krüger, R. Springer, and W. Lechner, "Global navigation satellite systems (gnss)," *Comput. Electron. Agric.*, vol. 11, no. 1, pp. 3–21, 1994. Global Positioning Systems in Agriculture.

[50] J. Paziewski, "Recent advances and perspectives for positioning and applications with smartphone GNSS observations," *Measurement Science and Technology*, vol. 31, p. 091001, jun 2020.

[51] S. Verhagen, "Performance analysis of gps, galileo and integrated gps-galileo," pp. 2208–2215, 01 2002.

[52] R. Li, S. Zheng, E. Wang, J. Chen, S. Feng, D. Wang, and L. Dai, "Advances in beidou navigation satellite system (bds) and satellite navigation augmentation technologies," *Satellite Navigation*, vol. 1, p. 12, 03 2020.

[53] L. Dong, H. Ling, and R. Heath, "Multiple-input multiple-output wireless communication systems using antenna pattern diversity," pp. 997 – 1001 vol.1, 12 2002.

[54] R. Hussain, A. Alreshaid, S. Podilchak, and M. Sharawi, "A compact 4g mimo antenna integrated with a 5g array for current and future mobile handsets," *IET Microwaves, Antennas & Propagation*, vol. 11, 02 2017.

[55] H. Du, C. Zhang, Q. Ye, W. Xu, P. Kibenge, and K. Yao, "A hybrid outdoor localization scheme with high-position accuracy and low-power consumption," *EURASIP J Wirel Commun Netw.*, vol. 2018, 01 2018.

[56] A. Hertelendy, K. Goniewicz, and A. Khorram-Manesh, "The applications of geographic information systems in disaster and emergency management in europe," *Disaster and Emergency Medicine Journal*, 10 2020.

[57] E. Colle and S. Galerne, "Mobile robot localization by multiangulation using set inversion," *Robotics and Autonomous Systems*, vol. 61, p. 39–48, 01 2013.

[58] Z. Xiao and Y. Zeng, "An overview on integrated localization and communication towards 6g," 06 2020.

[59] I. Vin, D. P. Gaillot, P. Laly, M. Liénard, and P. Degauque, "Overview of mobile localization techniques and performances of a novel fingerprinting-based method," *Comptes Rendus Physique*, vol. 16, no. 9, pp. 862–873, 2015. Radio science for connecting humans with information systems / L'homme connecté.

[60] T. Geok, K. Aung, M. Aung, M. Soe, A. Abdaziz, C. Liew, F. Hossain, C. Tso, and W. Yong, "Review of indoor positioning: Radio wave technology," *Applied Sciences*, vol. 11, p. 279, 12 2020.

[61] J. A. del Peral-Rosado, R. Raulefs, J. López-Salcedo, and G. Seco-Granados, "Survey of cellular mobile radio localization methods: From 1g to 5g," *IEEE Communications Surveys & Tutorials*, vol. 20, pp. 1124–1148, 2018.

[62] M. Laaraiedh, *Contributions on Hybrid Localization Techniques For Heterogeneous Wireless Networks*. PhD thesis, 12 2010.

[63] M. W. Khan, N. Salman, A. H. Kemp, and L. Mihaylova, "Localisation of sensor nodes with hybrid measurements in wireless sensor networks," *Sensors*, vol. 16, no. 7, 2016.

[64] C. Geng, T. Abrudan, V. M. Kolmonen, and H. Huang, "Experimental study on probabilistic toa and aoa joint localization in real indoor environments," 02 2021.

[65] K. Merry and P. Bettinger, "Smartphone gps accuracy study in an urban environment," *PLOS ONE*, vol. 14, pp. 1–19, 07 2019.

[66] M. B. Kjærgaard, H. Blunck, T. Godsk, T. Toftkjær, D. Christensen, and K. Grønbæk, "Indoor positioning using gps revisited," in *Pervasive*, 2010.

[67] J. Arias, A. Zuloaga, J. Lázaro, J. Andreu, and A. Astarloa, "Malguki: An rssi based ad hoc location algorithm," *Microprocessors and Microsystems*, vol. 28, pp. 403–409, 10 2004.

[68] R. Mehra and A. Singh, "Real time rssi error reduction in distance estimation using rls algorithm," in *2013 3rd IEEE International Advance Computing Conference (IACC)*, pp. 661–665, 2013.

[69] M. Dashti, M. Ghoraishi, K. Haneda, and J.-i. Takada, "Sources of toa estimation error in los scenario," in *2010 IEEE International Conference on Ultra-Wideband*, vol. 2, pp. 1–4, IEEE, 2010.

[70] M. Schüssel, "Angle of arrival estimation using wifi and smartphones," 2016.

[71] L. o. C. Science Reference Section, "What is a gps? how does it work? | library of congress." https://www.loc.gov/everyday-mysteries/item/what-is-gps-how-does-it-work/, November 2019. (Accessed on 09/08/2021).

[72] F. Zahradnik, "Gps smartphone apps vs. dedicated car gps devices." https://www.lifewire.com/smartphone-or-car-gps-1683388, July 2021. (Accessed on 08/15/2021).

[73] J. Kendrick, "Smartphone for gps navigation is better than a dedicated device | zdnet." https://www.zdnet.com/article/smartphone-for-gps-navigation-is-better-than-a-dedicated-device/, June 2011. (Accessed on 08/15/2021).

[74] C. Dunphy, "5g goes mainstream: Apple's iphone 12 debuts - mobile internet resource center." https://www.rvmobileinternet.com/5g-goes-mainstream-apples-iphone-12-debuts/. (Accessed on 08/16/2021).

[75] M. Sauter, "From gsm to lte-advanced: An introduction to mobile networks and mobile broadband: Second edition," pp. 1–441, 01 2014.

[76] M. I. M. Ismail, R. A. Dzyauddin, H. M. Kaidi, M. A. M. Izhar, S. Samsul, and N. A. Azmi, "Comparison of wireless sensor node localisation between trilateration and multi-lateration methods using rssi," in *2022 IEEE Symposium on Future Telecommunication Technologies (SOFTT)*, pp. 97–102, IEEE, 2022.

[77] A. Chatzimichail, A. Tsanousa, G. Meditskos, S. Vrochidis, and I. Kompatsiaris, *RSSI Fingerprinting Techniques for Indoor Localization Datasets*, pp. 468–479. 09 2020.

[78] D. Tse and P. Viswanath, *Fundamentals of wireless communication*. Cambridge university press, 2005.

[79] F. Afroz, R. Subramanian, R. Heidary, K. Sandrasegaran, and S. Ahmed, "Sinr, rsrp, rssi and rsrq measurements in long term evolution networks," *International Journal of Wireless & Mobile Networks*, vol. 7, pp. 113–123, 08 2015.

[80] I. Angri, A. Najid, and M. Mahfoudi, "Available bandwidth and rsrp based handover algorithm for lte/lte-advanced networks tested in lte-sim simulator," *International Journal of Electronics and Telecommunications*, vol. 65, pp. 85–93, 01 2019.

[81] F. Shang, W. Su, Q. Wang, H. Gao, and Q. Fu, "A location estimation algorithm based on rssi vector similarity degree," *International Journal of Distributed Sensor Networks*, vol. 2014, pp. 1–22, 08 2014.

[82] J. Lu and C. C. Wang, "A new monte carlo mobile node localization algorithm based on newton interpolation," *EURASIP Journal on Wireless Communications and Networking*, vol. 2018, pp. 1–8, 2018.

[83] V. Basnayake, D. N. K. Jayakody, V. Sharma, N. Sharma, P. Muthuchidambaranathan, and H. Mabed, "A new green prospective of non-orthogonal multiple access (noma) for 5g," *Information*, vol. 11, no. 2, 2020.

[84] J. Tang, J. Luo, M. Liu, D. So, E. Alsusa, G. Chen, K.-K. Wong, and J. Chambers, "Energy efficiency optimization for noma with swipt," *IEEE Journal of Selected Topics in Signal Processing*, vol. PP, pp. 1–1, 02 2019.

[85] H. I. Fitriasari, A. I. Lestari, D. L. Luhurkinanti, and R. F. Sari, "Performance evaluation of downlink multi-user ofdma scheduling in 5g new radio (nr)," in *2021 18th International Conference on Electrical Engineering/Electronics, Computer, Telecommunications and Information Technology (ECTI-CON)*, pp. 219–223, 2021.

[86] D. Thiyagarajan and P. Venkatesan, "Performance estimation of multicarrier cdma using adaptive brain storm optimization for 5g communication system in frequency selective fading channel," 12 2019.

[87] Y. Liu, W. Yi, Z. Ding, X. Liu, O. A. Dobre, and N. Al-Dhahir, "Developing noma to next generation multiple access (ngma): Future vision and research opportunities," *IEEE Wireless Communications*, pp. 1–8, 2022.

[88] J. Zhao, Y. Liu, K. K. Chai, Y. Chen, M. Elkashlan, and J. Alonso-Zarate, "Noma-based d2d communications: Towards 5g," in *2016 IEEE Global Communications Conference (GLOBECOM)*, pp. 1–6, 2016.

[89] Z. Ding, R. Schober, and H. V. Poor, "Unveiling the importance of sic in noma systems—part 1: State of the art and recent findings," *IEEE Communications Letters*, vol. 24, no. 11, pp. 2373–2377, 2020.

[90] F. M. Caceres, S. Kandeepan, and S. Sun, "Theoretical analysis of hybrid sic success probability under rayleigh channel for uplink cr-noma," *IEEE Transactions on Vehicular Technology*, pp. 1–16, 2022.

[91] K. Mehmood, M. T. Niaz, and H. S. Kim, "Dynamic fractional frequency reuse diversity design for inter-cell interference mitigation in non-orthogonal multiple access (noma) multicellular networks," *Wireless Communications and Mobile Computing*, vol. 2018, 07 2018.

[92] X. Su, H. Yu, W. Kim, C. Choi, and D. Choi, "Interference cancellation for non-orthogonal multiple access used in future wireless mobile networks," *EURASIP Journal on Wireless Communications and Networking*, vol. 2016, p. 231, Sep 2016.

[93] X. Wang, F. Labeau, and L. Mei, "Asynchronous uplink non-orthogonal multiple access (noma) with cyclic prefix," in *2018 IEEE Wireless Communications and Networking Conference (WCNC)*, pp. 1–6, 2018.

[94] M. Ganji, X. Zou, and H. Jafarkhani, "Asynchronous transmission for multiple access channels: Rate-region analysis and system design for uplink noma," *IEEE Transactions on Wireless Communications*, vol. 20, no. 7, pp. 4364–4378, 2021.

[95] X. Li, H. Liu, G. Li, Y. Liu, M. Zeng, and Z. Ding, "Effective capacity analysis of ambc-noma communication systems," *IEEE Transactions on Vehicular Technology*, pp. 1–6, 2022.

[96] W. Chen and Z. Tang, "Research on improved receiver of noma-ofdm signal based on deep learning," in *2021 International Conference on Communications, Information System and Computer Engineering (CISCE)*, pp. 173–177, 2021.

[97] C. Liu and N. C. Beaulieu, "Exact ber performance for symbol-asynchronous two-user non-orthogonal multiple access," *IEEE Communications Letters*, vol. 25, no. 3, pp. 764–768, 2021.

[98] H. Haci, H. Zhu, and J. Wang, "Performance of non-orthogonal multiple access with a novel asynchronous interference cancellation technique," *IEEE Transactions on Communications*, vol. 65, no. 3, pp. 1319–1335, 2017.

[99] S. Sadinov, "Simulation study of m-ary qam modulation techniques using matlab/simulink," pp. 547–554, 05 2017.

[100] A. Goldsmith, *Wireless communications*. Cambridge university press, 2005.

[101] A. Zappone, "A survey of energy-efficient techniques for 5g networks and challenges ahead," *IEEE Journal on Selected Areas in Communications*, vol. 34, 04 2016.

[102] Y. Zhang, H.-M. Wang, T.-X. Zheng, and Q. Yang, "Energy-efficient transmission design in non-orthogonal multiple access," *IEEE Transactions on Vehicular Technology*, vol. 66, pp. 2852 – 2857, 03 2017.

[103] J. Zhu, J. Wang, Y. Huang, S. He, X. You, and L. Yang, "On optimal power allocation for downlink non-orthogonal multiple access systems," *IEEE Journal on Selected Areas in Communications*, vol. 35, pp. 2744–2757, Dec 2017.

[104] L. Lei, D. Yuan, and P. Värbrand, "On power minimization for non-orthogonal multiple access (noma)," *IEEE Communications Letters*, vol. 20, pp. 2458–2461, Dec 2016.

[105] F. Fang, H. Zhang, J. Cheng, and V. Leung, "Energy-efficient resource scheduling for noma systems with imperfect channel state information," pp. 1–5, 05 2017.

[106] F. Fang, H. Zhang, J. Cheng, and V. C. M. Leung, "Energy efficiency of resource scheduling for non-orthogonal multiple access (noma) wireless network," in *2016 IEEE International Conference on Communications (ICC)*, pp. 1–5, May 2016.

[107] F. Fang, H. Zhang, J. Cheng, and V. C. M. Leung, "Energy-efficient resource allocation for downlink non-orthogonal multiple access network," *IEEE Transactions on Communications*, vol. 64, pp. 3722–3732, Sep. 2016.

[108] J. Choi, "Joint rate and power allocation for noma with statistical csi," *IEEE Transactions on Communications*, vol. PP, pp. 1–1, 06 2017.

[109] K. Senel and S. Tekinay, "Optimal power allocation in noma systems with imperfect channel estimation," in *GLOBECOM 2017 - 2017 IEEE Global Communications Conference*, pp. 1–7, Dec 2017.

[110] M. Zamani, M. Eslami, M. Khorramizade, and Z. Ding, "Energy efficient power allocation for noma with imperfect csi," *IEEE Transactions on Vehicular Technology*, vol. PP, pp. 1–1, 11 2018.

[111] Q. Sun, S. Han, C. I, and Z. Pan, "Energy efficiency optimization for fading mimo non-orthogonal multiple access systems," in *2015 IEEE International Conference on Communications (ICC)*, pp. 2668–2673, June 2015.

[112] H. Zhang, B. Wang, C. Jiang, K. Long, A. Nallanathan, V. C. M. Leung, and H. V. Poor, "Energy efficient dynamic resource optimization in noma system," *IEEE Transactions on Wireless Communications*, vol. 17, pp. 5671–5683, Sep. 2018.

[113] Z. Wei, D. W. K. Ng, and J. Yuan, "Power-efficient resource allocation for mc-noma with statistical channel state information," in *2016 IEEE Global Communications Conference (GLOBECOM)*, pp. 1–7, Dec 2016.

[114] F. Palacios-Gomez, L. Lasdon, and M. Engquist, "Nonlinear Optimization by Successive Linear Programming," *Management Science*, vol. 28, pp. 1106–1120, Oct. 1982. Publisher: INFORMS.

[115] F. Mourad, H. Snoussi, F. Abdallah, and C. Richard, "Anchor-based localization via interval analysis for mobile sensor networks," *IEEE Transactions on Signal Processing*, vol. 57, no. 8, pp. 3226–3239, 2009.

[116] M. Kieffer, L. Jaulin, E. Walter, and D. Meizel, "Robust autonomous robot localization using interval analysis," *Reliable Computing*, vol. 6, pp. 337–362, 08 2000.

[117] K. Kueviakoe, Z. Wang, A. Lambert, E. Frenoux, and P. Tarroux, "Localization of a vehicle: A dynamic interval constraint satisfaction problem-based approach," *Journal of Sensors*, vol. 2018, pp. 1–12, 04 2018.

[118] Z. Wang and A. Lambert, "A low-cost consistent vehicle localization based on interval constraint propagation," *Journal of Advanced Transportation*, vol. 2018, 06 2018.

[119] F. Mourad, H. Snoussi, F. Abdallah, and C. Richard, "Guaranteed boxed localization in manets by interval analysis and constraints propagation techniques," in *IEEE GLOBECOM 2008 - 2008 IEEE Global Telecommunications Conference*, pp. 1–5, 2008.

[120] V. Drevelle and P. Bonnifait, "Robust positioning using relaxed constraint-propagation," in *2010 IEEE/RSJ International Conference on Intelligent Robots and Systems*, pp. 4843–4848, 2010.

[121] E. Colle and S. Galerne, "Mobile robot localization by multiangulation using set inversion," *Robotics and Autonomous Systems*, vol. 61, no. 1, pp. 39–48, 2013.

[122] M. Mouhoub and B. Jashmi, "Heuristic techniques for variable and value ordering in csps," pp. 457–464, 01 2011.

[123] S. Mintonl, M. Johnston, A. B. Philips, and P. Laird, "Stolving large-scale constraint satisfaction an scheduling problems using a epair metho," 1990.

[124] M. Wahbi, *Algorithms and Ordering Heuristics for Distributed Constraint Satisfaction Problems*. 06 2013.

[125] W. U. Khan, M. A. Javed, T. Nguyen, S. Khan, and B. ElHalawany, "Energy-efficient resource allocation for 6g backscatter-enabled noma iov networks," *IEEE Transactions on Intelligent Transportation Systems*, vol. PP, pp. 1–11, 09 2021.

[126] S. Shakkottai, T. Rappaport, and P. Karlsson, "Cross-layer design for wireless networks," *IEEE Communications Magazine*, vol. 41, no. 10, pp. 74–80, 2003.

[127] M. S. M. Gismalla, A. I. Azmi, M. R. B. Salim, M. F. L. Abdullah, F. Iqbal, W. A. Mabrouk, M. B. Othman, A. Y. I. Ashyap, and A. S. M. Supa'at, "Survey on device to device (d2d) communication for 5gb/6g networks: Concept, applications, challenges, and future directions," *IEEE Access*, vol. 10, pp. 30792–30821, 2022.

[128] S. Gamboa, F. J. Cintron, D. Griffith, and R. Rouil, "Adaptive synchronization reference selection for out-of-coverage proximity services," in *2017 IEEE 28th Annual International Symposium on Personal, Indoor, and Mobile Radio Communications (PIMRC)*, pp. 1–7, 2017.

[129] F. Lu, M. Xu, L. Cheng, J. Wang, and G.-K. Chang, "Power-division non-orthogonal multiple access (noma) in flexible optical access with synchronized downlink/asynchronous uplink," *Journal of Lightwave Technology*, vol. 35, no. 19, pp. 4145–4152, 2017.

[130] X. Zou, B. He, and H. Jafarkhani, "An analysis of two-user uplink asynchronous non-orthogonal multiple access systems," *IEEE Transactions on Wireless Communications*, vol. 18, no. 2, pp. 1404–1418, 2019.

[131] X. Zou, B. He, and H. Jafarkhani, "On uplink asynchronous non-orthogonal multiple access systems with timing error," in *2018 IEEE International Conference on Communications (ICC)*, pp. 1–6, 2018.

[132] J. Liu, Y. Li, G. Song, and Y. Sun, "Detection and analysis of symbol-asynchronous uplink noma with equal transmission power," *IEEE Wireless Communications Letters*, vol. 8, no. 4, pp. 1069–1072, 2019.

[133] X. Zou, M. Ganji, and H. Jafarkhani, "Cooperative asynchronous non-orthogonal multiple access with power minimization under qos constraints," *IEEE Transactions on Wireless Communications*, vol. 19, no. 3, pp. 1503–1518, 2020.

[134] V. Basnayake, H. Mabed, D. N. K. Jayakody, P. Canalda, and M. Beko, "Adaptive emergency call service for disaster management," *Journal of Sensor and Actuator Networks*, vol. 11, no. 4, 2022.

[135] V. Basnayake, H. Mabed, P. Canalda, and D. N. K. Jayakody, "Enhanced convex hull based clustering for high population density avoidance under d2d enabled network," in *2021 IEEE 94th Vehicular Technology Conference (VTC2021-Fall)*, pp. 1–7, 2021.

[136] M. Ganji, X. Zou, and H. Jafarkhani, "Asynchronous transmission for multiple access channels: Rate-region analysis and system design for uplink noma," *IEEE Transactions on Wireless Communications*, vol. 20, no. 7, pp. 4364–4378, 2021.

[137] X. Zou, B. He, and H. Jafarkhani, "An analysis of two-user uplink asynchronous non-orthogonal multiple access systems," *IEEE Transactions on Wireless Communications*, vol. 18, no. 2, pp. 1404–1418, 2019.

[138] C. Liu and N. C. Beaulieu, "Exact ber performance for symbol-asynchronous two-user non-orthogonal multiple access," *IEEE Communications Letters*, vol. 25, no. 3, pp. 764–768, 2021.

[139] S. Qureshi, S. A. Hassan, and D. N. K. Jayakody, "Successive bandwidth division noma systems: Uplink power allocation with proportional fairness," in *2017 14th IEEE Annual Consumer Communications & Networking Conference (CCNC)*, pp. 998–1003, 2017.

[140] S. Rajkumar, D. Nalin, and D. N. Jayakody, "Backscatter assisted noma-plnc based wireless networks," *Sensors*, vol. 21, 11 2021.

[141] I. Raziah, Y. Yunida, Y. Away, R. Muharar, and N. Nasaruddin, "Adaptive relay selection based on channel gain and link distance for cooperative out-band device-to-device networks," *Heliyon*, vol. 7, no. 7, p. e07430, 2021.

[142] S. Kumarapandian and M. J. Sibley, "Complexity analysis of double-threshold based relay selection in d2d cooperative network," *Journal of Wireless Networking and Communications*, vol. 8, no. 1, pp. 1–6, 2018.

[143] P. S. Bithas, K. Maliatsos, and F. Foukalas, "An sinr-aware joint mode selection, scheduling, and resource allocation scheme for d2d communications," *IEEE Transactions on Vehicular Technology*, vol. 68, no. 5, pp. 4949–4963, 2019.

[144] O. Hayat, R. Ngah, S. Z. Mohd Hashim, M. H. Dahri, R. Firsandaya Malik, and Y. Rahayu, "Device discovery in d2d communication: A survey," *IEEE Access*, vol. 7, pp. 131114–131134, 2019.

[145] M. Koivisto, M. Costa, J. Werner, K. Heiska, J. Talvitie, K. Leppänen, V. Koivunen, and M. Valkama, "Joint device positioning and clock synchronization in 5g ultra-dense networks," *IEEE Transactions on Wireless Communications*, vol. 16, no. 5, pp. 2866–2881, 2017.

[146] A. A. Nasir, S. Durrani, H. Mehrpouyan, S. D. Blostein, and R. A. Kennedy, "Timing and carrier synchronization in wireless communication systems: A survey and classification of research in the last five years," *CoRR*, vol. abs/1507.02032, 2015.

[147] E. Che, H. D. Tuan, and H. H. Nguyen, "Joint optimization of cooperative beamforming and relay assignment in multi-user wireless relay networks," *IEEE Transactions on Wireless Communications*, vol. 13, no. 10, pp. 5481–5495, 2014.

[148] S. He, J. Yuan, Z. An, W. Huang, Y. Huang, and Y. Zhang, "Joint user scheduling and beamforming design for multiuser miso downlink systems," 2021.

[149] E. Björnson, M. Kountouris, and m. Debbah, "Massive mimo and small cells: Improving energy efficiency by optimal soft-cell coordination," 04 2013.

[150] X. Wang, L. Yan, and Q. Zhang, "Research on the application of gradient descent algorithm in machine learning," in *2021 International Conference on Computer Network, Electronic and Automation (ICCNEA)*, pp. 11–15, 2021.

[151] Ó. Gama, P. Carvalho, J. A. Afonso, and P. M. Mendes, "Trade-off analysis of a mac protocol for wireless e-emergency systems," in *Sensor Systems and Software* (S. Hailes, S. Sicari, and G. Roussos, eds.), Springer Berlin Heidelberg, 2010.

[152] V. Basnayake, H. Mabed, D. N. K. Jayakody, and P. Canalda, "M-help - multi-hop emergency call protocol in 5g," in *2020 IEEE 19th International Symposium on Network Computing and Applications (NCA)*, pp. 1–8, 2020.

[153] J.-S. Ahn, J.-H. Yoon, and K.-W. Lee, "Performance and energy consumption analysis of 802.11 with fec codes over wireless sensor networks," *Journal of Communications and Networks*, vol. 9, no. 3, pp. 265–273, 2007.

[154] P. Joshi, F. Ghasemifard, D. Colombi, and C. Tornevik, "Actual output power levels of user equipment in 5g commercial networks and implications on realistic rf emf exposure assessment," *IEEE Access*, 11 2020.

[155] A. Kumar and D. N. K. Jayakody, "Secure noma-assisted multi-led underwater visible light communication," *IEEE Transactions on Vehicular Technology*, vol. 71, no. 7, pp. 7769–7779, 2022.

[156] A. Abdalla, K. Powell, V. Marojevic, and G. Geraci, "Uav-assisted attack prevention, detection, and recovery of 5g networks," *IEEE Wireless Communications*, vol. 27, pp. 40–47, 2020.

[157] M. Y. Selim and A. Kamal, "Post-disaster 4g/5g network rehabilitation using drones: Solving battery and backhaul issues," *2018 IEEE Globecom Workshops (GC Wkshps)*, pp. 1–6, 2018.

[158] M. Casoni, C. A. Grazia, M. Klapez, N. Patriciello, A. Amditis, and E. Sdongos, "Integration of satellite and lte for disaster recovery," *IEEE Communications Magazine*, vol. 53, no. 3, pp. 47–53, 2015.

[159] Z. Kaleem, M. Yousaf, A. Qamar, A. Ahmad, T. Duong, W. Choi, and A. Jamalipour, "Uav-empowered disaster-resilient edge architecture for delay-sensitive communication," *IEEE Network*, vol. PP, pp. 1–9, 05 2019.

[160] C. Esposito, A. Gouglidis, D. Hutchison, A. Gurtov, B. Helvik, P. Heegaard, G. Rizzo, and J. Rak, "On the disaster resiliency within the context of 5g networks: The recodis experience," 2018.

[161] K. Gomez Chavez, L. Goratti, T. Rasheed, and L. Reynaud, "Enabling disaster resilient 4g mobile communication networks," *IEEE Communications Magazine*, 09 2014.

[162] L. Globa and I. Volvach, "Mobile networks disaster recovery," pp. 84–86, 02 2015.

[163] F. Malandrino, C.-F. Chiasserini, and G. Landi, "Towards failure resiliency in 5g: Service shifting," *ArXiv*, vol. abs/1902.06317, 2019.

[164] A. Reichman and S. I. Wayer, "Ad-hoc network recovery after severe disaster," *2019 IEEE International Conference on Microwaves, Antennas, Communications and Electronic Systems (COMCAS)*, pp. 1–3, 2019.

[165] H. Lee and D. Jeon, "A mobile ad-hoc network multi-path routing protocol based on biological attractor selection for disaster recovery communication," *ICT Express*, vol. 1, pp. 86–89, 2015.

[166] S. Alwan, I. Fajjari, and N. Aitsaadi, "D2d multihop energy-efficient routing and ofdma resource allocation in 5g networks," *2018 IFIP Networking Conference (IFIP Networking) and Workshops*, pp. 1–9, 2018.

[167] A. V. Bastos, C. Silva, and D. Da Silva Jr., "Assisted routing algorithm for d2d communication in 5g wireless networks," 04 2018.

[168] V. Basnayake, H. Mabed, D. N. K. Jayakody, and P. Canalda, "M-help - multi-hop emergency call protocol in 5g," in *2020 IEEE 19th International Symposium on Network Computing and Applications (NCA)*, pp. 1–8, 2020.

[169] T. standardization sector of ITU, "Itu-t focus group on disaster relief systems, network resilience and recovery," 2014. version 1.0.

[170] C. Luo, W. Miao, H. Ullah, S. McClean, G. Parr, and G. Min, *Unmanned Aerial Vehicles for Disaster Management*, pp. 83–107. 08 2019.

[171] K. Gomez Chavez, L. Goratti, T. Rasheed, and L. Reynaud, "Enabling disaster resilient 4g mobile communication networks," *IEEE Communications Magazine*, 09 2014.

[172] M. Casoni, C. A. Grazia, M. Klapez, N. Patriciello, A. Amditis, and E. Sdongos, "Integration of satellite and lte for disaster recovery," *IEEE Communications Magazine*, vol. 53, no. 3, pp. 47–53, 2015.

[173] Z. Kaleem, M. Yousaf, A. Qamar, A. Ahmad, T. Duong, W. Choi, and A. Jamalipour, "Uav-empowered disaster-resilient edge architecture for delay-sensitive communication," *IEEE Network*, vol. PP, pp. 1–9, 05 2019.

[174] F. Afroz, R. Subramanian, R. Heidary, K. Sandrasegaran, and S. Ahmed, "Sinr, rsrp, rssi and rsrq measurements in long term evolution networks," *International Journal of Wireless & Mobile Networks*, vol. 7, pp. 113–123, 08 2015.

[175] I. Angri, A. Najid, and M. Mahfoudi, "Available bandwidth and rsrp based handover algorithm for lte/lte-advanced networks tested in lte-sim simulator," *International Journal of Electronics and Telecommunications*, vol. 65, pp. 85–93, 01 2019.

[176] F. Shang, W. Su, Q. Wang, H. Gao, and Q. Fu, "A location estimation algorithm based on rssi vector similarity degree," *International Journal of Distributed Sensor Networks*, vol. 2014, pp. 1–22, 08 2014.

[177] 3GPP, "Ts 136 214 - v14.3.0 - lte; evolved universal terrestrial radio access (e-utra); physical layer; measurements (3gpp ts 36.214 version 14.3.0 release 14)," 10 2017.

[178] "Anylogic: Simulation modeling software tools & solutions for business." https://www.anylogic.com/. (Accessed on 10/23/2020).

[179] S. Peckham, A. Kelbert, M. Hill, and E. Hutton, "Towards uncertainty quantification and parameter estimation for earth system models in a component-based modeling framework," *Computers & Geosciences*, 03 2016.

[180] Y. Shang and Y. Qiu, "A note on the extended rosenbrock function," *Evolutionary Computation*, vol. 14, pp. 119–126, 03 2006.

[181] M. Katiyar, "Performance and sensitivity analysis of path loss models for wimax signals," 04 2013.

[182] S. Kang, T. Kim, and W. Chung, "Hybrid rss/aoa localization using approximated weighted least square in wireless sensor networks," *Sensors*, vol. 20, no. 4, 2020.

[183] M. Bertoni, S. Michieletto, R. Oboe, and G. Michieletto, "Indoor visual-based localization system for multi-rotor uavs," *Sensors*, vol. 22, no. 15, 2022.

[184] W. Wang and Q. Zhu, "Rss-based monte carlo localisation for mobile sensor networks," *Communications, IET*, vol. 2, pp. 673 – 681, 06 2008.

[185] A. Krishna, A. van Schaik, and C. S. Thakur, "Source localization using particle filtering on fpga for robotic navigation with imprecise binary measurement," *arXiv preprint arXiv:2010.11911*, 2020.

[186] C. Zhou, H. Tian, and B. Zhong, "An improved mcb localization algorithm based on weighted rssi and motion prediction," *Computer Science and Information Systems*, vol. 17, pp. 779–794, 01 2020.

[187] G. Li, J. Zhang, J. Chen, and Z. Xu, "A monte carlo box localization algorithm based on rssi," in *Proceedings of the 33rd Chinese Control Conference*, pp. 395–400, 2014.

[188] B. Abbache, N. Roumila, S. Rezzoug, M. Omar, and A. Tari, "Collaborative localization algorithm based on constraint programming," in *Proceedings of the International Conference on Big Data and Advanced Wireless Technologies*, BDAW '16, (New York, NY, USA), Association for Computing Machinery, 2016.

[189] F. Mourad, H. Snoussi, F. Abdallah, and C. Richard, "Anchor-based localization via interval analysis for mobile ad-hoc sensor networks," *IEEE Transactions on Signal Processing*, vol. 57, no. 8, pp. 3226–3239, 2009.

[190] M. Qin and R. Zhu, "A monte carlo localization method based on differential evolution optimization applied into economic forecasting in mobile wireless sensor networks," *EURASIP Journal on Wireless Communications and Networking*, vol. 2018, 02 2018.

[191] A. abu znaid, M. Yamani, M. Idris, A. Wahid, A. Wahab, L. Qabajeh, and O. MAHDI, "Sequential monte carlo localization methods in mobile wireless sensor networks: A review," *Journal of Sensors*, vol. 2017, 04 2017.

[192] D. C. Yuen and B. A. MacDonald, "A comparison between extended kalman filtering and sequential monte carlo techniques for simultaneous localisation and map-building," in *Proceedings of the 2002 Australasian Conference on Robotics and Automation*, pp. 111–116, Citeseer, 2002.

[193] A. Singh, "Extended kalman filter. in my previous blog i have covered… | by atul singh | towards data science." https://towardsdatascience.com/extended-kalman-filter-ee9bd04ac5dc, May 2018. (Accessed on 08/31/2021).

[194] F. Mourad, H. Snoussi, and C. Richard, "Interval-based localization using rssi comparison in manets," *IEEE Transactions on Aerospace and Electronic Systems*, vol. 47, no. 4, pp. 2897–2910, 2011.

[195] J. Fernández, M. Quispe, G. Kemper, J. Samaniego, and D. Diaz, "An improvement of the log-distance path loss model for digital television in lima," *XXX Simposio Brasilero de Telecomunications*, 09 2012.

[196] L. L. F. Palacios-Gomez and M. Engquist, "Nonlinear optimization by successive linear programming," *Management Science*, vol. 28, pp. 1106–1120, Oct. 1982. Publisher: INFORMS.

[197] S. Rohou *et al.*, "The Tubex library – Constraint-programming for robotics," 2017. http://simon-rohou.fr/research/tubex-lib/.

[198] E. Bisong, *Google Colaboratory*, pp. 59–64. Berkeley, CA: Apress, 2019.

[199] N. Hossein Motlagh, M. Bagaa, and T. Taleb, "Uav-based iot platform: A crowd surveillance use case," *IEEE Communications Magazine*, vol. 55, pp. 128–134, 02 2017.

[200] WHO, "What are the health risks related to overcrowding?." https://www.who.int/water_sanitation_health/emergencies, 2021. (Accessed on 05/04/2021).

[201] N. Kadi and M. Khelfaoui, "Population density, a factor in the spread of covid-19 in algeria: statistic study," *Bulletin of the National Research Centre*, vol. 44, 12 2020.

[202] N. Saeed, A. Bader, T. Y. Al-Naffouri, and M.-S. Alouini, "When wireless communication responds to covid-19: Combating the pandemic and saving the economy," *Frontiers in Communications and Networks*, vol. 1, p. 3, 2020.

[203] C. Y. Wei, *D2D Physical-Layer Design*, pp. 1–25. 05 2020.

[204] P. Kumar, S. Darshi, and S. Shailendra, "Drone assisted device to device cooperative communication for critical environments," *IET Communications*, vol. n/a, no. n/a.

[205] K. Khan, W. Albattah, R. Khan, A. Qamar, and D. Nayab, "Advances and trends in real time visual crowd analysis," *Sensors (Basel, Switzerland)*, vol. 20, 09 2020.

[206] H. Cevikalp, "High-dimensional data clustering by using local affine/convex hulls," *Pattern Recognition Letters*, vol. 128, pp. 427–432, 2019.

[207] "Cluster analysis." https://medium.com/mlearning-ai/cluster-analysis-6757d6c6acc9, January 2021. (Accessed on 04/15/2021).

[208] C. Guyeux, S. Chrétien, G. Bou Tayeh, J. Demerjian, and J. Bahi, "Introducing and comparing recent clustering methods for massive data management in the internet of things," *Journal of Sensor and Actuator Networks*, vol. 8, p. 56, 12 2019.

[209] "What is clustering? clustering in machine learning." https://developers.google.com/machine-learning/clustering/overview, 2020. (Accessed on 04/04/2021).

[210] E. Patel and D. S. Kushwaha, "Clustering cloud workloads: K-means vs gaussian mixture model," *Procedia Computer Science*, vol. 171, pp. 158–167, 2020. Third International Conference on Computing and Network Communications (CoCoNet'19).

[211] S. Nanjundan, S. Sankaran, C. R. Arjun, and G. P. Anand, "Identifying the number of clusters for k-means: A hypersphere density based approach," *CoRR*, vol. abs/1912.00643, 2019.

[212] R. Tibshirani, G. Walther, and T. Hastie, "Estimating the number of clusters in a data set via the gap statistic," *Journal of the Royal Statistical Society Series B*, vol. 63, pp. 411–423, 02 2001.

[213] B. Boehmke, "K-means cluster analysis." https://uc-r.github.io/kmeans_clustering. (Accessed on 04/08/2021).

[214] L. Liparulo, A. Proietti, and M. Panella, "Fuzzy clustering using the convex hull as geometrical model," *Advances in Fuzzy Systems*, vol. 2015, 04 2015.

[215] R. L. Graham and F. Frances Yao, "Finding the convex hull of a simple polygon," *Journal of Algorithms*, vol. 4, no. 4, pp. 324–331, 1983.

[216] C. Barber, D. Dobkin, and H. Huhdanpaa, "The quickhull algorithm for convex hulls," *ACM Transactions on Mathematical Software*, vol. 22, 02 1998.

[217] Z. Jiayin, G. Mei, N. Xu, and K. Yang, "A novel implementation of quickhull algorithm on the gpu," *arxiv*, 01 2015.

[218] C. H. Lin, R. Wu, W. K. Ma, C. Y. Chi, and Y. Wang, "Maximum volume inscribed ellipsoid: A new simplex-structured matrix factorization framework via facet enumeration and convex optimization," *SIAM Journal on Imaging Sciences*, vol. 11, 08 2017.

[219] U. Kar and D. Sanyal, "A critical review of 3gpp standardization of device-to-device communication in cellular networks," *SN Computer Science*, vol. 1, 10 2019.

[220] P. Ahrendt, *The Multivariate Gaussian Probability Distribution*. 2005.

[221] J. J. Nick Paine, "K-means clustering and gaussian mixture models." https://towardsdatascience.com/clustering-out-of-the-black-box-5e8285220717, February 2021. (Accessed on 05/13/2021).

[222] "Colaboratory." https://colab.research.google.com/notebooks/intro.ipynb. (Accessed on 04/01/2021).

[223] "sklearn.datasets.make_blobs — scikit-learn 0.24.1 documentation." https://scikit-learn.org/stable/modules/generated/sklearn.datasets.make_blobs.html. (Accessed on 04/01/2021).

[224] "Cvxpy 1.1.11 documentation." https://www.cvxpy.org, 2020. (Accessed on 04/01/2021).

[225] "scikit-learn 0.24.2 documentation." https://scikit-learn.org/stable/modules/generated/sklearn.metrics.silhouette_score.html, 2007. (Accessed on 05/11/2021).

[226] M. Chaudhary, "Silhouette analysis in k-means clustering." https://medium.com/@cmukesh8688/silhouette-analysis-in-k-means-clustering-cefa9a7ad111. (Accessed on 05/11/2021).

[227] A. Kumar, "Kmeans silhouette score explained with python example." https://dzone.com/articles/kmeans-silhouette-score-explained-with-python-exam, September 2020. (Accessed on 05/11/2021).

[228] S. Kumar, "Comparative analysis in between the k-means algorithm, k-means using with gaussian mixture model and fuzzy c means algorithm," 02 2017.

List of Figures

List of Tables

ACRONYMS AND ABBREVIATIONS

Acronyms:

A-NOMA	Asynchronous Non-Orthogonal Multiple Access
AWGN	Additive White Gaussian Noise
BER	Bit Error Rate
B5G	Beyond 5G
BGP	Border Gateway Protocol
CDMA	Code Division Multiple Access
CH	Cluster Head
Conv T-SIC	Conventional T-SIC
CSI	Channel State Information
CSP	Constraint Satisfaction Programming/Problem
eNB	eNodeB
D2D	Device to Device
EE	Energy Efficiency
ETI	Emergency Call occurring Time Interval
FDMA	Frequency Division Multiple Access
GD	Gradient Descent
GNSS	Global Navigation Satellite Systems
GPS	Global Positioning System
gNB	gNodeB
IC	Interference Cancellation
ICI	Inter-Carrier Interference
ISP	Internet Service Provider
LTE	Long Term Evolution
M2M	Machine to Machine
MA	Multiple Access
MANET	Mobile Cellular Network
MCS	Modulation and Coding Scheme
MEC	Multi-Access Edge Computing
mMTC	Massive Machine-Type Communication

MPR	Multi-Point Relay
NEC	Number of Emergency Calls
NoU	Number of UEs
NOMA	Non-Orthogonal Multiple Access
OFDMA	Orthogonal Frequency Division Multiple Access
OMA	Orthogonal Multiple Access
PSCCH	Physical Sidelink Control Channel
PRACH	Physical Random Access Channel
PSSCH	Physical Sidelink Shared Channel
ProSe	Proximity Services
PTT	Push To Talk
QoS	Quality of Service
RB	Resource Block
RIV	Resource Indicator Value
RSSI	Received Signal Strength Indicator
RSSI-MCL	RSSI Montecarlo Boxed Localization
SCI	Sidelink Channel Information
SC	Superposition Coding
SoC	State of Charge
SGD	Stochastic Gradient Descent
SIC	Successive Interference Cancellation
SLP	Successive Linear Programming
SINR	Signal to Interference plus Noise Ratio
T-SIC	Triangular SIC
TDMA	Time Division Multiple Access
ToA	Time of Arrival
TRP	Transmission Resource Pattern
UE	User Equipment
URLLC	Ultra-Reliable Low-Latency Communication
UAV	Umanned Aerial Vehicle
VANET	Vehicular Ad-hoc Network
WAA	Wireless Aerial Agent
5G-SOS	5G StandAlone Service

Symbols and Notations:

α_e	Energy attenuation factor
α_u	Iteration step size of $\boldsymbol{\lambda}, \boldsymbol{\delta}, \boldsymbol{\phi}, \boldsymbol{\mu}$ in SGD
α_r	Transmit power ratio of the legitimate user over jamming user
α_{RSSI}	Error margin of RSSI distance measurement
α_{AoA}	Error margin of AoA angle measurement
α_{ToA}	Error margin of ToA distance measurement
β	Time-varying distortion introduced by the frequency offset
β_u	Iteration step size of D_u in SGD
$\mathcal{B}$	Deformation matrix from unit circle to an ellipse
B	Bandwidth
$\tilde{\gamma}$	SINR threshold
$\gamma_k[s]$	SINR of the k-th user at the s-th symbol
c_c	Cluster centers
C_{m_i}	Emergency call initiated by m_i
C_s	Secrecy Capacity
C_m	Constant offset of Cost231 Hata model
δf	Frequency offset
Δf	Subcarrier spacing
$\Delta_{k^*,i}[s,\varsigma]$	Symbol time offset between k^*-th user symbol s and i-th user symbol ς
$d_{e_{[k^*]}}$	Half the distance between two nearest constellation points
$\boldsymbol{d}$	Vector representing the orientation of the ellipse
d_{ε^*}	Number of data points which are only inside the ε^*
$d_{rssi}(m_i, m_j)$	RSSI assisted m_i to m_j distance estimation
$d_{toa}(m_i, m_j)$	ToA assisted m_i to m_j distance estimation
d_{in}	Total number of data points in the dataset of UE locations
d_r	Data size reduction
d_{r_m}	Maximum data size reduction possible
D_b	Difference of two convex functions/sets constraints
$\boldsymbol{D_u}$	Binary decision variable of Cyclic T-SIC optimization problem
D_{u_k}	Binary decision of the data symbols to be decoded

ϵ_1	Error tolerance limit for optimal D_u
ϵ_2	Error tolerance limit for optimal λ
ε	Reciprocal of the transmitter power amplifier drain efficiency
ε^*	Maximum volume inscribed ellipse inside χ
E_c	Total energy consumption
E_{initial}	Initial energy level
E_{final}	Final energy level
E_{max}	Maximum initial energy of user device
g_i	Gain of the i-th user channel
g_m^k	Gain of legitimate user channel
g_e^k	Gain of eavesdropping user channel
h_{k^*}	Channel coefficient of k^*th user
$\mathbf{z}$	Latest detection status of the interfering symbols
$\eta_{k^*}[s]$	Multi-access interference
η_b	Number of messages in emergency call buffer
η	FIFO list of calls in the buffer to be relayed
η_p	Path-loss exponent
f	Signal transmission frequency of gNBs
$\Theta(m_i, m_j)$	AoA of m_i as estimated by m_j
$g(\boldsymbol{\lambda}, \boldsymbol{\delta}, \boldsymbol{\phi}, \boldsymbol{\mu})$	Lagrangian dual function
h_g	BS/gNB antenna effective height
h_m	UE antenna effective height
h_{k^*}	Channel coefficient of k^*th user
I_{th}	Interference power threshold
j	Imaginary unit of Complex number
k_{opt}	Optimal number of users' data to be decoded
k^*	Desired user within a cohort of K users
K	Maximum number of transmitters
K_{opt}	Optimum number of clusters
Λ	Distance of the interfering subcarrier to the desired subcarrier
$\lambda, \delta, \phi, \mu$	Dual variables of Lagrangian dual function

M	Modulation order
M_d	Set of 4/5G D2D enabled UEs
m_i	ith device in $m \in M$
ν	Received power ratio
N_{sym_k}	Number of symbols selected from an IC triangle per each k^{th} user
$N_{\text{T-SIC}}$	Number of repeated times of T-SIC decoding
n_0^u	Upper limit of re-transmissions
n_0	Additive White Gaussian Noise (AWGN)
n_{RS}	Number of relaying of data by the neighborhood
n_{Rt}	Re-transmission count of data signals
N_{sym_k}	Number of symbols selected per each kth user for the IC triangle
N	Number of subcarriers
N_l	Number of total UE locations
$N_{T_{SIC}}$	Fixed number of times Conv T-SIC is repeated between users
$N_{T_{SIC}\text{max}}$	Maximum range for NT_{SIC}
ϕ_i	GPS accuracy of the mobile m_i
P_i	Transmit power of the i-th user
P_g	Transmit power of gNB
$P(m_i)$	Priority value of m_i
$P_{C_{m_i}}$	Propagation path of C_{m_i}
$P(e_{k^*}[s])$	Error probability of sth symbol detection
P_i	Transmit power of the i-th user
P_{k^*}	Transmit power of k^* user
P_m^k	Transmit power of legitimate user
P_e^k	Transmit power of jamming user
P_{circuit}	Power dissipated by user device
P_{max}	Maximum transmit power
ρ	Ratio of δf to Δf
ρ_2	Volume of a planar unit circle
r_i	GPS accuracy radius of mobile m_i
$RS_{\text{th}}^{\text{max}}$	Maximum limit for RS_{th}
d	BS/gNB Link distance
$RS_{\text{threshold}}$	Threshold of relaying UEs
$RSSI(m_i, m_j)$	RSSI of m_i estimated by m_j
R_{min}^g	Minimum of GPS estimation radius
R_{max}^g	Maximum of GPS estimation radius
R_{min}	Minimum throughput threshold
R_{max}^e	Maximum throughput threshold for jammers
R_X	Receiver terminal
RR	Average number of requests per T_w during the last T_M period

σ^2	AWGN power
ς	Interfering symbol index
s	Symbol index
T_{d2d}	Data transfer delay by D2D mode
T_{max}	Initial Relay waiting time
T_0	Initial Emergency re-transmission waiting time
$ToA(m_i, m_j)$	ToA of m_i as estimated by m_j
T_0	Duration of the received superimposed signal
T_M	Fixed time period used to compute the average number of requests
T_N	Time duration over N symbols
t	Time index
τ_{min}	Minimum relative symbol time offset
τ_{max}	Maximum relative symbol time offset
u_a	Wireless aerial agent (WAA) that computes c_c locations
u_b	Upper bound of waiting time
ϕ	Relative symbol time offset
χ_c	Convex hull of the total UE locations
χ	List of calls already received and processed in the past
(x_{m_i}, y_{m_i})	The (x, y) coordinates of m_i
$X[n]$	Signal transmitted over the nth subcarrier
$X_{k^*}[s]$	The k^*th user's sth data symbol
$Y_{k^*}[s]$	Received signal at R_X for the k^*th user at the sth symbol

Mathematical Operator Notations and Symbols:

$\mathcal{L}(.)$	Lagrangian function
$Q(.)$	Q function
$\nabla_x f$	Sub-gradient of f with respect to x

Other Notations:

callID	Identifier of the emergency call
callIDGenerator	Function used by each UE to generate unique call IDs
DATA	Emergency call
deadline	latest time by which a waiting call is transmitted
nbAttempts	Count that *DATA* was transmitted or relayed
relay	relay device information content in DATA
srcID	Identifier of the source device
waitingCall	A call stored in η

Document generated with LaTeX and:
the LaTeX style for PhD Thesis created by S. Galland — http://www.multiagent.fr/ThesisStyle
the tex-upmethodology package suite — http://www.arakhne.org/tex-upmethodology/